NTNU
Norwegian University of
Science and Technology

Numerical Analysis of a Floating Wind Turbine

Global Load Effects in the Tower Structure

Mikal Hansson Espedal

Marine Technology
Submission date: June 2016
Supervisor: Trygve Kristiansen, IMT
Co-supervisor: Kjell Larsen, IMT
Erin Elizabeth Bachynski, IMT
Trond Landbø, Dr. Techn. Olav Olsen AS

Norwegian University of Science and Technology
Department of Marine Technology

NTNU Trondheim
Norwegian University of Science and Technology
Department of Marine Technology

MASTER THESIS IN MARINE TECHNOLOGY

SPRING 2016

FOR

Mikal Hansson Espedal

Numerical Analysis of a Floating Wind Turbine
– Global load Effects in the Tower Structure

Significant research within renewable energy sources has been performed the last decades. A renewable energy source with great potential is wind energy. Today onshore wind energy dominates the wind energy market, but it is expected that offshore wind energy will play an important role in the future.

Several designs, both bottom fixed and floating, have been proposed as options for offshore wind. Floating designs are mainly been TLP, semi-sub or spar types. The main problem with the offshore wind industry is the cost, making it dependent of governmental support.
The floater OO Star 10 MW is a semi-submersible floater developed by Dr.techn. Olav Olsen AS. It is designed to be built from concrete. A steel tower is mounted on the concrete floater, and this tower support the wind turbine with a satisfying vertical height. The bottom part of this steel tower is sensitive to fatigue damage, even though the steel thickness is close to both a practical and economical limit. It is therefore of interest to investigate possibilities to improve the fatigue lifetime of the steel tower. An increased lifetime will give a longer time to pay off the investment, making the design better suited for commercial energy companies.

Concrete is less sensitive to fatigue than steel, and the main task for the candidate is to investigate the effect on fatigue when increasing the transition point between concrete and steel. Important tasks for the thesis are:

- *In a proper way make use of important theory for a fatigue analysis of an offshore wind turbine. Relevant regulations should be used to provide needed results.*
- *Build a numerical model that is suitable for fatigue analysis of an offshore wind turbine. Relevant software can be applied.*
- *Perform relevant sensitivity studies to verify the numerical model.*
- *Make use of long-term statistic for a severe site to calculate fatigue damage. Point out loads contributing to fatigue.*

- *Make a comparison of fatigue lifetime for three different elevation levels between concrete and steel. If possible, make a conclusion whether or not an increased elevation level between concrete and steel is beneficiary for fatigue life time.*

The design of OO Star 10 MW is still in an ongoing process. If time, the candidate can therefore use the numerical model to look at additional design aspects for the design. Example of such design aspects are mooring system and pitch motions.

The thesis should be organized in a rational manner to give a clear exposition of results, assessments, and conclusions. The text should be brief and to the point, with a clear language. Telegraphic language should be avoided.

The thesis shall contain the following elements: A text defining the scope, preface, list of contents, summary, main body of thesis, conclusions with recommendations for further work, list of symbols and acronyms, reference and (optional) appendices. All figures, tables and equations shall be numerated.

The original contribution of the candidate and material taken from other sources shall be clearly defined.

Work from other sources shall be properly referenced using an acknowledged referencing system.

The thesis is to be submitted in DAIM.

Supervisor: Professor Trygve Kristiansen
Start: 10.01.2016
Deadline: 10.06.2016

Trygve Kristiansen
Supervisor

Abstract

The OO Star 10 MW is a semi-submersible floater that aims to support a 10 MW wind turbine. It consists of three outer columns with a shaft in the centre. The floater is designed to be built from concrete, and a steel tower is mounted on top of the concrete shaft providing a sufficient height for the wind turbine. Bottom part of the steel tower is sensitive to fatigue damage, even though steel thickness is close to both a practical and economical limit. A study of the effect on fatigue damage when increasing concrete shaft length is therefore performed.

Three cases with variable concrete shaft length are tested. The cases are named Case 0, Case 20 and Case 40. The number at each case represents increased concrete shaft length in metre compared to a base case. Small geometry modifications are done on Case 20 and Case 40 to maintain sufficient stability. Also the steel towers are slightly stiffer at comparable vertical positions for Case 20 and Case 40 compared to Case 0. Wind turbine is taken as the 10 MW DTU reference turbine, and hub height is kept constant for all three cases.

The problem is solved in time domain by use of the software SIMA. SIMA uses hydrodynamic forces calculated in the software Wadam and a turbulent wind field created by the software TurbSim. Calculations are performed for severe environmental conditions, and stress is calculated at several vertical positions on the steel tower. Stress concentration and safety factors are taken in accordance with regulations. Fatigue damage is estimated by use of a S-N curve.

A sensitivity study showed that first bending mode frequency for the steel tower is depending on the water plane stiffness, and that it is increased when the tower is mounted on a floater compared to being fixed. For current designs, this is found to be critical. All three cases have steel tower eigenfrequency close to the blade passing frequency (3p).

Contributions to fatigue is found to be wind, wave and 3p forces, where the latter one gives the largest contribution. Preliminary results show that an increased concrete shaft will improve fatigue life time, but due to the large 3p effects, none of the three designs have a sufficient life time. The fatigue life time is found to be 1.2 years for Case 0, 1.32 years for Case 20 and 1.39 years for Case 40. Fatigue life time for Case 40 is estimated to increase to 12.5 years if 3p effects are minimized. In addition to improving fatigue life time, an increase of concrete shaft with 40 metre will reduce the material cost by 5 mNOK.

Fatigue life time must be improved, and it is therefore recommended to modify the steel tower such that eigenfrequency is outside the 3p frequency range. Also using a steel tower with variable bending stiffness at different angular positions is found to be an option.

Additional design aspects were tested for Case 0 to be used in a screening process. Results indicate that mooring line tension, horizontal offset, pitch motion, acceleration at hub height and air gap is within requirements. Freeboard at outer column is found to be critical low, and the column risks being fully submerged during critical environmental conditions.

Abstrakt

OO Star 10 MW er en halvt nedsenkbar flyter som tar sikte på å støtte en 10 MW vindturbin. Den består av tre ytre søyler med et skaft i midten. Flyteren er designet for å bli bygget i betong, og et ståltårn er montert på toppen av betongskaftet for å gi tilstrekkelig høyde til vindturbinen. Nedre del av dette ståltårnet er sensitivt for utmatting, selv om ståltykkelsen som er brukt er nær både en praktisk og økonomisk grense. På grunn av dette er det gjennomført en studie som undersøker effekten av en økt lengde på betongskaftet med tanke på utmattingslevetid for ståltårnet.

Tre design med ulike lengder for betongskaft er testet, og disse er navngitt Case 0, Case 20 og Case 40. Tallet representerer antall meter som betongskaftet er forlenget sammenlignet med originalt design. Små geometriske modifikasjoner er gjort for Case 20 og Case 40 for å opprettholde nødvendig stabilitet. Også ståltårnet er litt stivere ved sammenlignbare vertikale posisjoner for Case 20 og Cased 40 sammenlignet med Case 0. 10 MW DTU referanseturbin er brukt, og denne har samme vertikale posisjon for alle tre designene.

Analysene er gjort i tidsplanet ved bruk av programmet SIMA. SIMA bruker hydrodynamiske krefter regnet ut i programmet Wadam og et turbulent vindfelt generert av programmet TurbSim. Beregningene er basert på relativt harde miljøkondisjoner, og spenningene er beregnet ved ulike vertikale posisjoner på ståltårnet. Stresskonsentrasjon og sikkerhetesfaktorer er tatt i henhold til regelverk. Utmattingskade er beregnet ved bruk av S-N kurve.

En sensitivitetstudie viste at første bøyemodefrekvens for ståltårnet avhenger av vannplanstivheten, og at denne frekvensen øker når tårnet er festet på en flyter sammenlignet med når det er fast. For nåværende design er denne effekten kritisk. Alle tre designene har en egenfrekvens for tårnet som er nær frekvensen for bladpassering (3p).

Analysene viser at det er vind, bølge og 3p krefter som bidrar til utmatting, hvor 3p krefter er den største bidragsyteren. Foreløpige resultater viser at utmattingslevetiden vil øke dersom betongskaftet blir forlenget, men på grunn av store 3p effekter har ingen av designene tilfredstillende levetid. Utmattingslevetiden er beregnet til 1.2 år for Case 0, 1.32 år for Case 20 og 1.39 år for Case 40. Utmattingslevetiden er estimert til å øke til 12.5 år for Case 40 dersom 3p effektene kan bli minimert. I tillegg til økt levetid vil en forlengelse av betongskaftet redusere materialkostnader med omtrent 5 mNOK.

Utmattingslevetiden må bli forbedret, og det er derfor anbefalt å modifisere ståltårnet slik at egenfrekvensen er utenfor rekkevidden for 3p frekvens. Det kan også være et alternativ å bruke et ståltårn hvor stivheten varier rundt tverrsnittet.

Også andre design aspekter er testet for Case 0. Resultatene kan bli brukt i et tidlig stadium for å kartlegge systemets egenskaper. Resultatene indikerer at linestrekk, horisontal forskyvning, stamp bevegelser, akselerasjoner ved sentrum av turbinen og avstand mellom roterende blad og vannivå er innen kravene. Fribord på ytre kolonne virker til å være kritisk lav, og kolonnen risikerer å bli fullt neddykket i kritiske miljøkondisjoner.

Preface

This master thesis has been carried out in the last semester of a masters degree within marine technology at NTNU. For several reasons, a new subject was chosen for the master thesis, and this work is therefore not a continuation of the project thesis carried out last semester.

The effect of an increased concrete shaft on fatigue life time for the floater OO Star 10 MW has been investigated by use of numerical tools. Background theory, methodology and results have been outlined in the report. Both workload and learning outcome has been significant.

I would like to thank my supervisor at NTNU, Trygve Kristiansen, for guiding me through the whole process. He has been a good support both on a personal and academic level during the thesis work. I would also like to thank my co-supervisors Erin Bachynski and Kjell Larsen. Erin's practical experience with software and wind turbines has been of large importance. Both Trygve, Erin and Kjell have been easy asking for guidance during the work, and this I appreciate.

The thesis is written in cooperation with the company Dr.techn. Olav Olsen AS. A sincere thanks goes to Trond Landbø for proposing the subject of the thesis. I appreciate that the company supported me with the opportunity to work at their office for some short periods. Several employees at the company have been of support, but a special thanks goes to Håkon S. Andersen and Jonas Gullaksen Straume.

– Mikal Hansson Espedal

Contents

Abstract **i**

Abstrakt **iii**

Preface **v**

Contents **ix**

List of Tables **xi**

List of Figures **xvi**

Nomenclature **xvii**

1 Introduction **1**
1.1 OO Star 10 MW 2
1.1.1 Wind Turbine 3
1.1.2 Cases 4
1.2 Report Layout 5

2 Background Theory **7**
2.1 Dynamic Analysis 7
2.1.1 Time Domain Analysis 10
2.1.2 Frequency Domain Analysis 11
2.1.3 Retardation Function 13
2.1.4 Dynamic Amplification Factor 14
2.2 Hydrodynamic Forces 15
2.2.1 Diffraction Problem 15
2.2.2 Radiation Problem 16
2.2.3 Excitation Loads (second order) 17
2.3 Aerodynamic Forces 18

2.3.1 Foil Theory . . . 18
2.3.2 Blade Element Momentum . . . 19
2.3.3 3p Effects . . . 20
2.4 Structural Forces . . . 22
2.5 Catenary Equation . . . 22
2.6 Processing of Results . . . 23
2.6.1 Filtering of Data . . . 23
2.6.2 Switching from Time Domain to Frequency Domain . . . 24
2.6.3 Normal Distribution . . . 25
2.7 Decay Analysis . . . 26
2.8 Fatigue . . . 28
2.8.1 Cycle Counting . . . 28
2.8.2 Miners Rule . . . 29
2.8.3 Stress Concentration Factors . . . 30

3 Methodology **33**
3.1 Discussion of Method . . . 33
3.2 Software . . . 34
3.3 Coordinate System and Floater Orientation . . . 35
3.4 Set-up for Model . . . 37
3.4.1 Floater Unit . . . 37
3.4.2 Tower Structure . . . 40
3.4.3 Wind Turbine . . . 43
3.5 Environmental Conditions . . . 46
3.5.1 Location . . . 46
3.5.2 Waves . . . 46
3.5.3 Wind . . . 47
3.5.4 Current . . . 48
3.5.5 Wind/Wave Relation . . . 49
3.6 Conditions for Analysis . . . 51
3.6.1 Numerical Parameters . . . 51
3.6.2 Decay Analysis . . . 51
3.6.3 Fatigue Analysis . . . 53

4 Verification and Sensitivity Studies **57**
4.1 Verification of Wind Turbine . . . 57
4.2 Sensitivity Studies . . . 59
4.2.1 Computational Time Step . . . 59
4.2.2 Quadratic Damping . . . 60
4.2.3 Second Order Wave Excitation Forces . . . 62
4.2.4 Structural Damping . . . 64
4.2.5 Effect on Tower Eigenfrequency When Mounted on a Semi-submersible Floater . . . 65

5 Results and Discussion for Fatigue **67**
5.1 Decay Analyses . . . 67

5.2 Eigenfrequency for First Tower Bending Mode . . . 69
5.3 Fatigue . . . 72
5.3.1 Contributions to Fatigue . . . 72
5.3.2 Case 0 . . . 72
5.3.3 Case 20 . . . 74
5.3.4 Case 40 . . . 74
5.3.5 Comparison of the Cases . . . 75
5.3.6 Critical Direction . . . 79
5.3.7 Critical Environment . . . 80
5.4 Cost Reduction . . . 82

6 Results and Discussion for Additional Design Aspects **83**
6.1 Mooring Line Tension . . . 84
6.2 Horizontal Offset . . . 85
6.2.1 Critical Direction . . . 85
6.2.2 Offset . . . 85
6.3 Pitch Motion . . . 87
6.4 Acceleration Hub Level . . . 88
6.5 Outer Column Freeboard . . . 89
6.6 Rotor Air Gap . . . 92

7 Conclusion **93**

8 Recommendations for Further Work **95**

References **97**

A Steel Tower Geometry **99**

B Environmental Data **103**

C Input TurbSim **109**

D Decay Analyses **113**

E Hydrodynamic Forces **115**
E.1 Frequency Dependent Added Mass . . . 115
E.2 Frequency Dependent Linear Damping Coefficient . . . 116
E.3 First Order Wave Force Transfer Function . . . 119

List of Tables

1.1 Key features for the 10 MW DTU reference wind turbine (Bak et al., 2013). 3
1.2 Key features for the three different cases. 4

3.1 Fastening points on body for mooring lines. Same body points are used for all three cases. 39
3.2 Drag coefficients tower. 43
3.3 Decay forces/moments for constant time range (200s − 300s) 52
3.4 Parameters for S-N curve D (DNV, 2010). 53

5.1 Results for decay analyses for Case 0, Case 20 and Case 40. Note that it is the damped natural period that is given, which for low damping ratios is approximately equal to undamped natural period. 68
5.2 Eigenfrequency first tower bending mode. 69
5.3 Operation conditions for wind turbine for variable environments. Environment numbers are taken according to Table B.1 and Table B.2. 81
5.4 Estimation for total material cost (steel and concrete) for the three different design cases. The material cost is here taken for floater and tower, i.e. material cost for rotor blades is not included. 82

B.1 Environmental conditions table 1. 106
B.2 Environmental conditions table 2. The table is a continuation of table 1 above. 107

List of Figures

1.1 Isometric view of the OO Star 10 MW concept (Landbø, 2016b). 2

2.1 Illustration mathematical solutions for the equation of motion. $\xi = 0.06$, $\omega_0 = 1.2$ rad/s, $\omega = 1.0$ rad/s. 9
2.2 Continuous and discrete solution (Larsen, 2014). 10
2.3 Illustration of a wave spectrum, response amplitude operator and corresponding response spectrum. 12
2.4 Dynamic amplification factor as a function of frequency ratio. Inspiration from Larsen (2014) 14
2.5 Illustration of radiation and diffraction problem (Faltinsen, 1990). 15
2.6 Illustration of a solution on damping and added mass in pitch-pitch motion from potential flow theory (by use of the software Wadam). Illustration represents values for Case 40. 16
2.7 Illustration of forces on a two-dimensional foil section (Bachynski, 2015). 18
2.8 Actuator disk rotor model used in one dimensional momentum theory (Bachynski, 2015). 19
2.9 Simple illustration of reasons for 3p effects. 21
2.10 Mooring line with symbols (Faltinsen, 1990). 23
2.11 Illustration of different filtering options (Steen, 2014). 24
2.12 Example of a normal distribution with mean values equal to zero and standard deviation equal to one. 25
2.13 Illustration of a decay test in heave direction performed in the software SIMA. 26
2.14 Measured damping from a heave decay test. 27
2.15 Illustration on how rainflow counting technique is used on a load cycle. Inspired by (Lee et al., 2012). 29
2.16 Example on how to find numbers of cycles to failure by use of a S-N curve. The curve is based on data for S-N curve D in DNV (2010). 30
2.17 Illustration of variables (DNV, 2010). 31
2.18 Illustration of variables (DNV, 2010). 31

3.1 Workflow between software. Italics represent modules in the main software. 34
3.2 Coordinate system used for modelling in SIMA. 36
3.3 Orientation of the system compared to true headings for given location. . 36
3.4 Decay test surge direction for Case 0 and Case 40. Decay tests were done before additional damping coefficient for Case 40 was modified. 39
3.5 Illustration of bending stiffness and outer radius for steel towers. 41
3.6 Illustration of modelling of concrete shaft flexibility (Landbø, 2016b). . . 41
3.7 Drag coefficient for a smooth 2D cylinder (Greco, 2012). Note that the angle θ is not similar as used elsewhere in the report. 42
3.8 Decay test with with constant wind included. 45
3.9 Illustration of SIMA model for Case 0. 45
3.10 West of Barra proposed site location (Gómez et al., 2015) 46
3.11 Annual mean wind speed for given site (reference location: West of Barra) (Gómez et al., 2015). 48
3.12 Illustration of heading probability for wind and wave for given site (Gómez et al., 2015). Note that the rose for direction X indicates the probability for the environment to come from this heading. 49
3.13 Illustration of applied force in a decay test. The ramp and constant force is applied in order to stabilize the system before releasing it. 51
3.14 Effect of using high-pass filter in order to avoid negative damping for a decay test in roll. 52
3.15 Illustration on how distribution of points are done if using 8 points. It illustrates two dimensional cross section of the steel tower seen from above. Point 1 is located the same place independent on number of points, while the rest is evenly distributed counter-clockwise. The figure is given in accordance with the specified coordinate system, as described in section 3.3. 54

4.1 Aerodynamic properties for DTU 10 MW turbine. 58
4.2 Aerodynamic properties for DTU 10 MW turbine. 58
4.3 Sensitivity of time step on fatigue damage. The figure present damage difference compared to previous time step in percentage. Note that x-axis is not to scale. 59
4.4 Comparison of linear damping versus quadratic damping amplitude. . . . 61
4.5 Damage variation as a function of $C_{scaling}$ (as used in equation (4.3)). . 62
4.6 Wave excitation forces in pitch. 63
4.7 Damage variation as a function of $C_{scaling}$ as used in equation (4.4). . . 64
4.8 Damage variation as a function of $C_{scaling}$ as used in equation (4.4). . . 65
4.9 Eigenmode steel tower for Case 0 when the tower is fixed, and not mounted on a floater. 65
4.10 Illustration of methods to find eigenfrequency of first tower bending mode when mounted on a semi-submersible. 66

5.1 Decay tests for Case 0 in SIMA. 68
5.2 Transfer functions for tower structure. They are taken in the bottom part of the steel tower, i.e. variable vertical position for the three cases. 70
5.3 Example of rotor speed in rated condition. 71

5.4 Illustration of 3p frequency compared to the natural frequency for the tower structure. 71
5.5 Illustration of peaks in a typical spectrum of a FFT of bending moment in steel tower. Note that there is a clear peak in natural frequency for pitch that is probably caused by wind loads. Fatigue damage for lower frequencies than this is also caused by wind loads. 72
5.6 Fatigue damage for Case 0. Damage is taken equal damage for the most critical point (out of eight). Wind/wave contributions and 3p effects are estimated by use of low-pass and band-pass filtering, respectively. 73
5.7 Fatigue damage for Case 20. Damage is taken equal damage for the most critical point (out of eight). Wind/wave contributions and 3p effects are estimated by use of low-pass and band-pass filtering, respectively. 74
5.8 Fatigue damage for Case 40. Damage is taken equal damage for the most critical point (out of eight). Wind/wave contributions and 3p effects are estimated by use of low-pass and band-pass filtering, respectively. 75
5.9 Total damage as function of vertical position relative to transition point between concrete and steel. 76
5.10 Total damage as function of vertical position relative to baseline. 77
5.11 Damage due to 3p effects estimated by use of a band-pass filter. Presented as function of vertical position relative to baseline. 77
5.12 Damage due to wind and wave forces. Damage is estimated by use of a low-pass filter. Presented as function of vertical position relative to baseline. 78
5.13 Damage for various points around the tower. Vertical position taken in bottom part of steel tower for each case. Point location is described by the angle θ, as described in Figure 3.15. 79
5.14 Damage for various points around the tower. Vertical position taken in bottom part of steel tower for each case. Point location is described by the angle θ, as described in Figure 3.15. 80
5.15 Weighted damage bottom part of steel tower in each case. Damage is taken as most critical out of 8 points for each run. Environmental condition number corresponds to environments given in Table B.1 and Table B.2. . 81
5.16 Probability for environmental conditions. Environmental condition number corresponds to environments given in Table B.1 and Table B.2. 81

6.1 Tension in mooring line located at windward side for Case 0 in variable environmental loads propagating in NE direction. 84
6.2 Offset for equal wind/wave environment, but with different propagation directions. 86
6.3 Offset for variable environmental conditions for Case 0 when environment is propagating in SW direction. 86
6.4 Pitch motion for variable environmental conditions for Case 0. Environment is propagting in true SW direction. 87
6.5 Acceleration in x-direction at hub level for variable environment propagating in true SW direction. Mean value is equal to zero, and the results are presented as $1.96 \cdot$ std. 88

6.6 Freeboard for outer column with variable environment propgating in true SW direction. 90
6.7 Time series of freeboard for environment wind speed at hub height equal to 19.1 m/s, significant wave height equal to 5.13 metre and a mean wave period of 10.81 second. 90
6.8 Time series of freeboard for environment corresponding to a wind speed at hub height equal to 19.1 m/s, significant wave height equal to 5.13 metre and a mean wave period of 10.81 second. 91
6.9 Rotor air gap for variable environmental conditions propagating in true SW direction. 92

A.1 Tower geometry for Case 0. Provided by Dr.techn. Olav Olsen AS. 100
A.2 Tower geometry for Case 20. Provided by Dr.techn. Olav Olsen AS. . . . 101
A.3 Tower geometry for Case 40. Provided by Dr.techn. Olav Olsen AS. . . . 102

B.1 Scatter Hs/Tp for location West of Barra (Gómez et al., 2015). 103
B.2 Scatter Hs/α_{Wa} for location West of Barra (Gómez et al., 2015). 104
B.3 Scatter Uw/α_{Wi} for location West of Barra (Gómez et al., 2015). 104
B.4 Scatter wind/wave for location West of Barra (Gómez et al., 2015). 105

D.1 Decay tests for Case 20. 113
D.2 Decay tests for Case 40. 114

E.1 Frequency dependent added mass from Wadam in surge-surge (s-s) and heave-heave (h-h) direction. 115
E.2 Frequency dependent added mass from Wadam in pitch-pitch (p-p) and yaw-yaw (y-y) direction. 116
E.3 Frequency dependent added mass from Wadam in surge-pitch (s-p) direction. 116
E.4 Frequency dependent linear damping coefficient from Wadam in surge-surge (s-s) and heave-heave (h-h) direction. 117
E.5 Frequency dependent linear damping coefficient from Wadam in pitch-pitch (p-p) and yaw-yaw (y-y) direction. 117
E.6 Frequency dependent linear damping coefficient from Wadam in surge-pitch (s-p) direction. 118
E.7 First order wave force transfer function in surge direction for wave heading 0 degrees. 119
E.8 First order wave force transfer function in heave direction for wave heading 0 degrees. 119
E.9 First order wave force transfer function in pitch direction for wave heading 0 degrees. 120

Nomenclature

1p	-	rotational frequency of turbine rotor
3p	-	blade passing frequency
CoG	-	Centre of Gravity
DAF	-	Dynamic Amplification Factor
DOF	-	Degree of Freedom
FEM	-	Finite Element Method
FFT	-	Fast Fourier Transformation
P-M	-	Pierson-Moskowitz
RAO	-	Response Amplitude Operator
RWT	-	Reference Wind Turbine
SCF	-	Stress Concentration Factor
α	-	angle of attack
α_{Wa}	-	wave propagation direction
α_{Wi}	-	wind propagation direction
β	-	frequency ratio
β_t	-	time integration parameter
γ	-	time integration parameter
δ	-	misalignment
ϵ	-	phase
ζ	-	wave elevation
ζ_A	-	wave amplitude
$\dot{\eta_x}$	-	relative velocity in direction x
θ	-	angle to describe point location
κ	-	correction factor
μ_Y	-	mean value
ν	-	kinematic viscosity
ξ	-	damping ratio
ρ	-	fluid density
σ	-	solidity ratio
σ_Y	-	standard deviation
τ	-	time difference
ϕ	-	angle accounting for both angle of attack and blade pitch angle
ϕ_{rs}	-	rotor speed error
ψ	-	angular velocity imparted to the free stream
ω	-	frequency [rad/s]
ω_0	-	natural frequency [rad/s]
ω_d	-	damped natural frequency [rad/s]
ω_t	-	eigenfrequency tower structure [rad/s]

Λ	-	logaritmic decrement
Ω	-	angular velocity of rotor
a	-	axial induction factor
a'	-	angular induction factor
a_1	-	stiffness proportional damping coefficient
a_2	-	mass proportional damping coefficient
aa	-	S-N curve parameter
b	-	number of blades
c	-	chord length
d	-	diameter
f	-	frequency [Hz]
f_t	-	eigenfrequency frequency tower structure [Hz]
g	-	gravity constant
h	-	retardation function
h_t	-	time step
h_z	-	water depth
k	-	S-N curve parameter
m	-	sum of mass and added mass
m_s	-	S-N curve parameter
m_n	-	n'th moment
n_i	-	number of stress cycles
p_1	-	linear damping coefficient divided by the mass
p_2	-	quadratic damping coefficient divided by the mass
p_N	-	force normal to rotor plane
p_T	-	force tangential to rotor plane
r	-	radial distance
s	-	line length from touch down point to point where tension is measured
t	-	time
v_0	-	inlet velocity
v_1	-	outlet velocity
w	-	weight per unit length in water
x	-	system displacement
x_0	-	response amplitude
$\dot{x}$	-	system velocity
$\ddot{x}$	-	system acceleration
x_H	-	homogeneous solution
x_P	-	particular solution
z_0	-	surface roughness length
z_f	-	freeboard outer column
z_{f0}	-	initial freeboard
A	-	added mass coefficient
A_C	-	constant from initial condition

A_{cs}	-	cross sectional area
A_{line}	-	cross sectional area of the line
A_p	-	projected area
B	-	damping coefficient
B_1	-	linear damping coefficient
B_2	-	quadratic damping coefficient
B_C	-	constant from initial condition
C	-	stiffness coefficient
C_D	-	drag force coefficient
C_L	-	lift force coefficient
C_n	-	normal coefficient
$C_{scaling}$	-	scaling coefficient
C_t	-	thrust coefficient
D	-	fatigue damage
D_{3p}	-	estimated 3p damage from band-pass filtering
$D_{wind/wave}$	-	estimated wind/wave damage from low-pass filtering
D_C	-	characteristic cumulative damage
D_D	-	design cumulative damage
D_{FF}	-	design fatigue factor
F	-	excitation force
F_0	-	excitation force amplitude
F_L	-	lift force
F_D	-	drag force
H	-	transfer function
H_s	-	significant wave height
I	-	mass moment of inertia
M_x	-	bending moment around x-axis
N_i	-	number of cycles to failure
R_{xx}	-	Auto correlation function
S_i	-	stress range
S_{xx}	-	load spectrum
S_{yy}	-	response spectrum
T	-	line tension
T_{jj}	-	natural period direction j-j
T_H	-	horizontal line tension
T_m	-	mean wave period
T_W	-	wave period
T_{jk}^{ic}	-	second order transfer function
T_{jk}^{is}	-	second order transfer function
U_M	-	maximum particle velocity
U_{ref}	-	mean wind speed at reference height
U_w	-	wind speed
V_{rel}	-	relative velocity

Chapter 1

Introduction

There has been a large focus on the drawbacks of the non-renewable energy sources the last decade. Heavy use of oil, gas and coal has been pointed out as the main source for environmental pollution and global warming. Anyhow, people are used to a certain standard of living, and this standard consumes a certain amount of energy. It is hard to force a downgrade on people's living standard, and therefore either more efficient ways to use energy, or improved methods to produce renewable energy, are needed in order to reduce consumption of non-renewable energy.

One renewable energy source with great potential is wind energy. Onshore wind energy is today dominating, but it is expected that offshore wind will play an important role in the future (EWEA, 2013). Offshore wind has the advantage of improved wind properties due to lower turbulence and wind shear. Larger wind turbines are also made possible offshore due to possibility of transporting larger constructions. Finally, offshore wind has the advantage of low visuality and noise disturbance to residents.

Cost is a major problem for the offshore wind energy industry. For offshore wind energy projects to be more attractive for commercial companies, and less dependent on governmental support, the total cost must be reduced. Closely connected to the cost is the expected lifetime of the system. A long lifetime provides longer time to pay off the investment. Fatigue related problems often determines the lifetime on offshore wind construction parts. Fatigue can also drive the amount of material which is needed, which is a major factor in the cost. This thesis will focus on improving the fatigue lifetime on the steel tower of the floating wind turbine system OO Star 10 MW.

1.1 OO Star 10 MW

The OO Star 10 MW is a semi-submersible floater that aims to support a 10 MW wind turbine. It consists of three outer columns with a shaft in the centre. Three pontoons connects the shaft with the columns. An illustration of the design is provided in Figure 1.1.

Figure 1.1: Isometric view of the OO Star 10 MW concept (Landbø, 2016b).

The floater is designed by Dr.techn. Olav Olsen AS, and it is designed to be built from concrete. A steel tower is mounted on top of the mid shaft of the floater, supporting the wind turbine with sufficient height. Technical data and specifications in this thesis are provided in cooperation with Dr.techn. Olav Olsen AS.

OO Star 10 MW is based on a similar design developed for 6 MW wind turbines. Significant research has been executed in order to optimize the 6 MW design. The work with the OO Star 10 MW is still in the early stage process, and there are still parts of the design that can be further optimized.

For the current design, the bottom part of the steel tower is sensitive to fatigue damage,

even though the steel thickness is close to both a practical and economical limit. It is therefore of interest to investigate options to improve this, and one possible option is to increase the elevation level of the transition point between concrete and steel.

Concrete is less sensitive to fatigue than steel. A longer concrete shaft, and equally shorter steel tower, will reduce the stress from wind moment loads on bottom part of the steel tower. In addition to an increased fatigue lifetime, the steel weight will be reduced. Hopefully the total material cost from concrete and steel will be reduced, helping to decrease the new building cost.

As mentioned is the work on the OO Star 10 MW not yet finished, and especially the steel tower needs to be improved. During the work with the thesis, it was found that the natural frequency for the first tower bending mode was close to the blade passing frequency (3p frequency). This gives a large fatigue contribution, and this finding has influenced both the results and focus of the thesis.

1.1.1 Wind Turbine

The wind turbine used is the 10 MW DTU reference wind turbine (RWT). This wind turbine is well suited to use in the design process, and it is designed for offshore sites. This is due to the assumption that turbines with this size most likely will be dedicated to offshore locations since transport of these constructions are a problem onshore. The 10 MW DTU RWT is an upwind turbine, i.e. it is facing the wind. Key features of the RWT is presented in Table 1.1, and a detail description can be found in Bak et al. (2013).

Bak et al. (2013) also provides a reference tower, which is designed to be a bottom fixed tower. Note that this tower is not used in the thesis. The tower structure used is designed by Dr.techn. Olav Olsen AS, and will be further described later on.

Table 1.1: Key features for the 10 MW DTU reference wind turbine (Bak et al., 2013).

Key feature	**Value**
Cut in wind speed	4 m/s
Cut out wind speed	25 m/s
Rated wind speed	11.4 m/s
Rated power	10 MW
Number of blades	3
Rotor diameter	178.3 m
Hub height	119 m
Minimum rotor speed	6 rpm
Maximum rotor speed	9.6 rpm
Shaft tilt angle	5 degrees
Rotor mass	227.962 t
Nacelle mass	446.036 t

1.1.2 Cases

In order to investigate the effect on fatigue lifetime when increasing the transition point between concrete and steel, three similar designs will be tested. The three designs are named Case 0, Case 20 and Case 40 in this report.

- ***Case 0***: Original design. Elevation level between concrete and steel equal to 37.5 metre relative to base line.
- ***Case 20***: Modified design. Elevation level between concrete and steel equal to 57.5 metre relative to base line.
- ***Case 40***: Modified design. Elevation level between concrete and steel equal to 77.5 metre relative to base line.

The hub height is kept constant for all three cases, meaning that the steel tower is decreased with the same length as the concrete shaft is increased. An increase for the transition point between concrete shaft and steel tower moves the centre of gravity (CoG) up, and hence lowers the stability of the system. This is accounted for by modifying the design on Case 20 and Case 40 compared to the base case (Case 0). Key features of the three models are given in Table 1.2.

Table 1.2: Key features for the three different cases.

Key feature	**Case 0**	**Case 20**	**Case 40**
Elevation level between concrete and steel [m]	37.5	57.5	77.5
Draught [m]	22.5	22.5	22.5
Shaft diameter in water plane [m]	9.44	8.9	9.56
Column diameter in water plane [m]	13.0	13.2	13.6
Distance shaft centre to column centre [m]	38.0	38.25	38.65
Mass displacement [t]	24355.8	25091.0	25611.0
Centre of gravity relative to water plane [m]	-9.22	-8.5	-7.609

The key features are given in order to provide a suitable impression of the three different cases. Optimally, one should have added the technical drawings for each case as appendix, but due to confidentiality this is not done. The thesis can only be kept confidential for a maximum of three years.

All three cases use the same wind turbine specification. The steel tower is, as mentioned, decreased with same magnitude that concrete shaft is increased. A further comparison of the three towers will be given in section 3.4.2.

1.2 Report Layout

This report is divided in five main chapters:

2. **Background Theory**: This chapter will cover the background theory that has been of importance for the thesis.
3. **Methodology**: This chapter describes software, methods, assumptions and simplifications used. It also gives a description of the environmental conditions. The chapter gives a relative short description of the procedure used to obtain results.
4. **Verification and Sensitivity Studies**: In this chapter the results from several sensitivity studies are given. They are given both to verify the numerical model and quantify if tested parameters affect the fatigue lifetime. The wind turbine is also verified according to reference values.
5. **Results and Discussion for Fatigue**: In this chapter results from the fatigue analysis are presented and discussed. Sensitivity for increased elevation height between concrete and steel on the fatigue lifetime will be discussed in particular. Also decay analyses and eigenfrequencies for first tower bending mode will be given.
6. **Results and Discussion for Additional Design Aspects** In this chapter results for some additional design aspects, such as mooring force, horizontal offset and pitch angle, will be given. These results are obtained by the numerical model used to calculate fatigue, and the method has therefore some limitations. Anyhow, the results can be useful in a screening process to check if the design seems reasonable.

In the end, conclusion and recommendations for further work is given.

Chapter 2

Background Theory

This chapter contains a description of important background theory. The theory that is included has either been used directly, or been important in order to provide and evaluate results from software in a proper way.

The tasks in this thesis have required a wide theoretical background knowledge. At first, the dynamic equation of motion, and possible methods to solve this, will be given. Then background theory for hydrodynamic and aerodynamic loads, and the structural response from these, will be described.

After this, theory for decay analysis, processing of results and catenary equation for mooring system is described. In the end, background theory for fatigue analysis will be given.

2.1 Dynamic Analysis

For a floating concept for offshore wind, dynamic analysis plays an important role for estimating both motions and structural responses. The dynamic equation of motion is evaluated based on Newton's second law:

$$M\ddot{x}(t) = F(t) \tag{2.1}$$

Where $F(t)$ is force working on the system at time t, $\ddot{x}(t)$ the system acceleration and M the mass of the system. For a hydrodynamic problem, the force, $F(t)$, will consist of the so-called excitation and radiation problem. Excitation forces are normally caused by environmental loads, such as waves, while radiation problem is the forces created due to the motions of the structure. The radiation problem consists of added mass (A), damping

(B) and stiffness (C) force/moment. The equation of motion for a linear uncoupled motion then becomes:

$$(M_j + A_{jj})\ddot{x_j}(t) + B_{jj}\dot{x_j}(t) + C_{jj}x_j(t) = F_j(t) \tag{2.2}$$

Here j is the degree of freedom. Note that for simplicity the theory will be described for uncoupled system in this chapter. Coupled effects are of importance, and are included in software calculations. Also some additional terms are added in the equation in the software, and these accounts for quadratic damping, mooring stiffness etc.

The natural period for a system described by the linear uncoupled motion can be found as:

$$T_{jj} = 2\pi\sqrt{\frac{M + A_{jj}}{C_{jj}}} \tag{2.3}$$

Note that mass, M, is only used for translational degrees of freedom. For rotational degrees of freedom, mass is replaced by mass moment of inertia, I_{jj}.

Mathematical Solution

The mathematical solution for equation (2.2) can be found by dividing the solution into two subsolutions; the homogeneous (x_H) and particular solution (x_P). The total solution is found as the sum of these two:

$$x(t) = x_H(t) + x_P(t) \tag{2.4}$$

The homogeneous solution is found by solving the equation of motion with no excitation force, while the particular solution accounts for the excitation force. A more detailed explanation of the two solutions can be found in Larsen (2014).

An illustration of a homogeneous and a particular solution is given in Figure 2.1. Also the total solution is illustrated in the same figure. Note that the homogeneous part will die out after time, and the particular solution will then dominate. This is called the steady-state part of the solution. The part also affected by the homogeneous part, is called the transient part.

The solution is depending on the frequency ratio, β, and the critical damping ratio, ξ, for the system. These are found as:

$$\xi = \frac{B}{B_{cr}} = \frac{B}{2(M + A)\omega_0} \tag{2.5}$$

$$\beta = \frac{\omega}{\omega_0} \tag{2.6}$$

Where ω_0 is the natural frequency and ω the load frequency. The solution also depends on the damped natural frequency, found as:

$$\omega_d = \omega_0 \sqrt{1 - \xi^2} \tag{2.7}$$

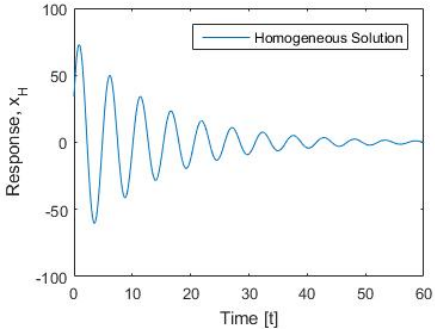

(a) Example of a homogeneous solution.

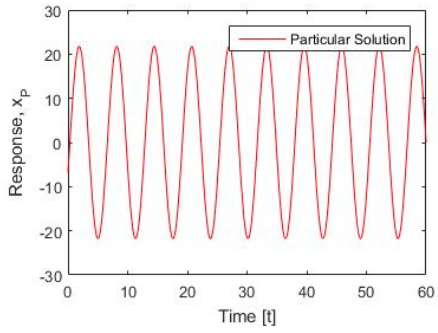

(b) Example of a particular solution.

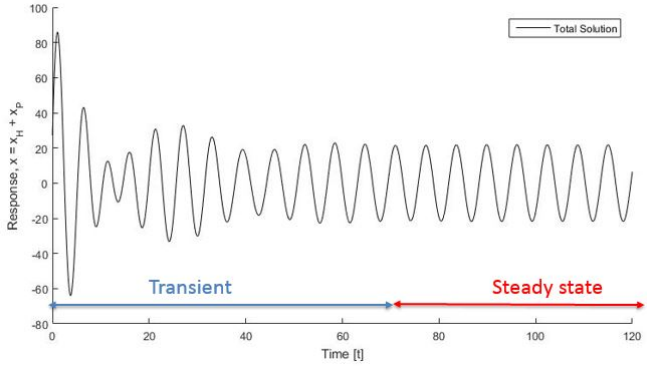

(c) Example of a total solution. The figure is taken as the sum of Figure 2.1a and Figure 2.1b

Figure 2.1: Illustration mathematical solutions for the equation of motion. $\xi = 0.06$, $\omega_0 = 1.2$ rad/s, $\omega = 1.0$ rad/s.

The mathematical solution is normally not used in computational tools. The equation is normally solved discrete in time domain or in frequency domain.

2.1.1 Time Domain Analysis

Solving the equation of motion in the time domain means to solve the problem for time, t, by use of numerical calculations. This method must be used if non-linear conditions and/or transient conditions (first part in Figure 2.1c) are of interest. Below is a list of typical non-linear effects that may be of importance for a dynamic analysis:

- Hydrodynamic sum frequency effects
- Hydrodynamic difference frequency effects
- Quadratic damping
- Aerodynamic thrust and lift

Time domain analysis is well-suited for a coupled dynamic analysis, where both wind and wave loads are to be included. The main advantage by solving the problem in time domain is that non-linear effects can be included. The main drawback is the computational time. Statistical values often requires several realizations with variable seed, and this is more time-consuming than finding statistical values from frequency domain (which will be further explained in section 2.1.2).

When solving the dynamic equation in time domain, the solution is not solved as a continuous function, but it is solved for discrete time steps. This means that the solution is correct (as correct as the method allows) for these points in time, but not necessarily between the points. This is illustrated in Figure 2.2, and the accuracy of the calculation is depends on the selected time step. Errors in the numerical calculation (such as numerical damping) is reduced by decreasing the time step, but this also increases the computational time.

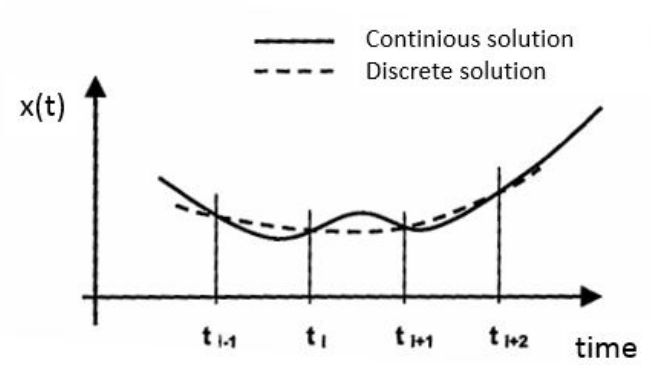

Figure 2.2: Continuous and discrete solution (Larsen, 2014).

Newmark Beta Method

The Newmark Beta method is a numerical method to solve the equation of motion. Theory for the method is taken from Larsen (2014), where also a more detailed description can be found. The three following equations are used to solve the equation for time step $i+1$:

$$(M+A)\ddot{x}_{i+1} + B\dot{x}_{i+1} + Cx_{i+1} = F_{i+1} \tag{2.8}$$

$$\dot{x}_{i+1} = \dot{x}_i + (1-\gamma)h_t\ddot{x}_i + \gamma h_t\ddot{x}_{i+1} \tag{2.9}$$

$$x_{i+1} = x_i + h_t\dot{x}_i + (\frac{1}{2} - \beta_t)h_t^2\ddot{x}_i + \beta_t h_t^2\ddot{x}_{i+1} \tag{2.10}$$

Here h_t is the time step. These three equations can be used to solve displacement (x_{i+1}), velocity ($\dot{x}_{i+1}$) and acceleration ($\ddot{x}_{i+1}$) at time step $i+1$. β_t and γ are time integration parameters. There are several methods within the Newmark Beta method, and type of method is determined by these parameters.

When solving the equation, one wants to avoid numerical instability. The requirements for the method to be unconditional numerical stable are:

$$\gamma \geq \frac{1}{2} \quad and \quad \beta_t \geq \frac{1}{4}(\gamma + \frac{1}{2})^2 \tag{2.11}$$

2.1.2 Frequency Domain Analysis

As an alternative to solving the equation of motion in time domain, frequency domain can be used. In frequency domain, the solution is solved for steady-state condition (ref. Figure 2.1c). For the frequency domain analysis it is assumed that the excitation is a harmonic oscillating force:

$$F(t) = F_0 sin(\omega t) \tag{2.12}$$

The steady state solution will be a harmonic oscillating response with a phase difference (ϵ) compared to the excitation load:

$$x(t) = x_0 sin(\omega t - \epsilon) \tag{2.13}$$

Newland (1993) sums up the frequency response method in a good way: ”By making measurements at a series of closely spaced frequencies, amplitude ratio and phase angle can be plotted as a function of frequency, and in theory if the frequency range extends from zero to infinity then the dynamic characteristics of the system are completely defined”.

Stochastic Spectral Analysis

Normally the response amplitude operator (RAO) is calculated in the frequency domain analysis for closely spaced frequencies. RAO is the transfer function of the system, and is defined as the ratio between the response, x_0, and the excitation amplitude, F_0:

$$RAO(\omega) = |H(\omega)| = \frac{x_o}{F_0} \tag{2.14}$$

The transfer function has a peak at natural frequency of the system. When executed to excitation forces close to this, large responses may occur. This frequency dependent effect is a dynamic effect related to the so-called dynamic amplification factor, which will be further described in section 2.1.4.

Further the RAO is used in spectral analysis to find the response. Knowing the spectra of the excitation load, $S_{xx}(\omega)$, and the transfer function, $|H(\omega)|$, the response spectrum, $S_{yy}(\omega)$, is found the following way:

$$S_{yy}(\omega) = |H(\omega)|^2 S_{xx}(\omega) \tag{2.15}$$

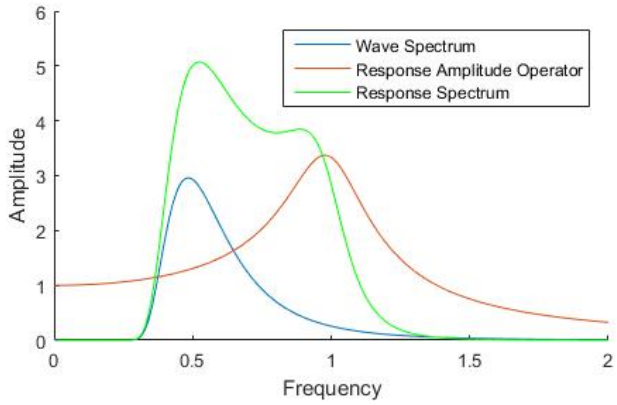

Figure 2.3: Illustration of a wave spectrum, response amplitude operator and corresponding response spectrum.

When knowing the response spectrum, the spectral characteristics can easily be found by calculating the n'th moment (see equation (2.16)). Characteristics such as standard deviation and significant value can then be statistically determined.

$$m_n = \int_0^\infty \omega^n S_{yy}(\omega) d\omega \tag{2.16}$$

Performing calculations in the frequency domain has both advantages and drawbacks. The main advantage is that calculations in the frequency domain has a high computational efficiency, and the results are well suited to find stochastic values. The main drawback is that the method mainly is suited for linear analyses, and that non-linear effects are not included.

2.1.3 Retardation Function

If the hydrodynamic loads are calculated in the frequency domain and should be integrated in a coupled dynamic analysis in the time domain, the retardation function is of importance. The retardation function makes it possible to use frequency dependent added mass, damping and excitation loads in the time domain. A short summary from the SIMO theory manual on the retardation function is given below (Marintek, 2015b).

The dynamic equation is written the following way:

$$(M + A(\omega))\ddot{x}(t) + B(\omega)\dot{x}(t) + Cx(t) = f'(t) \tag{2.17}$$

Where $f'(t)$ is the excitation load and non frequency dependent damping. The frequency dependent loads are gathered on one side of the equal sign:

$$A(\omega)\ddot{x} + B(\omega)\dot{x} = f(t) = f'(t) - Cx(t) - M\ddot{x}(t) \tag{2.18}$$

The frequency dependent load in time, $f(t)$, can be solved by use of added mass constant for infinitely frequency, A_∞, and the retardation function, h:

$$A_\infty\ddot{x}(t) + \int_{-\infty}^{\infty} h(t-\tau)\dot{x}(\tau)d\tau = f(t) \tag{2.19}$$

And the retardation function, $h(\tau)$, can be computed by a transform of the frequency-dependent added-mass and and damping:

$$h(\tau) = \frac{1}{2\pi}\int_{-\infty}^{\infty}[b(\omega) + i\omega a(\omega)]e^{i\omega t}d\omega \tag{2.20}$$

Where $a(\omega)$ and $b(\omega)$ represents the frequency dependent part of $A(\omega)$ and $B(\omega)$:

$$A(\omega) = a(\omega) + A_\infty \tag{2.21}$$

$$B(\omega) = b(\omega) + B_\infty \tag{2.22}$$

2.1.4 Dynamic Amplification Factor

Dynamic amplification factor (DAF) gives the ratio between static and dynamic response. The ratio for a damped linear system is given by the magnitude of critical damping ratio, ξ, and the frequency ratio, β. DAF for a damped linear system is found by use of the particular solution, and equals (Larsen, 2014):

$$DAF = |\frac{x_{max}}{x_{static}}| = \frac{1}{[(1-\beta^2)^2 + (2\xi\beta)^2]^{\frac{1}{2}}} \tag{2.23}$$

DAF for different values of critical damping ratios is presented in Figure 2.4. The figure gives information about two important aspects that should be accounted for when designing systems:

1. In resonance area the excitation load has a frequency close to natural frequency of the system, i.e. $\beta \approx 1$. In this area the dynamic effects are large and may cause large response on the system. Normally one wants to design the system such that the natural frequency is outside the load frequency. Large responses of the system due to resonance are then avoided.

2. How sensitive the system is to excitation loads at resonance is solely dependent on the critical damping ratio.

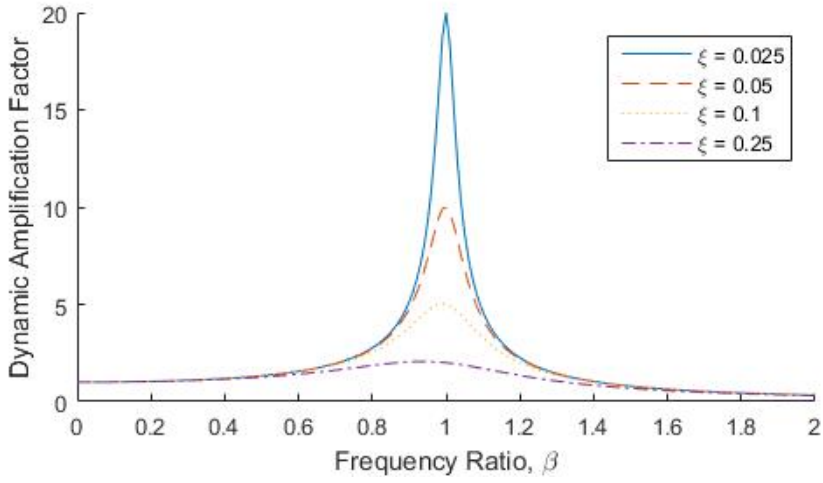

Figure 2.4: Dynamic amplification factor as a function of frequency ratio. Inspiration from Larsen (2014)

2.2 Hydrodynamic Forces

The hydrodynamic forces working on the system can be calculated based on potential flow theory. The problem is then solved for steady-state condition with oscillating wave forces in the frequency domain. The forces are later used in time-domain simulations via retardation functions, as described in section 2.1.3. There are three basic assumptions when solving the potential flow theory problem:

- Inviscid fluid
- Irrotational flow
- Incompressible fluid

Due to linearity, the superposition principle is valid for linear potential flow theory. The hydrodynamic force is divided in two; the diffraction problem and the radiation problem. Total hydrodynamical forces is taken as the sum of these contributions.

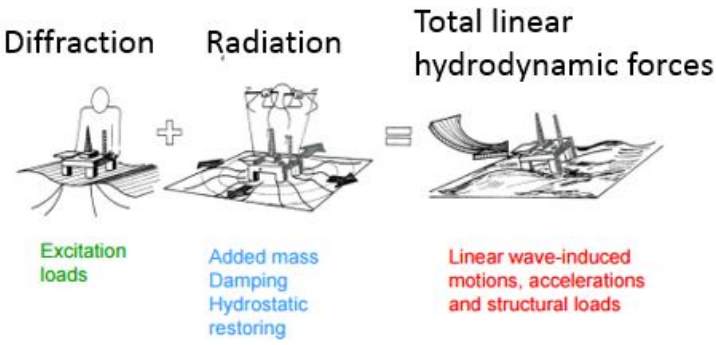

Figure 2.5: Illustration of radiation and diffraction problem (Faltinsen, 1990).

2.2.1 Diffraction Problem

For the diffraction problem the body is kept fixed and affected by incoming waves. The diffraction problem is further divided into two sub-problems in order to describe the excitation load:

Froude-Kriloff loads + Diffraction loads = Excitation loads

The Froude-Kriloff contribution comes by letting the waves penetrate the body as if it was not there, while the diffraction loads are found as the effect of the diffracted waves caused by the impermeability of the body. The Froude-Kriloff force is found by integrating the incident wave dynamic pressure over the mean wetted hull surface, while the diffraction force is found by integrating the diffraction dynamic pressure over the same surface (Greco, 2012).

2.2.2 Radiation Problem

The radiation problem means to solve for the hydrodynamical forces when the body is forced to oscillate with a frequency, ω, in all six degrees of freedom and with no incident waves. The forces found in the radiation problem is the added mass, damping and restoring force (as was given in equation (2.2)). Note that it is the linear damping contribution that is found by linear potential flow theory.

When the body is forced to oscillate, it will generate waves. It is due to the body's motion that added mass and damping forces are created. The geometry of the body is "forcing" the water particles in the surroundings to move, and this creates hydrodynamic forces. The restoring force is due to a variation in the hydrostatic pressure from the buoyancy when the body is oscillating.

The magnitude of added mass and damping depends upon geometry and oscillation frequency. An example illustration of added mass and damping for different frequencies are given in Figure 2.6. If the radiation problem is solved in the frequency domain, the retardation function (see section 2.1.3), makes it possible to use the values also in the time domain.

There is a relation between radiation and diffraction problem, and this is called the Haskind relation. Note that the Haskind relation makes it possible to use the radiation problem to solve the diffraction problem. This might be of use where the radiation problem is easier to solve than the diffraction problem, e.g. when using strip theory on slender structures.

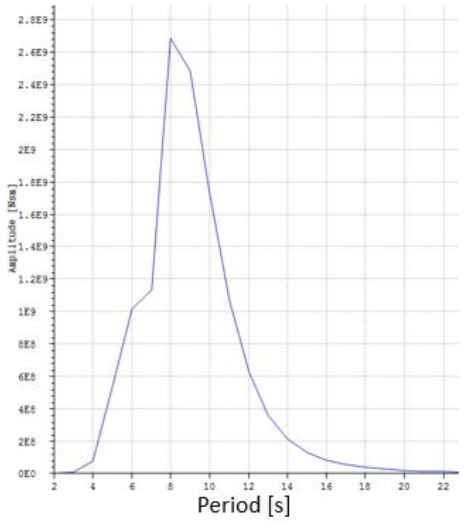

(a) Frequency dependent damping

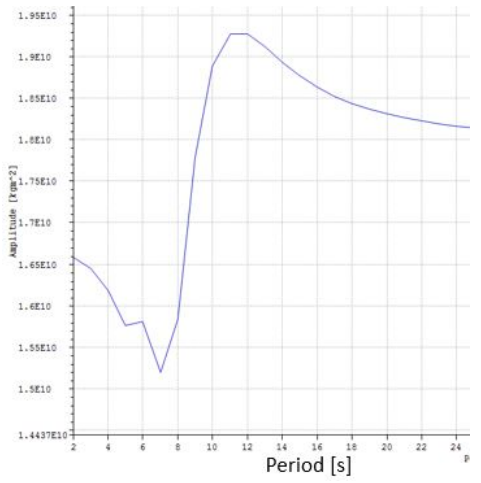

(b) Frequency dependent added mass

Figure 2.6: Illustration of a solution on damping and added mass in pitch-pitch motion from potential flow theory (by use of the software Wadam). Illustration represents values for Case 40.

2.2.3 Excitation Loads (second order)

Second order wave excitation forces are normally of lower magnitude than first order. Wave drift (mean), sum-frequency and difference-frequency forces are examples of second order excitation forces, where the two latest contributes with an oscillating force with a frequency different from first order excitations. For a floating offshore wind system (with relatively high natural period in pitch), the difference-frequency excitation force may excite the natural frequency in pitch, and hence cause large motions. Faltinsen (1990) gives the following formal expression for slow-drift excitation loads:

$$F_i^{SV} = \sum_{j=1}^{N}\sum_{k=1}^{N} \zeta_{Aj}\zeta_{Ak}[T_{jk}^{ic} \cdot cos[(\omega_k - \omega_j)t + (\epsilon_k - \epsilon_j)] + T_{jk}^{is} \cdot sin[(\omega_k - \omega_j)t + (\epsilon_k - \epsilon_j)]] \tag{2.24}$$

Where ζ_A is the wave amplitude, ω the wave frequency and ϵ the phase difference. T_{jk}^{ic} and T_{jk}^{is} are the second order transfer functions. To find the second order transfer functions, Newman's approximation is used:

$$T_{jk}^{ic} = T_{kj}^{ic} = 0.5(T_{jj}^{ic} + T_{kk}^{ic}) \tag{2.25}$$

$$T_{jk}^{is} = T_{kj}^{is} = 0 \tag{2.26}$$

The important advantage of using Newman's approximation is that the second order transfer functions can be found from the mean drift loads found by solving the first order velocity potential (Greco, 2012). The formula for slow drift excitation load is simplified by use of Newman's approximation, and becomes:

$$F_i^{SV} = \sum_{j=1}^{N}\sum_{k=1}^{N} \zeta_{Aj}\zeta_{Ak}[T_{jk}^{ic} cos[(\omega_k - \omega_j)t + (\epsilon_k - \epsilon_j)]] \tag{2.27}$$

2.3 Aerodynamic Forces

Aerodynamic forces are important for analyses where a wind turbine is included, giving both aerodynamic thrust due to drag forces, and making the system able to generate power due to lift forces ability to rotate the turbine. This section describes shortly basic theory for aerodynamic forces, and it is mainly based on lecture notes by Bachynski (2015). The section is divided in three subsections describing foil theory, blade element momentum theory and 3p effects.

2.3.1 Foil Theory

The basic principle of foil theory is that relative fluid velocity, in combination with circulation, provides a lift force normal to the relative velocity. The force is created by moving the foil, fluid passing the flow, or a combination of both. The shape of the foil, and it's angle of attack compared to the incoming flow, determines the magnitude of lifting force.

The forces on a two-dimensional foil section when used on a wind turbine blade, can be illustrated as in Figure 2.7. F_L is the lift force normal to incoming velocity, V_{rel}, while F_D is the drag force. p_N is the force normal to rotor plane and p_T the force tangential to the rotor plane. The angle ϕ accounts for both the angle of attack, α, and blade pitch angle.

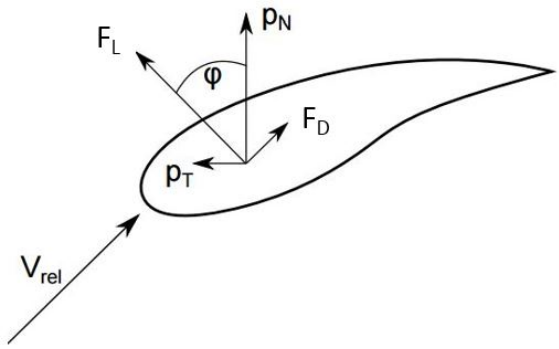

Figure 2.7: Illustration of forces on a two-dimensional foil section (Bachynski, 2015).

Lift and drag is normally determined by use of non-dimensional coefficients, given as C_L and C_D, respectively. The coefficients are given by use of fluid density (ρ), relative velocity (V_{rel}), chord length (c) and span of the airfoil (l) for a 2-D foil section.

$$C_L = \frac{\frac{F_L}{l}}{\frac{1}{2}\rho V_{rel}^2 c} \tag{2.28}$$

$$C_D = \frac{\frac{F_D}{l}}{\frac{1}{2}\rho V_{rel}^2 c} \tag{2.29}$$

2.3.2 Blade Element Momentum

Aerodynamic loads for the wind turbine can be calculated by use of blade element momentum (BEM) theory. This method estimates the loads by combining momentum theory for the rotor disk with foil theory.

Momentum theory is used in order to establish expressions for axial (a) and angular induction factor (a'). A more detailed description on how this is done can be found in Hansen (2015).

$$v_1 = v_0(1 - 2a) \tag{2.30}$$

$$a' = \frac{\psi}{2\Omega} \tag{2.31}$$

The axial induction factor gives a relation between inlet (v_0) and outlet velocity (v_1), as shown in Figure 2.8. The angular induction factor gives a relation between angular velocity imparted to the free stream (ψ) and the angular velocity of the rotor (Ω) for an ideal turbine with wake rotation.

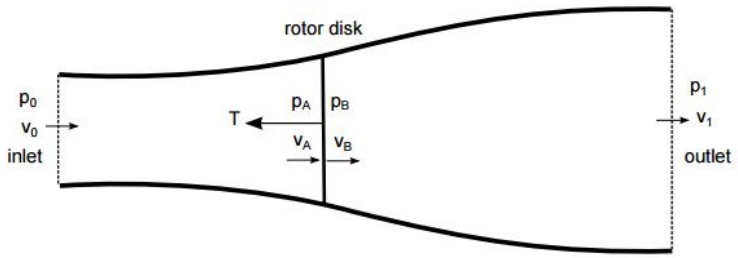

Figure 2.8: Actuator disk rotor model used in one dimensional momentum theory (Bachynski, 2015).

By combining momentum theory and foil theory, the induction factors can be obtained as:

$$a = \frac{1}{\frac{4sin^2(\phi)}{\sigma C_n} + 1} \tag{2.32}$$

$$a' = \frac{1}{\frac{4sin(\phi)cos(\phi)}{\sigma C_t} + 1} \tag{2.33}$$

Where C_n is the normal coefficient, C_t thrust coefficient and σ solidity ratio.

$$C_n = C_L cos(\phi) + C_D sin(\phi) \tag{2.34}$$

$$C_t = C_L sin(\phi) - C_D cos(\phi) \tag{2.35}$$

$$\sigma = \frac{bc}{2\pi r} \tag{2.36}$$

Here b is number of blades, c chord length and r radial distance. The induction factors are found by iteration in BEM. A typical solution procedure for BEM is given by Bachynski (2015) (quoted list):

1. Guess starting values for a and a'.
2. Calculate ϕ and consequently α, C_l and C_d.
3. Update a and a' using eq. (2.32) and (2.33).
4. Check for convergence within a given tolerance, if not, repeat (starting from the updated values).

In order to use BEM on a physical problem, some corrections are needed. Prandtl factor is used to account for tip and hub loss due to finite number of blades. Glauert correction factor is used in in order to make BEM valid also for large induction factors (if not used, BEM is only valid for a <0.5). The dynamic effects are included by use of dynamic wake and dynamic stall. A more detailed description on how the corrections are included in the calculations can be found in Appedix A of Marintek (2015a).

2.3.3 3p Effects

When the blades of the wind turbine rotate, out of plane loading appears with a frequency equal to the rotation frequency or three times the rotation frequency (if three blades are used). The loads with a frequency equal three times the rotation frequency are 3p effects, and due to a large number of cycles it may cause a significant fatigue load. A short description of important reasons for 3p effects are given in the current section.

Shaft Tilt and Yawed Flow

In order to maintain sufficient clearance between rotor blades and tower, the shaft is often tilted for upwind turbines. This is also the case for 10 MW DTU reference turbine, which has a shaft tilt angle equal to 5 degrees (Bak et al., 2013). The tilt angle gives variable relative wind speed on the foil. The drag and lift force vary with square of the wind speed, and will, due to a variable relative wind speed, vary depending on the azimuth angle. The azimuth angle describes the angular position of the blades. This variation in relative wind speed provides a variable out of plane bending moment with frequency equal blade passing frequency (3p).

Similar as for a shaft tilt angle will a yawed inflow for the wind cause variable wind speed dependent on the azimuth angle, and hence out of plane bending.

Wind Shear

Due to shear forces will the wind speed vary with vertical position (see also section 3.5.3). Rotating blades will then be exposed to variable incoming wind speeds, and hence variable force tangential to rotor plane. This out of plane bending moment has a frequency equal to 3p.

Tower Shadow

The tower geometry will block the wind and reduce the wind speed in regions both fore and aft of the tower. This leads to a lower drag force when the blade passes the tower structure, and hence a variation in the out of plane bending moment with frequency 3p. The effect of tower shadow is depending on the clearance between tower and blade structure.

For an upwind turbine, the tower influence on wind speed is calculated based on a potential flow model. The model is used to calculate influence factors which, when multiplied by the wind speed, gives the reduced wind speed in front of tower. A more detailed description on this can be found in Appendix A in Marintek (2015a).

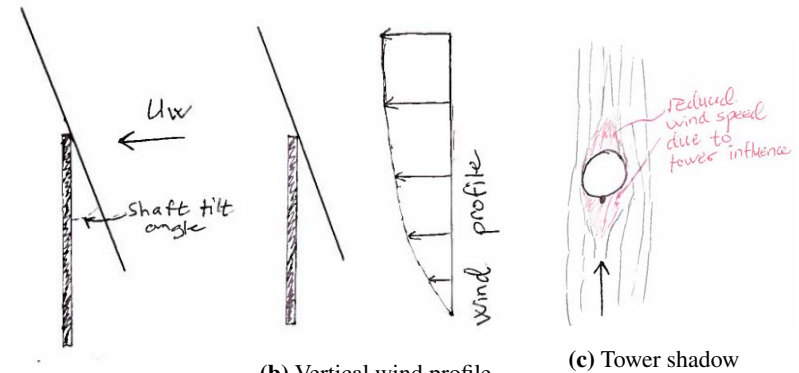

(a) Shaft tilt angle

(b) Vertical wind profile

(c) Tower shadow

Figure 2.9: Simple illustration of reasons for 3p effects.

2.4 Structural Forces

When calculating fatigue damage, one needs to know the internal forces on the structure when the system is exposed to aerodynamic and hydrodynamic forces. It is normal to divide the structure into several finite elements in order to solve the problem numerical, and this is called the finite element method (FEM).

The steel tower structure can be modelled by use of multiple beam elements. The elements may have different cross sectional properties, and they consist of two nodes located at the ends of the element. Each node has 3 translations and 3 rotational degrees of freedom, as opposite to a bar element which has only 3 translation degrees of freedom at each node.

Structural response due to external forces are calculated in each node by use of beam theory. The beam theory is based on the following assumptions (Marintek, 2015a) (quoted list):

- A plane section of the beam initially normal to the x-axis, remains plane and normal to the x-axis during deformations.
- Lateral contraction caused by axial elongation is neglected.
- The strain are small.
- Shear deformations due to lateral loading are neglected, but St. Venant torsion is accounted for.
- Coupling effects between torsion and bending are neglected. Thus, warping resistance and torsional stability problems are not considered.

A more detailed explanation on how the structural response is calculated can be found in chapter 2 in Marintek (2015a).

2.5 Catenary Equation

A semi-submersible floater is kept in position by use of mooring lines. Static analysis for a mooring line can be performed using the catenary equations. The catenary equation is based on the assumption of a horizontal sea bed with no friction, and where bending stiffness, dynamic effects in the line, line elasticity and forces from current are neglected. In the catenary equation mass provides horizontal restoring force due to geometric stiffness. A full outline of the method for catenary equation can be found in Chapter 8 in Faltinsen (1990), and the final three equations are presented below.

$$s = \frac{T_H}{w} sinh(\frac{w}{T_H}x) \tag{2.37}$$

$$z + h_z = \frac{T_H}{w}[cosh(\frac{w}{T_H}x) - 1] \tag{2.38}$$

$$T = T_H + wh + (w + \rho g A_{line})z \tag{2.39}$$

Where T is the line tension and s line length from touch down point to the point where T is found. T_H is horizontal tension at water plane level, h_z water depth, w weight per unit length in water and A_{line} cross sectional area of the line. An illustration of the problem is given in Figure 2.10.

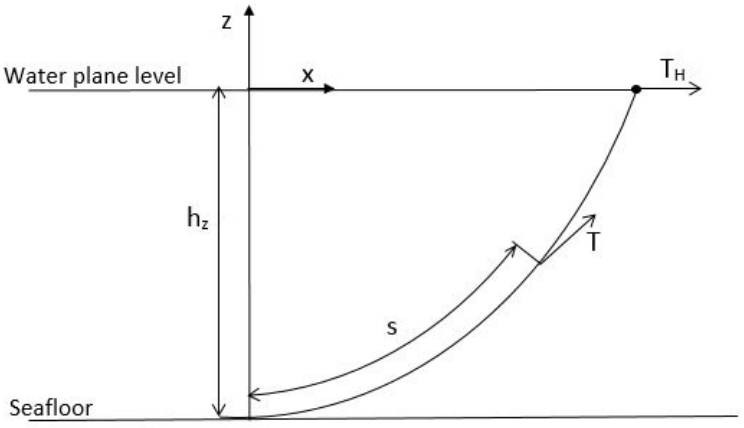

Figure 2.10: Mooring line with symbols (Faltinsen, 1990).

2.6 Processing of Results

In current section, background theory used when processing and evaluating the results are given. Filtering of data, switching from time domain to frequency domain and normal distribution have been used in order to process and present results in a proper way.

2.6.1 Filtering of Data

The basic principle behind filtering of data is that certain frequency bands are removed. One defines so-called cut-off frequencies, and these determine what frequencies in the time series that are to be removed. Three filters that are often used are listed below:

- Low pass filter; removes part of the time series which has a frequency higher than cut-off frequency.
- High pass filter; removes part of the time series which has a frequency lower than cut-off frequency.
- Band pass filter; removes part of the time series which has a frequency lower than low cut-off frequency and higher than high cut-off frequency.

The three methods are illustrated in Figure 2.11. Ideally one should remove all frequencies that are not wanted, and keep all frequencies that is wanted. Anyhow, in a real problem,

this is not possible, and frequencies close to the cut-off frequency may be both removed and kept. It is therefore important to chose a proper cut-off frequency. If one wants to keep frequencies under 0.2 Hz, and frequencies close to 0.2 Hz are important, it may be beneficial to set the cut-off frequency slightly higher than 0.2 Hz.

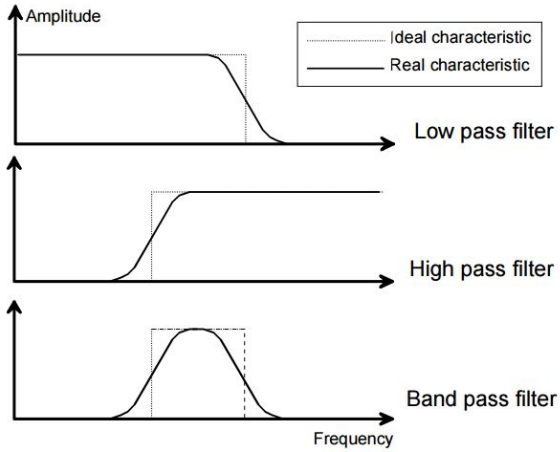

Figure 2.11: Illustration of different filtering options (Steen, 2014).

2.6.2 Switching from Time Domain to Frequency Domain

When performing a time-domain analysis, it may be of use to switch the results from time-domain to frequency domain in order to determine dominating frequencies. The time domain results can then be presented as a frequency spectrum.

One method to switch from time domain to frequency domain is by performing a Fourier transformation. Having a time series, $x(t)$, the frequency domain spectrum, $X(\omega)$, can be found the following way:

$$X(\omega) = \frac{1}{2\pi} \int_{-\infty}^{\infty} x(t) e^{-i\omega t} dt \tag{2.40}$$

It is normal to solve a Fourier transformation by use of a fast Fourier transformation (FFT) algorithm. A FFT algorithm solves the discrete Fourier transformation.

As an alternative to the Fourier transformation, an energy spectrum can be calculated based on the time series. The energy spectrum, S_{xx}, is found by:

$$S_{xx}(\omega) = \frac{1}{2\pi} \int_{-\infty}^{\infty} R_{xx}(\tau) e^{i\omega\tau} d\tau \tag{2.41}$$

Where $R_{xx}(\omega)$ is the autocorrelation function, which for a stationary process is defined as the expected value when multiplying two values of x with time difference τ:

$$R_{xx}(\tau) = E[x(t)x(t+\tau)] \tag{2.42}$$

2.6.3 Normal Distribution

It is often useful to present results by statistical functions. Normal (Gaussian) distribution is a continuous probability function. The probability is evenly distributed around a mean value, μ_Y. The mean value, together with standard deviation, σ_Y, determines the probability density function:

$$f_Y(y) = \frac{1}{\sqrt{2\pi}\sigma_Y} exp[-\frac{1}{2}(\frac{y-\mu_Y}{\sigma_Y})] \tag{2.43}$$

An illustration of a probability density function for a normal distributed process is given in Figure 2.12.

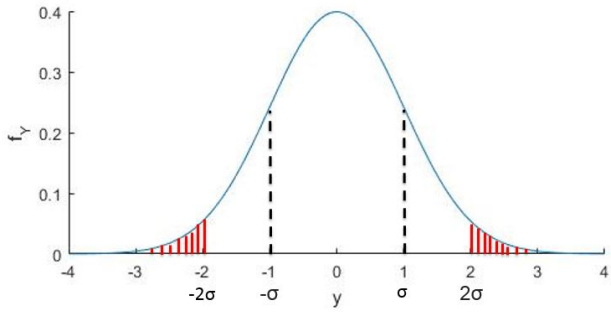

Figure 2.12: Example of a normal distribution with mean values equal to zero and standard deviation equal to one.

For a normal distributed process, one can find a confidence interval. A confidence interval defines a range of values which will happen with a certain probability. The probability is defined by a factor, Θ, that are multiplied with the standard deviation. The confidence interval is found as:

$$Y_p = [\mu_Y - \Theta_p\sigma_Y, \mu_Y + \Theta_p\sigma_Y] \tag{2.44}$$

A confidence interval of 95 % is normal to use, and for this interval Θ equals 1.96. A confidence interval of 95 % is given as the part of probability density function in Figure 2.12 that are not marked red. The probability for the process to be within the red areas are therefore equal to 5 %.

2.7 Decay Analysis

Important information such as natural period, added mass and damping (both linear and quadratic) can be found from a decay analysis. A decay analysis is performed by giving a specified force or moment on the system and release it. No environmental loads are applied, and the system will oscillate with its (damped) natural frequency.

When the model is released it will start to oscillate. This is illustrated in Figure 2.13 for a heave decay test.

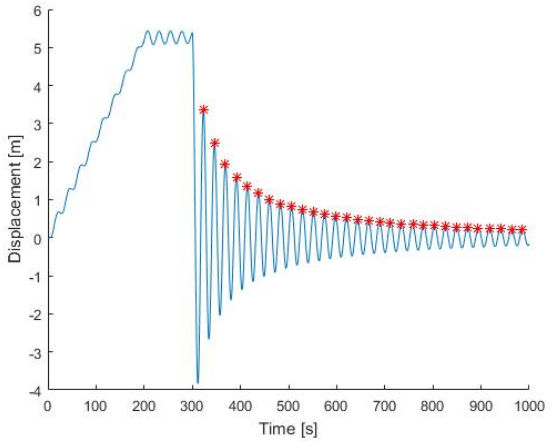

Figure 2.13: Illustration of a decay test in heave direction performed in the software SIMA.

Steen (2014) gives a description on how to use data from a decay test in order to find wanted parameters for a one-degree of freedom system with quadratic damping and time dependent equation of motion, as given in equation (2.45). Note that this is a similar equation of motion as in equation 2.2, but now also allowing for non-linear damping effects. Linear stiffness is assumed. The theory in this section is based upon his work.

$$m\ddot{x} + B_1\dot{x} + B_2\dot{x}|\dot{x}| + Cx = 0 \tag{2.45}$$

Here m represent total mass contribution, i.e. sum of mass and added mass. In order to find the damping coefficients, the equation of motion in divided by the mass contribution, m. Further, equivalent linearization is applied, and the equivalent linear term is determined from the requirement of equal damping energy pr. cycle. The equation of motion then becomes:

$$\ddot{x} + p_{EQ}\dot{x} + p_3 x = 0 \tag{2.46}$$

where

$$p_{EQ} = p_1 + \frac{8}{3\pi}\omega x_0 p_2 \tag{2.47}$$

In eq. (2.47), p_1 and p_2 are the linear and quadratic damping term divided by the mass contribution, respectively. x_0 is the motion amplitude and ω is the oscillation frequency. The logarithmic decrement can then be found for each period by taking the logarithmic value of the ratio between two amplitudes located one natural period apart:

$$\Lambda = ln(\frac{x_i}{x_{i+1}}) \tag{2.48}$$

The damping ratio, ξ, which is defined as the ratio between actual and critical damping, can then be found for each measured period. For low damping ratios (typically $\xi < 0.2$) the formula is:

$$\xi = \frac{\Lambda}{2\pi} \tag{2.49}$$

The damping ratio, ξ, can then be plotted together with mean amplitude for the corresponding period. A linearization is performed, and the linear damping ratio is the intersection with the abscissa, while the quadratic damping ratio is taken equal to the slope. An example corresponding to the heave decay test shown in Figure 2.13, is given in Figure 2.14:

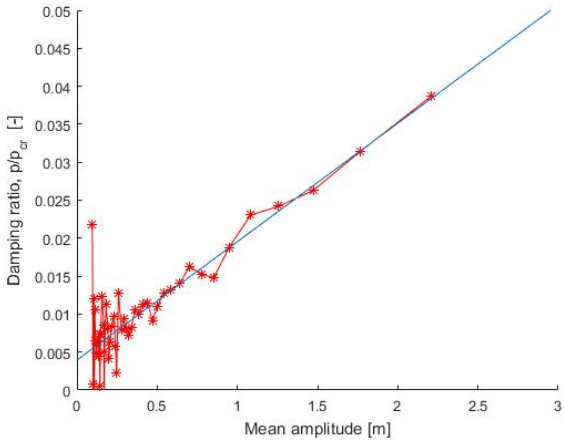

Figure 2.14: Measured damping from a heave decay test.

2.8 Fatigue

Fatigue is damage due to repetitive stress cycles over time. Each stress cycle (if it is above fatigue limit) contributes to a damage, and the sum of all cycles may in time cause fracture. DNV (2013) states that 20 years should normally be used as a minimum requirement for fatigue lifetime of offshore wind components.

2.8.1 Cycle Counting

In order to estimate total damage, one needs to extract cycles from a load history into a total number of cycles with a given stress range. A normal counting methodology is the so-called rainflow counting method.

Rainflow Counting

Rainflow counting is often used as a common name for several counting methods, such as range-pair counting, ordered overall range counting etc. The different methods give either identical or similar results (Berge, 2006). A short description of the principle behind rainflow counting will be given in this section.

The Japanese researchers Matsuishi and Endo developed the rainflow method in 1968, and the name ”rainflow” was inspired by flow of rain falling on a pagoda roof (Lee et al., 2012). Lee et al. (2012) summarize the rainflow cycle counting in the following way (quoted list):

1. Rotate the loading history 90 degrees such that the time axis is vertically downward and the load time history resembles a pagoda roof.
2. Imagine a flow of rain starting at each successive extreme point.
3. Define a loading reversal (half-cycle) by allowing each rainflow to continue to drip down these roofs until:
   (a) It falls opposite a larger maximum (or smaller minimum) point.
   (b) It meets a previous flow falling from above.
   (c) It falls below the roof.
4. Identify each hysteris loop (cycle) by pairing up the same counted reversals.

An illustration of the method is given for a load cycle history in Figure 2.15. Note that load cycle history is taken by drawing a straight line between maxima and minima in the time history for stress.

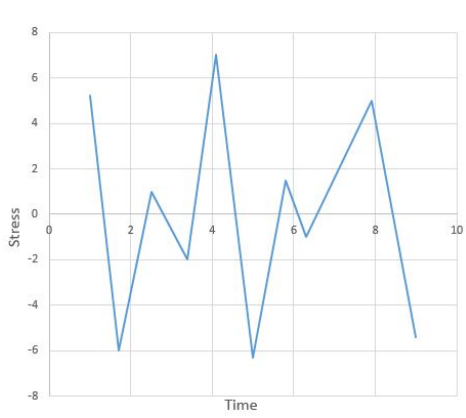

(a) Load cycle history

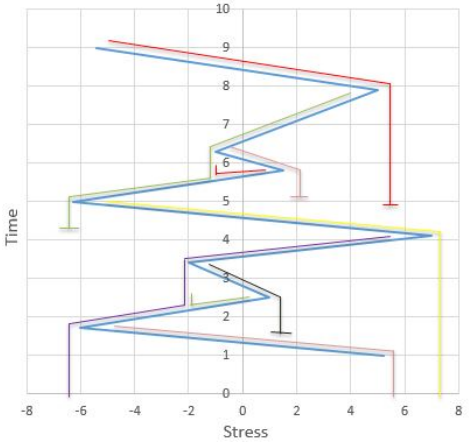

(b) Illustration of rainflow counting technique

Figure 2.15: Illustration on how rainflow counting technique is used on a load cycle. Inspired by (Lee et al., 2012).

2.8.2 Miners Rule

As mentioned, fatigue is defined as damage due to repetitive stress cycles. To estimate the total damage for a large number of stress cycles, the Miner sum can be used. The Miner sum is presented in equation (2.50).

$$D = \sum_i \frac{n_i}{N_i} \tag{2.50}$$

Where D is the total damage. If D is equal to 1.0, failure will occur. The time duration for the damage D varies depending on the specific case. In this report the damage will always be given as a yearly fatigue damage. n_i is the number of cycles with stress amplitude S_i found by use of rainflow counting. N_i is the total number of cycles with stress range S_i to failure, and is found by use of a so-called S-N curve.

S-N Curves

S-N curves are developed by regulation companies (such as DNV GL), and they are based on experimental fatigue tests. The probability of survival when using a S-N curve to estimate number of cycles to failure is 97.7 $\%$ (DNV, 2010). There are several types of S-N curves, and which one to use depends on geometry, technical parameters (such as how the weld is created) and load direction relative to the weld. The curve is described by equation (2.51).

$$log(N_i) = log(aa) - m_s \cdot log(S_i[\frac{t}{t_{ref}}]^k) \tag{2.51}$$

Where m_s is the negative inverse slope, $log(aa)$ the interception of $log(N)$ axis, k the thickness exponent and t_{ref} the reference thickness. An example on how to find number of cycles to failure, N_i, for a stress range S_i by use of a S-N curve is given in Figure 2.16.

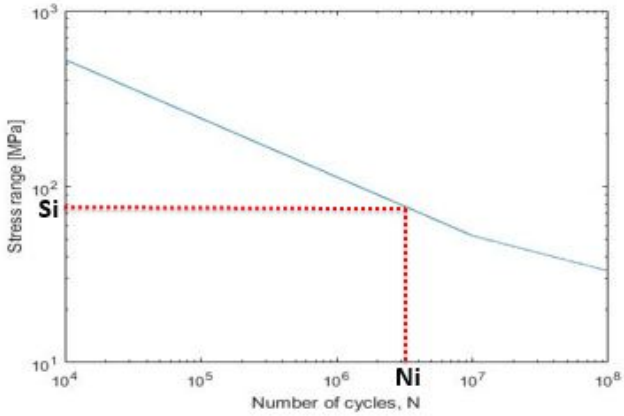

Figure 2.16: Example on how to find numbers of cycles to failure by use of a S-N curve. The curve is based on data for S-N curve D in DNV (2010).

2.8.3 Stress Concentration Factors

Stress concentration factor (SCF) is the ratio between the hot-spot stress and the nominal stress, where hot-spot stress is a local increase in stress due to weld geometry. DNV (2010) states that when using S-N curve for a hollow section one must include SCF to allow for any thickness change and for fabrication tolerances.

Estimates for the SCF is normally found by finite element analysis or by use of parametric formulas in the design process. The latter method is more time-efficient, and parametric formulas can be found in regulations. DNV (2010) provides following parametric formula for the SCF:

$$SCF = 1 + \frac{6(\delta_t + \delta_m - \delta_0)}{t} \cdot \frac{1}{1 + (\frac{T}{t})^q} e^{-u} \tag{2.52}$$

where

$$u = \frac{1.82L}{\sqrt{dt}} \cdot \frac{1}{1 + (\frac{T}{t})^q} \tag{2.53}$$

$$q = 1.5 - \frac{1}{log(\frac{d}{t})} + \frac{3}{[log(\frac{d}{t})]^2} \tag{2.54}$$

$\delta_0 = 0.1t$ is misalignment inherent in the SN-data provided in regulations. Illustrations of the variables are given below.

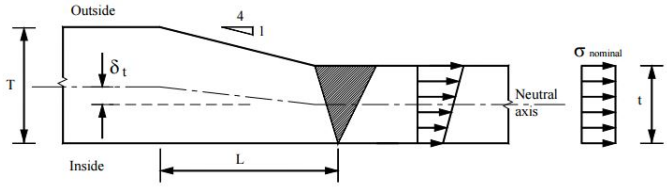

Figure 2.17: Illustration of variables (DNV, 2010).

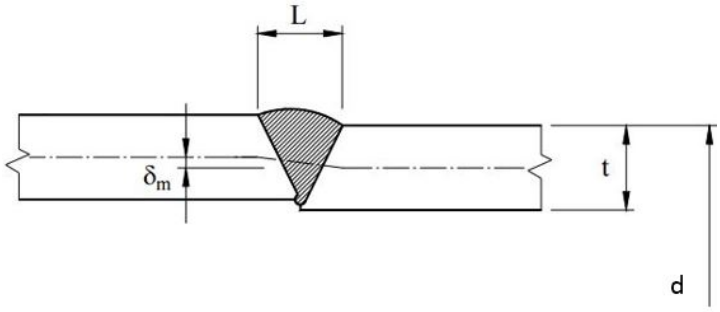

Figure 2.18: Illustration of variables (DNV, 2010).

Chapter 3

Methodology

Current chapter gives a relative short, but to the point, description on how the results have been established. It describes methods that are used in order to evaluate the effect of an increased transition point between concrete and steel on fatigue lifetime.

The chapter will describe relevant software, and how the set-up for the numerical model has been done. Also the environmental conditions are described. Finally some specified conditions when running the analyses are given. During the chapter, assumptions and simplifications will be pointed out.

3.1 Discussion of Method

It was early decided to use numerical tools in order to solve the problem. It could have been an option to study the effect of increased elevation between concrete and steel by use of experimental methods, but it has some drawbacks; high cost, scaling issues and difficulties when simulating wind environment. It could have been beneficiary to use experimental methods on some parts of the project, such as determining viscous forces, but it was concluded not worth the cost.

When using numerical tools to perform coupled dynamic analysis, it is a question whether to use time domain simulations or frequency domain simulations. The theory behind the two methods was described in section 2.1.2 and section 2.1.1.

Time domain simulations can include non-linear effects, while frequency domain assumes that both load and response is a harmonic oscillation. Examples of non-linear effects are quadratic damping and aerodynamic thrust force. The main drawback with time domain simulations is that they are less computationally efficient than frequency domain. Each simulation requires a significant computational time. If one want to establish sta-

tistical distributions, such as maximum values, several runs with variable seeds must be performed.

Anyhow, the time domain simulation method was chosen for the analysis. It is ability to include non-linear loads in a coupled dynamic analysis that was the main reason. It was also found that the main drawback, computational time, was within acceptable limits.

Kvittem and Moan (2015) published a paper on the subject frequency versus time domain fatigue analysis of a semi-submersible wind turbine tower. For calculations with combined wind and wave, the relative error between frequency and time domain analysis in fatigue damage was 8-50 %, dependent on the environmental conditions. Knowing that time domain is the most accurate method, this supports the choice of using time domain simulations to estimate the fatigue.

3.2 Software

Results are obtained by use of several software. An illustration of the workflow between software is provided in Figure 3.1, and a short description of important software is given below. Note that the candidate has performed all analyses himself (except creating surface panel models in GeniE).

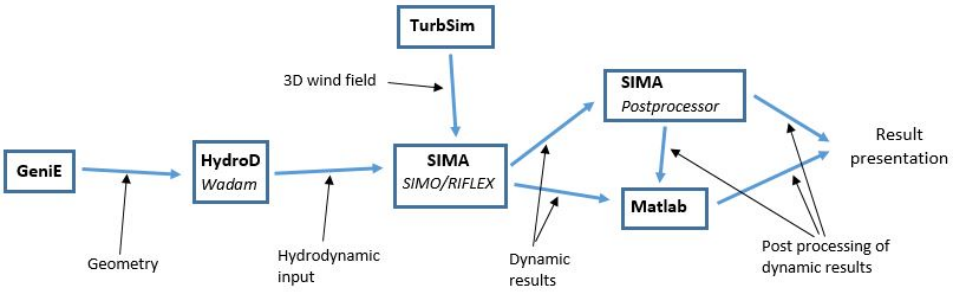

Figure 3.1: Workflow between software. Italics represent modules in the main software.

HydroD

HydroD is a hydrodynamical tool developed by DNV. It is part of the SESAM-package, and is an "application for computation of hydrostatics and stability, wave loads and motion response for ships and offshore structures" (DNV, 2011). Wadam is a module in HydroD, and it is able to solve wave load calculations in the frequency domain by use of potential theory.

TurbSim

TurbSim is a stochastic, full-field, turbulent-wind simulator developed by NREL. From user-defined input files (see Appendix C), it creates time series of three-component wind-speed vectors numerically by use of a statistical model (Jonkmann and Kilcher, 2012). The output files are used in SIMA to simulate the wind environment.

SIMA

SIMA is a simulation and analysis tool developed by Marintek. It is well suited to simulate and analyse marine operations (such as fatigue on a floating offshore wind concept). The software can perform non-linear time domain analysis. Environmental loads from wind, waves and current can be included. The software is based on several submodules.

SIMO is a submodule in the software SIMA, and it is a computer program for simulation of motions and station-keeping behaviour of complex systems of floating units (Marintek, 2015b).

RIFLEX is also a submodule in the software SIMA. It is well suited to analyse structural response on flexible risers or other slender structures. It is possible to run a coupled RIFLEX/SIMO analysis in SIMA in order to simulate both hydrodynamic and structural forces/response.

SIMA has an own module for post-processing results from its submodules (such as SIMO and RIFLEX).

Matlab

Matlab is a numerical programming tool from MathWorks. It is well suited for performing larger calculations and visualising results.

3.3 Coordinate System and Floater Orientation

The coordinate system used when modelling in SIMA is shown in Figure 3.2. Origo is located in still water level, with z-axis pointing upwards. Environmental loads in SIMA is given a heading. The direction of the heading relative the the floater is shown in Figure 3.2.

In this report, the heading of environmental loads is described by their propagation direction. If wind propagates in N direction, this means that it is coming from S and going towards N. The largest probability of occurence is environments propagating in NE direction (Gómez et al., 2015), and this will be further described in section 3.5.

One wanted to locate the system such that the environment with largest probability propagated in the direction of a mooring line. The SIMA model, as shown in Figure 3.2, has

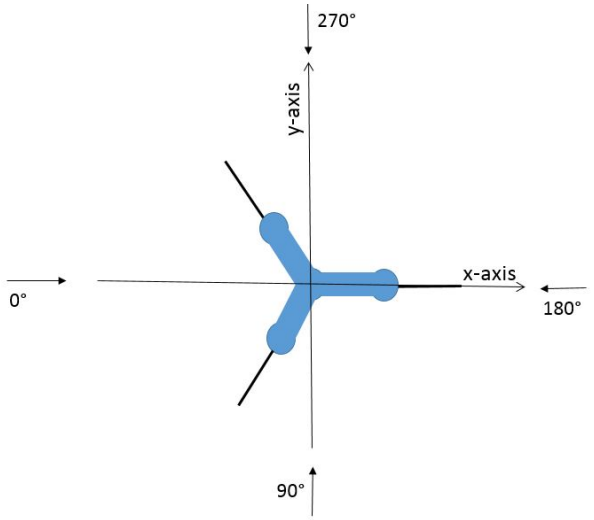

Figure 3.2: Coordinate system used for modelling in SIMA.

one line in the true south-west direction, as shown in Figure 3.3. Practically this means that environmental input to SIMA are modified in order to simulate forces with correct propagation direction when the model is oriented with one line in true SW direction.

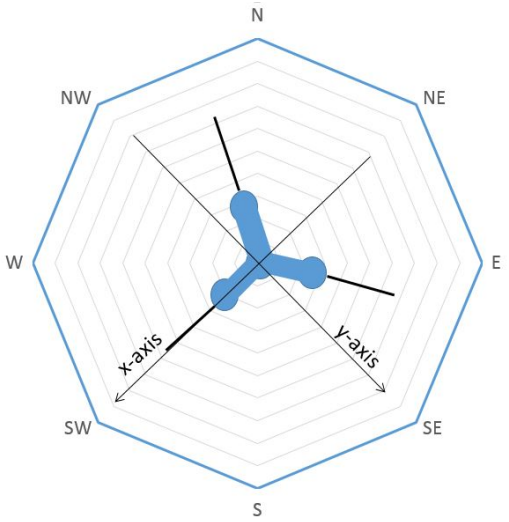

Figure 3.3: Orientation of the system compared to true headings for given location.

3.4 Set-up for Model

In this section, a description on how the model is established is given. The model is built as a coupled RIFLEX/SIMO model. Description of model set-up is divided in three parts; floater, tower and wind turbine. An illustration of a finished model is given in Figure 3.9.

3.4.1 Floater Unit

The floater unit is modelled in SIMO. Hydrodynamic properties such as added mass, linear damping and excitation forces are imported from Wadam calculations in the frequency domain. Retardation functions, also calculated by Wadam, are then used in order to use the coefficients in time domain analysis (see section 2.1.3 for theory). Frequency dependent added mass and damping are given in Appendix E.

Updating Coefficients When Going from Wadam to SIMA

In Wadam the calculations are performed with the correct total mass in order to find hydrodynamic coefficients. When importing values from Wadam to SIMA, the floater is given values from the run in Wadam. In SIMA, the mooring system, tower and turbine will be modelled later on, and then also contribute with a mass. Note that the tower is here defined as all parts modelled in RIFLEX with a mass, i.e. both flexible part of concrete shaft and steel tower (see also section 3.4.2). Properties affected by the mass must hence be updated in SIMA for the floater.

The total mass of the floater is modified by subtracting the mass of wind turbine (WT) system, tower and the effective mass of the mooring system (equation (3.1)). By the effective mass of the mooring system it is meant the mass corresponding to the vertical force, i.e. buoyancy is accounted for. The centre of gravity (CoG) for the floater is set accordning to mass distribution for the floater, and not for the total system.

$$M_{floater} = M_{total} - M_{tower} - M_{WT} - M_{mooring_{eff}} \tag{3.1}$$

SIMO takes care of hydrostatic aspects in a SIMO/RIFLEX computation. For the software to understand that the buoyancy is larger than the floater mass and mooring force given in SIMO, a specified force equal to the mass of RIFLEX parts is defined. By RIFLEX parts it is meant the parts modelled in RILFEX, i.e. tower and wind turbine.

The mass moment of inertia in pitch and roll for the floater is found by use of parallel axis theorem. Knowing the mass moment of inertia for the total system around origo, I_0, the mass moment of inertia around origo for the floater ($I_{0_{floater}}$) is found the following way:

$$I_{0_{floater}} = I_{0_{total}} - z^2_{tower} M_{tower} - I_{tower} - z^2_{WT} M_{WT} - I_{WT} \tag{3.2}$$

Where z_{tower} is the vertical distance between origo and CoG for the tower, and I_{tower} is the mass moment of inertia for the tower around its own CoG. Similar applies to z_{WT} and I_{WT}. Note that due to symmetry, this formula is valid for both roll and pitch moment. If further assuming that the contribution from tower and wind turbine around its own centre of gravity (CoG) is small compared to other contributions, the mass moment of intertia around origo for the floater is estimated the folloing way:

$$I_{0_{floater}} \approx I_{0_{total}} - z_{tower}^2 M_{tower} - z_{WT}^2 M_{WT} \tag{3.3}$$

Also the hydrostatic stiffness coefficients in roll and pitch are modified. For these coefficients, one needs to account for the fact that floater buoyancy is taken larger than the mass in SIMO. The reduction of the stiffness in roll and pitch due to RIFLEX parts is included later on. The formula for hydrostatic stiffness coefficients in SIMO is taken as:

$$C_{44} = \rho g V GM = \rho \cdot g \cdot V \cdot KB + I_{xx_{WP}} \cdot \rho \cdot g - KG_{floater} \cdot M_{floater} \cdot g \tag{3.4}$$

Where C_{44} is the stiffness in roll direction, GM the metacentric height, g is the gravity constant, $I_{xx_{WP}}$ area of moment around x-axis in water plane, KB vertical distance between base line and centre of buoyancy and $KG_{floater}$ the vertical distance between base line and CoG for floater.

Modified Additional Damping Term

In addition to the coefficients mentioned above, is the additional damping term modified for Case 20 and Case 40. This value is calculated in Wadam, and is originally added in order to avoid negative damping frequencies after cut-off frequency when using the retardation function. It should normally only have a small impact on the damping. When performing decay tests for Case 20 and Case 40 this value was found to be much larger than expected in sway and surge. This is illustrated in Figure 3.4 by comparing decay tests in surge direction for Case 0 and Case 40. It is seen that for Case 40 the system damped out quickly.

Due to this, the additional damping coefficients for Case 20 and Case 40 in surge and sway are modified, and taken equal to the coefficients for Case 0. The system will then damp out slower, and this is also supported by comparing the decay tests performed for a similar design in Xu (2015).

From Figure 3.4, it is seen that Case 40 has a larger offset when it is released. Knowing that the two designs are similar, and with a similar stiffness in surge, it is expected that this offset difference would be small if the system had achieved equilibrium. A longer time duration for the constant force is needed to achieve equilibrium, but it would take longer computational time, and it should not have any influence on the results from decay tests.

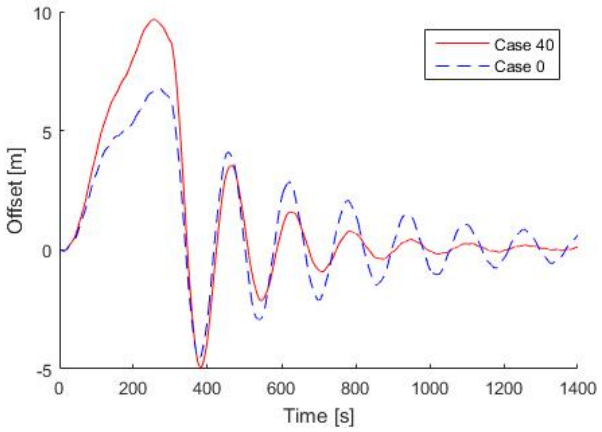

Figure 3.4: Decay test surge direction for Case 0 and Case 40. Decay tests were done before additional damping coefficient for Case 40 was modified.

Mooring System

The mooring system is modelled by the so-called shooting method in SIMO. Each line is divided into 50 segments, and iteration on boundary conditions at one end is performed in order to satisfy specified boundary conditions at the other (Marintek, 2015b). The method is a quasi-static mooring analysis. In quasi-static mooring analysis, mooring forces are calculated statically, and dynamic load effects are added by use of a dynamic amplification factor (ref. section 2.1.4). The static solution is found by use of catenary equations (ref. section 2.5).

The mooring system consists of three lines mounted on the columns. Fastening points for the lines are presented in Table 3.1. Line type is taken as 147 mm GL-R4s studless chain common link, and technical data are collected from Vicinay (2016). Weight in water is 3689 N/m and weight in air equals 4240 N/m.

Table 3.1: Fastening points on body for mooring lines. Same body points are used for all three cases.

Line	x	y	z
1	44.0	0.0	6.95
2	-22.0	38.11	6.95
3	-22.0	-38.11	6.95

Input data was given as 80 metric tons vertical force (on each line) with a length equal to 600 meters. Pretension for each line was calculated by use of catenary equations, and found to be 1007 kN.

Viscous Forces

Only linear damping is included when importing hydrodynamic coefficients from Wadam to SIMO. The quadratic damping due to viscous forces must therefore be included by use of drag coefficients.

For most environmental cases, the KC number for the columns are low. The KC number is given as:

$$KC = \frac{U_M T_W}{d} \tag{3.5}$$

Where U_M is maximum particle velocity, T_W is the wave period and d the diameter. Bearman et al. (1985) states that for a circular cylinder with low KC-numbers (KC$<$10), the drag coefficient equal 0.2 times the KC number: $C_D = KC \cdot 0.2$. The drag coefficient for columns and shaft below still water level are therefore taken equal to 0.2.

For the three pontoons binding the columns to the shaft, the drag coefficient was taken equal to the coefficient for a rectangular 2D geometry with similar breadth to height ratio. The coefficient was found to be $C_D = 2.5$ in vertical direction and $C_D = 1.6$ in horizontal direction (Blevins, 1992).

The effect of viscous forces will be further discussed in section 4.2.2.

3.4.2 Tower Structure

The tower structure is modelled in RIFLEX by use of beam elements with defined cross-sectional properties. The RIFLEX model is connected to the SIMO model by use of a master-slave connection. A node in bottom part of the steel tower is defined as slave, and a point at the floater in still water level is defined as master. They are rigidly connected, and the slave node follows the motions of its master node.

Steel Tower

The geometry of the steel tower was given by Dr.techn. Olav Olsen AS. The three different cases have a similar tower, but Case 0 has a lower outer radius compared to Case 20 and Case 40 when comparing at the same level above baseline. Note that the hub height is unchanged, i.e. the steel tower length is decreased with the same value as the concrete shaft length is increased. Tower specification is given in Appendix A, and a comparison of the three cases for both outer radius and bending stiffness is given in Figure 3.5.

The steel tower is modelled by use of 26 beam elements, where each element is given a cross sectional property. The elasticity modulus is set equal 206 GPa for steel.

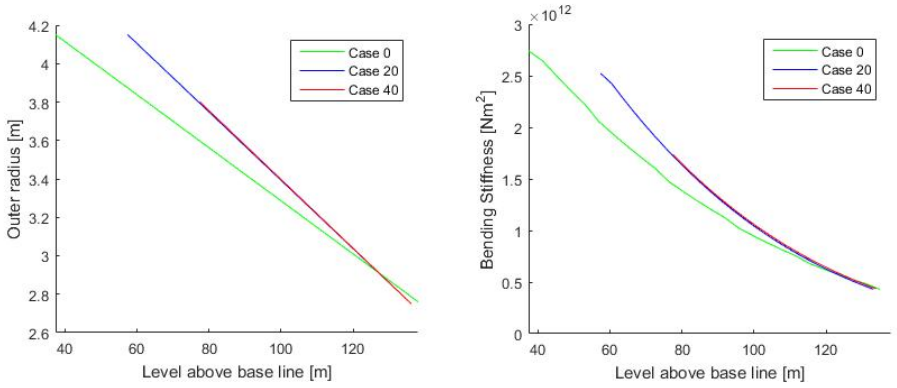

(a) Outer radius **(b)** Bending stiffness

Figure 3.5: Illustration of bending stiffness and outer radius for steel towers.

Flexibility of Concrete Shaft

The flexibility of the concrete shaft is modelled from the point where cone shape of the shaft ends, and up to the transition between concrete and steel. Below this level the floater is assumed to be rigid. This is illustrated in Figure 3.6. The flexibility was taken based on the thickness of the shaft. The modulus of elasticity was taken equal to 30 GPa and the density equal to 2275 $\frac{kg}{m^3}$ for concrete.

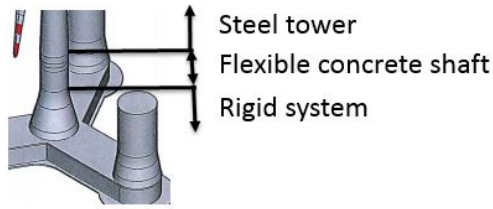

Figure 3.6: Illustration of modelling of concrete shaft flexibility (Landbø, 2016b).

Structural Damping

The structural damping is defined by use of Rayleigh formulation for both steel and concrete. Only flexible part of the concrete shaft is given a structural damping (see section 3.4.2). Rayleigh damping is defined as:

$$B_{Rayleigh} = a_1 M + a_2 C \tag{3.6}$$

The damping is assumed to be stiffness proportional with a factor of 0.007:

$$B_{Rayleigh} = a_2 C = 0.007 \cdot C \tag{3.7}$$

The relation between Rayleigh stiffness coefficient and critical damping for a system, which has stiffness proportional damping only, is:

$$\xi_i = \frac{1}{2} a_2 \omega_i \tag{3.8}$$

Where ω_i is the frequency of interest given in rad/s.

Drag Forces

Drag forces on both the steel tower and concrete shaft are modelled by use of drag coefficients. The drag coefficient is depending on the Reynolds number and the shape of the structure. The Reynolds number is defined as:

$$R_e = \frac{U_w d}{\nu} \tag{3.9}$$

If using a kinematic viscosity for dry air in 10 degrees ($\nu = 1.41 \cdot 10^{-5}$ (DNV, 2014)), wind speed (U_w) between 5 m/s and 25 m/s and a diameter (d) between 8.25 and 5.55 metre, the Reynolds number will vary between approximately $1.4 \cdot 10^7$ and $2.0 \cdot 10^6$. This means that the flow regime will be in both the subcritical and transcritical range.

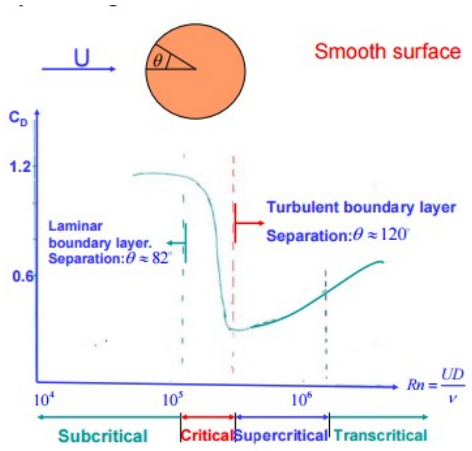

Figure 3.7: Drag coefficient for a smooth 2D cylinder (Greco, 2012). Note that the angle θ is not similar as used elsewhere in the report.

DNV (2014) states that one should account for the fact that the cylinder has finite length. A correction factor, κ, is found to be approximately 0.85 if using a length on the tower

equal to 100 m and a mean diameter equal to 6.5 m. The drag coefficients for finite tower in Table 3.2 are implemented in SIMA, and the software use interpolation between these values of Reynolds number to find the needed drag coefficient (and hence drag force).

Table 3.2: Drag coefficients tower.

R_n	C_D (infinite tower)	C_D (finite tower)
0	0.5	0.43
$3 \cdot 10^5$	0.35	0.3
10^6	0.5	0.43
$5 \cdot 10^6$	0.6	0.51
10^7	0.7	0.6
$5 \cdot 10^7$	0.7	0.6

3.4.3 Wind Turbine

The wind turbine is taken as the 10 MW DTU reference turbine, as described in section 1.1.1. This wind turbine is pre-modelled by the developer in a SIMA example, where the properties are taken according to Bak et al. (2013).

The wind turbine is an upwind type, meaning that it is facing the wind. The wind turbine is defined to rotate according to wind for the fatigue analysis, i.e. always facing the incoming wind.

In parked condition some problems occured when using BEM in SIMA. The blades vibrated with a high frequency, causing a large fatigue damage. This problem was solved by avoiding the use of BEM in parked condition, i.e. not calculating induction factors. Lift and drag forces on the blades were still calculated, and the blades was manually pitched in order to minimize the aerodynamic thrust in parked condition.

Control System

The control system used is based on 10 MW DTU reference turbine, which is pre-modelled in SIMA. 10 MW DTU reference turbine is a bottom fixed concept, and the control system would not necessarily be stable in rated condition for a floating concept due to horizontal motions. Some modifications on the proportional integral (PI) pitch angle control of the rotor speed is needed.

Jonkman et al. (2009) gives the following equation of motion for the rotor-speed error, ϕ_{rs}:

$$
\begin{aligned}
&(I_{Drivetrain} + \frac{1}{\Omega_0}(-\frac{\partial P}{\partial \theta})N_{gear}K_D) \cdot \ddot{\phi_{rs}} \\
&+[\frac{1}{\Omega_0}(-\frac{\partial P}{\partial \theta})N_{gear}K_P - \frac{P_0}{\Omega_0^2}] \cdot \dot{\phi_{rs}} \\
&+[\frac{1}{\Omega_0}(-\frac{\partial P}{\partial \theta})N_{gear}K_I] \cdot \phi_{rs} = 0
\end{aligned} \tag{3.10}
$$

Where $I_{Drivetrain}$ is the drivetrain inertia cast to low-speed shaft, Ω_0 rated low-speed shaft rotational speed, $\frac{\partial P}{\partial \theta}$ is the sensitivity of aerodynamic power to the rotor-collective blade-pitch angle and N_{gear} is the high-speed to low-speed gearbox ratio. K_P, K_I and K_D are the blade-pitch controller proportional, integral and derivative gains, respectively.

Further the derivative gain is neglected and the negative damping term is ignored, as recommended by Hansen et al. (2005). This gives the following formulas for the blade-pitch controller proportional and integral:

$$K_P = \frac{2I_{Drivetrain}\Omega_0\xi_{\phi_{rs}}\omega_{\phi_{rs}n}}{N_{gear}(-\frac{\partial P}{\partial \theta})} \tag{3.11}$$

$$K_I = \frac{I_{Drivetrain}\Omega_0\omega_{\phi_{rs}n}^2}{N_{gear}(-\frac{\partial P}{\partial \theta})} \tag{3.12}$$

Where $\omega_{\phi_{rs}n}$ is the natural frequency of the rotor-speed error, while $\xi_{\phi_{rs}}$ is the damping ratio. To make the control system stable, the coefficients for the blade-pitch controller proportional and integral is modified by changing the natural frequency. The natural frequency equals 0.06 Hz for the full load controller for 10 MW DTU reference turbine (Bak et al., 2013). The blade-pitch controller proportional and integral is changed according to a decrease in natural frequency from 0.06 Hz to 0.02 Hz, which is lower than natural frequency in pitch for the system.

The effect of changing the natural frequency is seen by performing a decay test in pitch where a constant wind of 15 m/s is included (see Figure 3.8). The system is given a time-dependent moment until 300 seconds, and then released. The original control system provides a negative aerodynamic damping, and the total damping from hydrodynamic and aerodynamic is eventually zero, even if the system oscillates. The modified control system provides a larger damping making the system stable, and the pitch motion dies out eventually.

The modified control system is not optimal, and a it is recommended to investigate how to further optimize the control system for the OO Star 10 MW design. Anyhow, the modified system is stable when the turbine is mounted on a floater, and is better to use than the original control system that is designed for bottom fixed turbines.

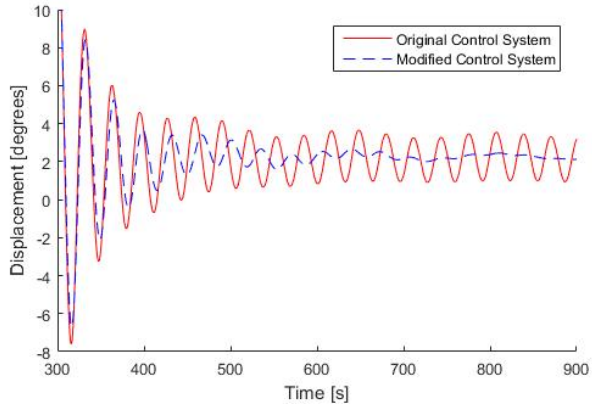

Figure 3.8: Decay test with with constant wind included.

An illustration on the model set-up is given in Figure 3.9. In this figure, both floater, tower and wind turbine is illustrated, and it shows the finished SIMA model for Case 0.

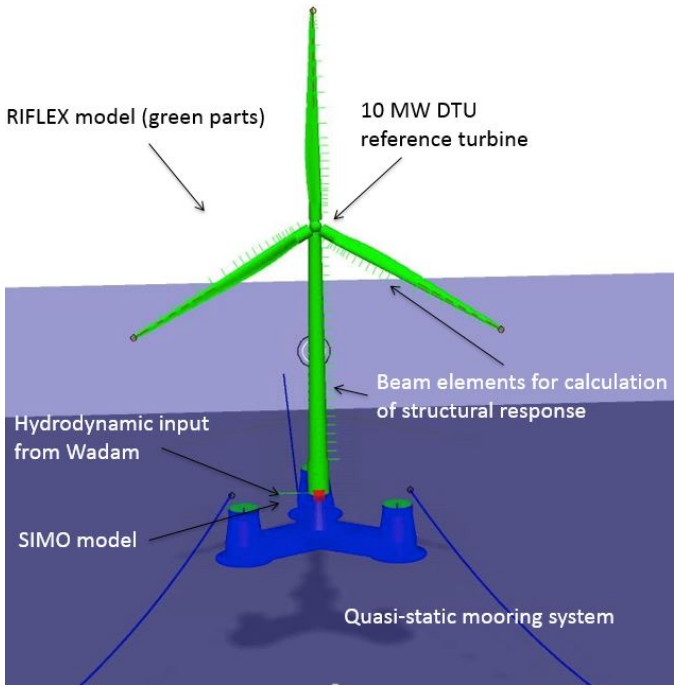

Figure 3.9: Illustration of SIMA model for Case 0.

3.5 Environmental Conditions

3.5.1 Location

OO Star 10 MW is part of the research project LIFES50+, where the goal is to develop innovative floating substructures for 10 MW wind turbines at water depths greater than 50 metre. Three possible sites are given for this project; A, B and C. Site C has the most severe environment, and this location is therefore chosen for the analyses. The reference location for site C is given as West of Barra - Scotland. The mean water depth in the location is 95 meter. All environmental data used in this report are taken with respect to this location, and environmental data in this section are based on Gómez et al. (2015), unless noted otherwise.

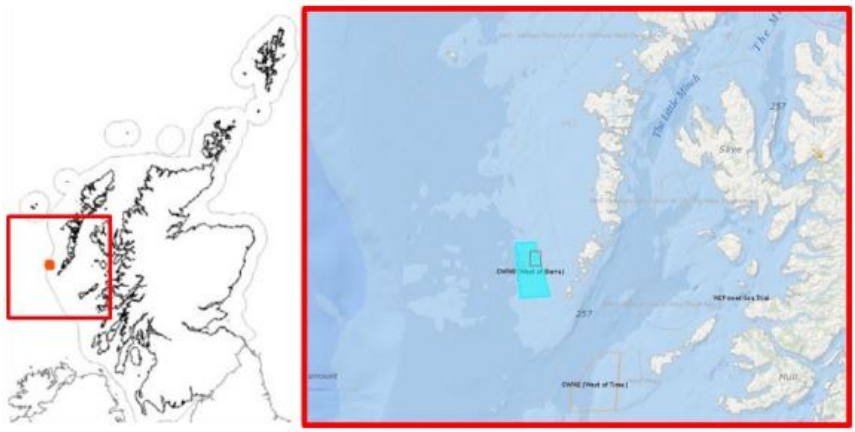

Figure 3.10: West of Barra proposed site location (Gómez et al., 2015)

3.5.2 Waves

The wave climate for long time statistics is given by scatter diagrams for H_s/T_m and H_s/α_{Wa}, where α_{Wa} is the wave propagation direction. The scatter diagrams are provided in Appendix B.1 and B.2. Note that the direction in the scatter diagrams is given as clockwise from true north, i.e. true north is 0 degrees, and that the direction describes from where the weather is coming from.

Generation of Waves

When analysing fatigue on the steel tower, short-time statistics is used. Multiple environmental cases are performed with a statistical weighted damage.

Short-time statistics for waves are given by wave spectrum. There is no information for West of Barra to determine the most suitable wave spectrum, but ISO (2005) indicates that the region has swell waves that has moved out of the area in which they were generated. Hence, Gómez et al. (2015) advise to use a Pierson-Moskowitz (P-M) type spectrum.

A P-M ISSC spectrum is used in the simulations, and significant wave height and mean period is given as input. The wave elevation (ζ) in time domain at a given point is then found by dividing the spectrum in multiple pieces with density $\Delta\omega$ to find amplitude (ζ_A), and then sum all contributions:

$$\zeta_{An} = \sqrt{2S(\omega_n)\Delta\omega} \tag{3.13}$$

$$\zeta(t) = \sum_{n=1}^{N} \zeta_{An} cos(\omega_n t + \epsilon_n) \tag{3.14}$$

3.5.3 Wind

The wind speed is described by Gómez et al. (2015). The long-term statistic is given by a scatter diagram showing mean wind speed at 10 meters height and direction of wind propagation (see appendix B.3). Note that direction in the scatter diagram describes incoming wind direction.

Wind is generated by the software TurbSim (ref. section 3.2) as a three dimensional wind field. The generation is based on an input file. Example of such input file is given in Appendix C, and only the mean wind speed at reference height and seed number varies for different wind fields. One wind field is created for each wind speed. Optimally one should had several wind fields with variable seed for each wind speed, but due to large computational time and storing capacity, this was not possible. A discussion on some critical aspects when generating wind field is given below.

Wind Profile

Due to shear forces will the wind speed vary in vertical direction. There are several wind shear profiles that can be used to describe the wind profile in vertical direction. Gómez et al. (2015) states that logarithmic law is best suited to describe the wind profile. The logarithmic law is given as:

$$U_w(z) = U_{ref} \frac{ln(\frac{z}{z_0})}{ln(\frac{z_{ref}}{z_0})} \tag{3.15}$$

Where $U_w(z)$ is the wind speed at height z. U_{ref} is the mean wind speed at a reference height, chosen to be 10 meter, since available scatter diagrams are for mean wind speed at 10 meter. z_0 is the surface roughness length, representing the vertical level at which the mean wind speed becomes zero in neutral atmosphere, and is taken equal to 0.0002. A comparison for annual mean wind speed for measured values and values by use of logarithmic law is given in Figure 3.11.

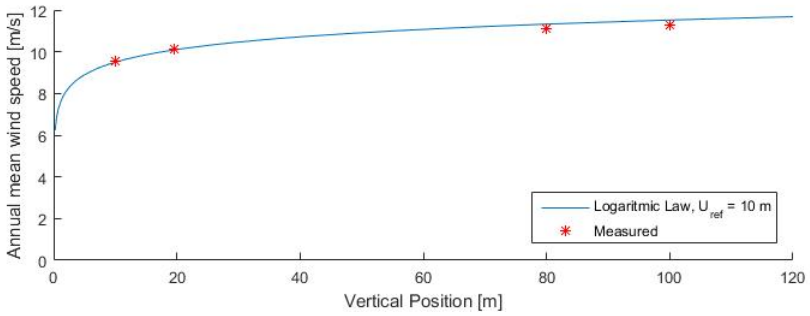

Figure 3.11: Annual mean wind speed for given site (reference location: West of Barra) (Gómez et al., 2015).

Turbulence Model and Intensity

A turbulence model is used in order to generate a turbulent wind field in TurbSim. IEC (2005) gives three requirements for a turbulence model. These requirements are for the standard deviation, the longitudinal turbulence scale parameter and model for the coherence. Two models, the Mann uniform shear turbulence model and the Kaimal spectrum and exponential coherence model, satisfies these requirements, and are hence recommended to use. The Kaimal model defined in IEC (2005) is chosen to model the turbulence in TurbSim. Note that this IEC Kaimal model differs slightly from the original Kaimal spectral model. The turbulence type is taken as Normal Turbulence Type (NTM) according to IEC (2005).

One can choose between different turbulence intensities in the input file for TurbSim. Predefined choices are A, B and C, where the turbulence intensity follows the same order. Turbulence intensity B is used, which gives medium turbulence intensity. This is assumed valid since the unit is located offshore, where fewer elements will trigger the turbulence.

3.5.4 Current

Current will contribute with a mean force on the system. It will also change the viscous forces due to a change in relative particle velocity when the body oscillates. Non of these effects are assumed to contribute with any significance to fatigue, and current is hence not included in the calculations.

3.5.5 Wind/Wave Relation

When performing a fatigue analysis, it is of importance to simulate environmental conditions suitable for the given area. The long-term statistic is used to do so, and several environmental cases contributes with a weighted damage (based on statistically value of occurrence).

The correlation between wind speed and significant wave height is given by a scatter diagram in Gómez et al. (2015) (see Appendix B.4). For the correlation of wind direction and wave direction, no met-ocean data are provided for the area. The rose for wave and wind, describing the probability for propagation direction, is given in Figure 3.12. Note that the rose for direction X indicates the probability for the environment to come from this heading. It is seen that the highest probability of occurrence for both wind and wave is from SW/W, i.e. environment propagating in NE/E direction. Probability is more evenly distributed for wind. In the simulations it is assumed that the waves are wind driven, and the direction for wave propagation is set equal to wind propagation direction.

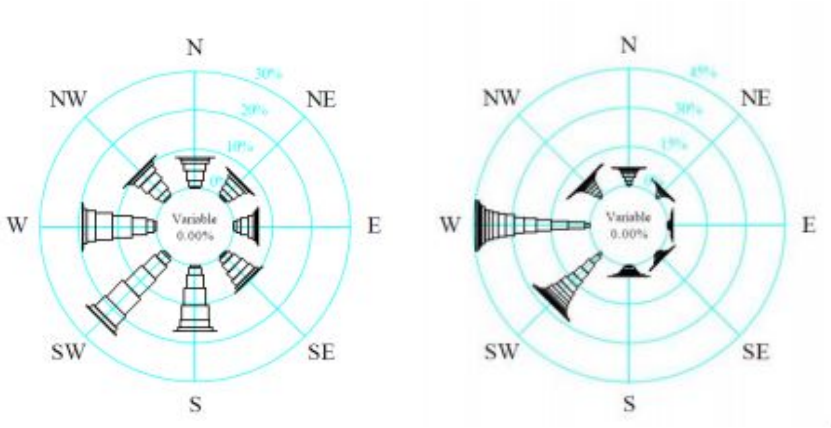

(a) Wind rose

(b) Wave rose

Figure 3.12: Illustration of heading probability for wind and wave for given site (Gómez et al., 2015). Note that the rose for direction X indicates the probability for the environment to come from this heading.

If assuming wind generated waves with same propagation direction, four parameters will affect the total number of simulations when calculating the fatigue; propagation direction (α_{Wi}), wind speed (U_w), significant wave height (H_s) and mean wave period (T_m). In long-term statistic, these parameters represents a certain range of values. In simulations the mean value of the range is used. Each environmental condition will have a probability equal to:

$$p(EC) = p(\alpha_{Wi} \cap U_w \cap H_s \cap T) \tag{3.16}$$

If using long-term environment statistic provided for the site, this will lead to approximately 8000 single conditions for each design case. In order to calculate these, either more time, or stronger computational power, is needed. In order to reduce number of runs, the probability of each environment is defined according to direction and wind speed, while the significant wave height is taken as the most probable for the given wind speed. The wave period is taken as the most probable for given significant wave height.

$$p(EC) = p(\alpha_{Wi} \cap U_w) = p(\alpha_{Wi}) \cdot p(U_w|\alpha_{Wi}) \tag{3.17}$$

$$Hs = E[Hs|U_w] \tag{3.18}$$

$$T_m = E[T|Hs] \tag{3.19}$$

Total number of runs is reduced to 70. Environmental realizations are described in Table B.1 and B.2. Note that environments with wind speed equal to 0.95 m/s is added to those with a wind speed of 2.5 m/s. The direction is also modified in order to simulate environment for wanted orientation of the system (see section 3.3).

Each realization is simulated with a duration of 4000 seconds. First 400 seconds are not taken into considerations in order to avoid transient effects. Each environmental condition is simulated for one wave seed and one wind seed. Optimally one should have performed realizations with several wind and wave seeds, and with a longer time duration. Anyhow, this would also require a longer computational time. Since fatigue not depends on one peak, but on the stress distribution, it is assumed that the environmental simulations are valid to use in the calculations.

3.6 Conditions for Analysis

Current section will describe conditions for analyses that are performed. It described how decay analysis practically are done in the software. It also gives an description on how fatigue damage is calculated in SIMA.

3.6.1 Numerical Parameters

As already mentioned, the problem was solved numerically in time domain in SIMA. Newmark Beta method was used to solve the equation of motion, and the parameters γ and β_t needed to be defined. The background theory for this method was given in section 2.1.1. The following values for the parameters was used in the numerical calculation:

$$\gamma = 0.505 \qquad and \qquad \beta_t = \frac{1}{3.9} \tag{3.20}$$

In practice, this means that there is a small numerical damping, but this will not affect the results in any way. These values satisfy the requirement for the method to be unconditional numerical stable (see equation 2.11).

3.6.2 Decay Analysis

The background theory for a decay analysis was described in section 2.7. The method on how this analysis is performed in SIMA is further described in this section. In SIMA, the force, or moment, is applied over a time range before the body is released. Total time range is 300 seconds, where in the first 200 seconds the force is increasing linearly. A constant force is applied from 200s. to 300s. This is illustrated in Figure 3.13. Magnitudes of the forces and moments are given in Table 3.3. Note that the wind turbine generator is parked for the decay tests in order to minimize its contribution.

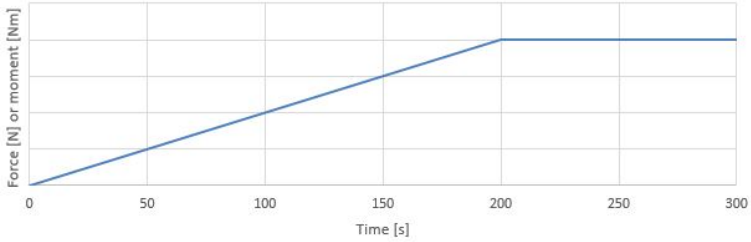

Figure 3.13: Illustration of applied force in a decay test. The ramp and constant force is applied in order to stabilize the system before releasing it.

Roll and pitch are found to have a coupling effect with sway and surge, respectively. As a consequence, multiple frequencies are present in the signal, as can be seen in Figure 3.14a.

Table 3.3: Decay forces/moments for constant time range (200s − 300s)

Direction	Surge/sway	Heave	Roll/pitch	Yaw
Force/moment	$5 \cdot 10^5$ N	$2.5 \cdot 10^7$ N	$1.9 \cdot 10^8$ Nm	$6 \cdot 10^6$ Nm

Due to multiple frequencies in the signal, some cycles will have a negative damping. A negative damping causes larger deviations when estimating the damping effects by use of decay test measurement. To avoid this negative damping, the results for pitch and roll decay is filtered by use of a high-pass filter.

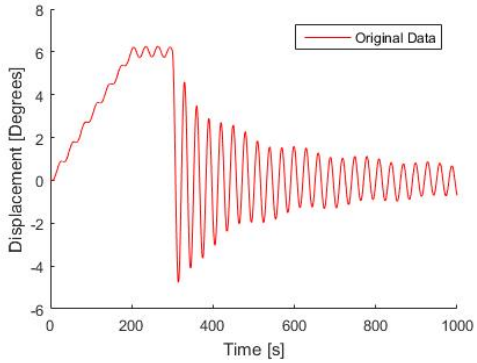

(a) Roll decay before high-pass filtering.

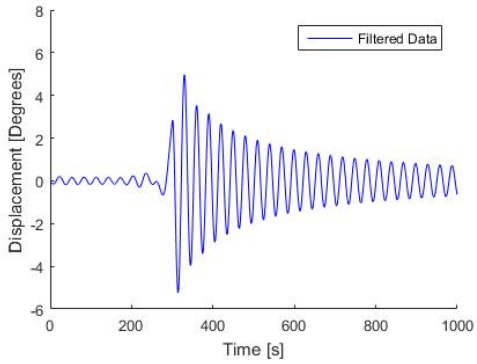

(b) Roll decay after high-pass filtering.

Figure 3.14: Effect of using high-pass filter in order to avoid negative damping for a decay test in roll.

3.6.3 Fatigue Analysis

The theoretical background for fatigue analysis was described in section 2.8. Assumptions and methods are described in this section. As mentioned in the theory part, the choice of S-N curve depends on geometry, technical parameters and load direction of the weld. The steel tower structure is assumed to be hollow with circumferential butt weld made from both sides. The loading direction is assumed normal to the weld. The corresponding S-N curve for this tower is then type D, and is taken according to DNV (2010). Parameters for S-N curve D, as used in equation (2.51), are given in Table 3.4.

N $<= 10^7$ cycles		N $> 10^7$ cycles		Thickness exponent, k
m_s	log(aa)	m_s	log(aa)	
3	12.164	5	15.606	0.2

Table 3.4: Parameters for S-N curve D (DNV, 2010).

How to use Miners rule to find damage was described in section 2.8. DNV (2013) differentiate between characteristic cumulative damage, D_C, and the design cumulative damage D_D.The characteristic cumulative damage is found by Miners rule when knowing the stress history. The design cumulative damage is found by use of the characteristic damage and by use of a design fatigue factor (D_{FF}), as found in Table 7.3 in DNV (2013):

$$D_D = D_{FF} \cdot D_C \tag{3.21}$$

For an external structure, accessible for regular inspection and repair in dry and clean conditions with a normal safety class, the design fatigue factor equals 2.0. All results presented as either total life time or damage in this report has included this design fatigue factor and hence used D_D as damage.

Stress Concentration Factor

SCF was found by use of parametric formulas (see section 2.8.3). Some assumptions have been made due to lack of information about detail engineering for the steel tower. First it is assumed that $\delta_t = 0$ due to no changes in the neutral axis for the tower structure. Further the length of the weld, L, is assumed to be equal the thickness t, and the misalignment is assumed to be 20 percent of the steel thickness. This gives a stress concentration factor equal to 1.32 for all nodes in the tower section.

Calculation of Stress

The resultant axial stress, σ_{as}, is calculated in order to find the total fatigue damage. This stress is multiplied with the SCF, and then counted by use of Rainflow counting method. The stress is found as the sum of axial bending (σ_{ab}) and true wall axial (σ_{tw}) stress in SIMA:

$$\sigma_{as} = \sigma_{tw} + \sigma_{ab} = \frac{N}{A_{cs}} + \frac{M_y r}{I_y}\sin(\theta) + \frac{M_x r}{I_x}\cos(\theta) \tag{3.22}$$

Where N is the axial force, A_{cs} the cross sectional area, M_y and M_x the bending moments, I_y and I_x the second moment of area and r the distance from centreline. θ is the angle determining the position at which the stress should be calculated, as shown in Figure 3.15. Note that the stress is calculated at the outer part of the hollow cylinder.

Distribution of Stress Points

In order to estimate the fatigue, the stress in several points evenly distributed around the 2D cross section of the cylinder is estimated. This is illustrated in Figure 3.15. Unless noted otherwise, the total number of points is 8 in the calculations.

If only one damage is given in the results, this is taken as the maximum out of the 8 points. In some cases, point 1-4 are given, and due to symmetry this also gives an approximation for damage at point 5-8.

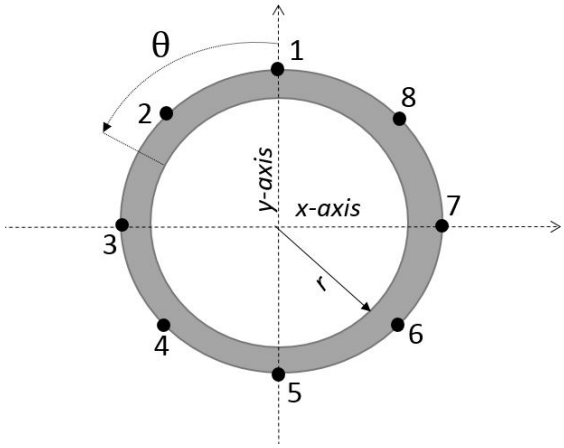

Figure 3.15: Illustration on how distribution of points are done if using 8 points. It illustrates two dimensional cross section of the steel tower seen from above. Point 1 is located the same place independent on number of points, while the rest is evenly distributed counter-clockwise. The figure is given in accordance with the specified coordinate system, as described in section 3.3.

Weighted Fatigue Damage

When calculating the fatigue on the three steel towers, several environmental conditions are used (as was described in section 3.5.5). A weighted damage for each environment is taken according the the probability for the respective environment, and the damage at each point is then found as the sum of all conditions:

$$D = \sum_{i=1}^{N_{EC}} D_i \cdot p(EC_i) \tag{3.23}$$

Here N_{EC} represents the total number of environmental conditions. $p(EC_i)$ is the probability and D_i the damage for environment i.

Note that for sensitivity studies, which is performed in order to evaluate and verify the numerical modal, only one environment is used when calculating the fatigue. This will be further explained in chapter 4.

Chapter 4

Verification and Sensitivity Studies

This chapter will present results from sensitivity and verification studies. A verification study is performed for the wind turbine system, and the results are compared to reference values in order to verify the wind turbine in SIMA.

The sensitivity studies are performed in order to quantify the importance of different parameters when calculating the fatigue lifetime. This is helpful both to understand the different parameters contribution to fatigue, and to verify assumptions for the relevant parameters when building the numerical model.

Some of the sensitivity studies use an environment. Depending on the type of study, they need either combined wind/wave, only wind, only wave or none. The environment is propagating with a direction of 0 degrees in SIMA, i.e. towards true SW. If needed, the following environment is used in the sensitivity studies (unless noted otherwise):

- Waves: P-M ISSC spectra with $H_S = 4m$ and $T_m = 10s$
- Turbulent wind field with $U_{w_{10}} = 15m/s$

4.1 Verification of Wind Turbine

As mentioned in the methodology chapter, the wind turbine was pre-modelled in SIMA, and only a modification on the control system was performed. The wind turbine is verified according to values given in Bak et al. (2013) by performing multiple runs with constant wind.

The results are given in Figure 4.1 and Figure 4.2. The reference values are based on simulations in HAWCStab2 for 10 MW DTU reference turbine performed by Bak et al. (2013). HAWCStab2 is a tool able to compute aerodynamic performance.

It is seen that there are some deviations in the comparison, especially for rotor speed with a wind velocity between 6 and 12 m/s. This deviation may be caused by different use of BEM theory in the software, or the fact that reference values are taken from a bottom fixed system, while values calculated from SIMA is for a floating design with a mean pitch angle. Also mean generator power at wind speeds above 20 m/s has some deviations to the reference (which is 10 MW in rated condition). It seems like the minimum pitch angles defined in control system are slightly too high for these wind speeds, even though they are taken equal to reference values. Anyhow, the comparison shows that the model in SIMA is quite similar to the reference, and should hence be valid to use in the computations.

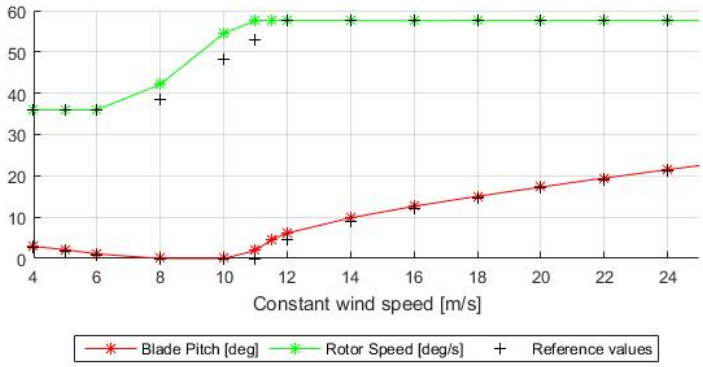

Figure 4.1: Aerodynamic properties for DTU 10 MW turbine.

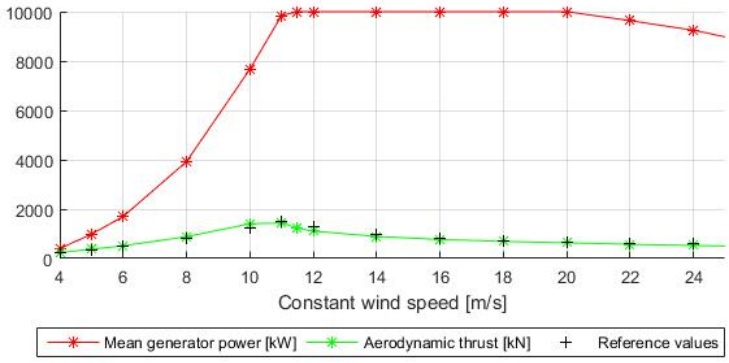

Figure 4.2: Aerodynamic properties for DTU 10 MW turbine.

4.2 Sensitivity Studies

This section will describe results from relevant sensitivity studies. The studies are performed to estimate the effect, and verify the use, of the following parameters; computational time step, quadratic damping, second order wave excitation forces, structural damping and tower eigenfrequency when mounted on a semi-submersible floater.

4.2.1 Computational Time Step

As described in section 2.1.1, the solution in time domain is solved for discrete time steps. The accuracy of calculations is depending on the computational time step, and possible errors are reduced when the time step is reduced. At the same time, a reduced time step require longer computational time, and it is therefore of interest to choose a time step that are sufficiently low in order to provide accurate results, but at the same time not smaller than needed in order to limit the total computational time.

In SIMA two time steps are used; one for hydrodynamical loads (SIMO) and one for structural and wind forces (RIFLEX). The time step in RIFLEX is of large importance for fatigue damage, and is recommended to be as low as 0.005 seconds by the developers of the software. To verify this, yearly damage for a given environment with combined wind/wave was estimated.

Figure 4.3 shows percentage difference in damage compared to previous time step. A self-defined convergence criteria of 1 percent for all four points was set, and the results shows that a time step equal to 0.005 seconds is sufficient, as recommended by the developers of the software. This time step was then used in all further calculations.

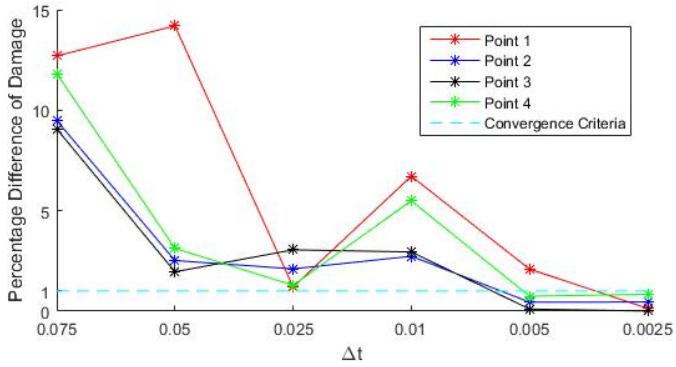

Figure 4.3: Sensitivity of time step on fatigue damage. The figure present damage difference compared to previous time step in percentage. Note that x-axis is not to scale.

4.2.2 Quadratic Damping

In this subsection a study of the quadratic damping effect will be given. The sensitivity of quadratic damping force was tested in two ways; first it was compared to linear damping force and then the sensitivity of quadratic damping on fatigue damage was investigated. Only the latter one included environmental forces (combined wind/wave).

Quadratic Damping Versus Linear Damping

In potential theory, only linear damping is calculated, as described in section 2.2.2. The quadratic damping is not calculated when using potential theory, and must be modelled by in SIMA by use of drag coefficients (ref. section 3.4.1).

The linear damping term is found by multiplying the velocity with coefficient for linear damping. The coefficient for linear damping is calculated by Wadam. The quadratic term is found by:

$$F_D = \frac{1}{2}\rho C_D A_p \dot{\eta}_x |\dot{\eta}_x| \tag{4.1}$$

Where A_p is projected area, C_D drag coefficient, $\dot{\eta}_x$ relative velocity in direction x and ρ fluid density. The comparison is done for the radiation problem (harmonic oscillation with no incoming waves). This method is assumed valid to compare the two damping terms (even though waves would have an effect - especially on the quadratic term). The velocity of the floater oscillation, $\dot{\eta_x}$, is found as the derivative of the displacement:

$$\dot{\eta}_x = \frac{d\eta_x}{dt} = \frac{d(\eta_{xa} sin(\omega t))}{dt} = \eta_{xa} \cdot \omega \cdot cos(\omega t) \tag{4.2}$$

Here η_{xa} is the displacement amplitude. Viscous forces was calculated in matlab. In surge direction it is assumed that the main contribution is from the columns and shaft, while in heave direction the pontoons is assumed to make the largest contribution. The problem was therefore simplified by excluding the pontoons in surge and the columns and shaft in heave direction. A comparison of the damping amplitudes are given in Figure 4.4. It is seen that the importance of quadratic damping is dependent on oscillation frequency and amplitude of motion. Linear damping goes to zero at high and low periods. Quadratic damping goes to zero for high periods, while for short periods velocity will increase, and hence also the quadratic damping force. For current drag coefficients, it appears that heave motion is more affected by the quadratic damping than surge motion. All in all, viscous damping if found to be of importance for the hydrodynamic model, and is therefore included in SIMA.

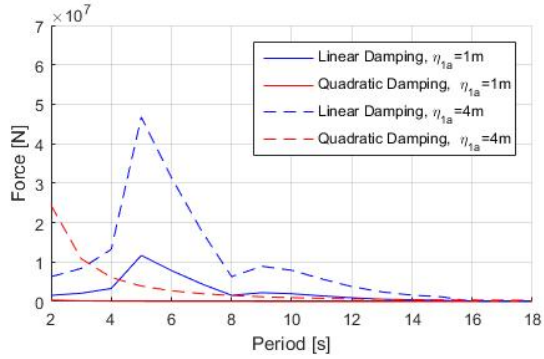

(a) Surge

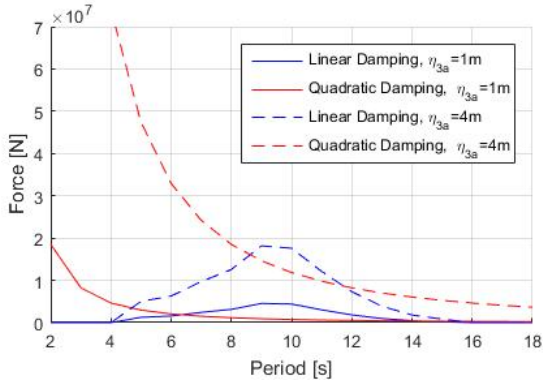

(b) Heave

Figure 4.4: Comparison of linear damping versus quadratic damping amplitude.

Viscous Force Sensitivity on Fatigue

As discussed above, the viscous forces will affect the hydrodynamical damping of the system. Slender systems with drag coefficients were therefore modelled to account for drag forces on pontoons and cylinders. Due to lack of detailed information, the drag coefficients was estimated based on drag coefficients for more simple geometries (see section 3.4.1). To verify the use of these when estimating fatigue, yearly damage was found for different drag coefficients. The drag coefficients were taken the following way:

$$C'_D = C_D \cdot C_{scaling} \tag{4.3}$$

Where C_D is the original drag coefficient used in SIMA modelling (as described in section 3.4.1), and $C_{scaling}$ is a scaling coefficient. The difference in damage (given in percentage) is presented in Figure 4.5. The reference value was set to be the damage when using the original drag coefficient, i.e. $C_{Scaling} = 1$.

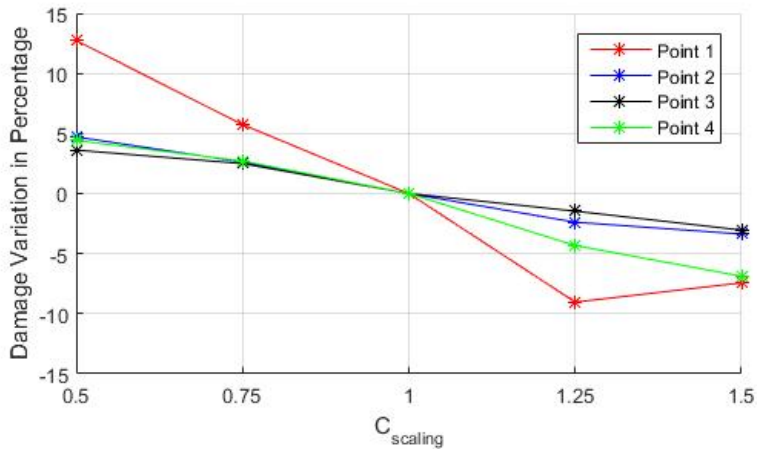

Figure 4.5: Damage variation as a function of $C_{scaling}$ (as used in equation (4.3)).

As seen in Figure 4.5 will an increase by 50 % on the drag coefficients only decrease the fatigue damage by approximately 5 %. It is hence concluded that the drag coefficients are valid to use in the calculations, even though they were estimated from more simple geometries. Therefore, no further research (such as an experiment) were established to determine these.

Note that 3p effects will dominate the fatigue damage for the given design, and this will be further outlined in section 5.3. For other cases, where the 3p effects don't dominate fatigue, the viscous forces may be of higher importance, and a new sensitivity study is then recommended.

4.2.3 Second Order Wave Excitation Forces

Wadam calculates first order velocity potential, and the hydrodynamic excitation forces used in SIMA are hence of first order. First order forces are of a higher magnitude, but second order forces may in some cases be important if they have periods close to the natural period of the system.

It is of interest to estimate the effect of second order forces on fatigue for the steel tower. The second order forces in roll and pitch are therefore investigated. The natural period in pitch/roll of the system (for all three cases) is approximately 29 seconds. This will be further explained in section 5.1. First order wave forces will not excite this natural frequency, but second order different frequency may. The response in pitch/roll when excitation load is close to the natural frequency can be high due to dynamic effects, as described in section 2.1.4. It is therefore of interest to compare first order and second order excitation forces to see if the response from second order wave forces is of importance.

Both first and second order results are based on a wave spectrum, as given in beginning of

the chapter. This wave spectrum is a conservative choice, representing a rougher weather than most in the long-term weather statistic. Second order excitation forces are found by use of Newman's approximation (see theory in section 2.2.3), and wave drift forces in pitch. The first order results are calculated by use of wave force transfer function in pitch. Drift forces and transfer functions are calculated by use of Wadam.

The result for second order different frequency forces is presented in Figure 4.6a. Both second order and first order excitation forces are given in 4.6b, and it is seen that second order forces are negligible. Second order forces are found to be approximately 0.1 % of first order forces. The first order forces are in addition of a higher frequency, which causes more cycles in a given time range. It is concluded that excluding different frequency forces in pitch and roll will not affect the final fatigue results.

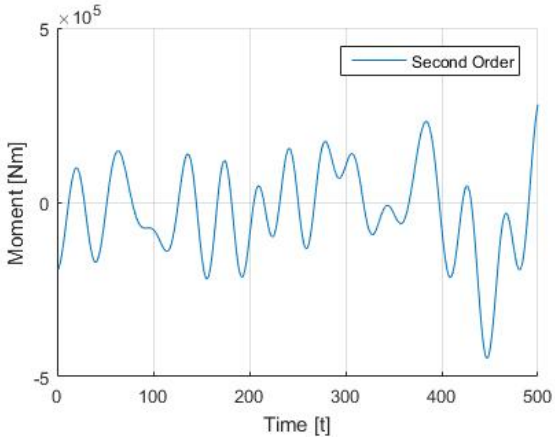

(a) Second order

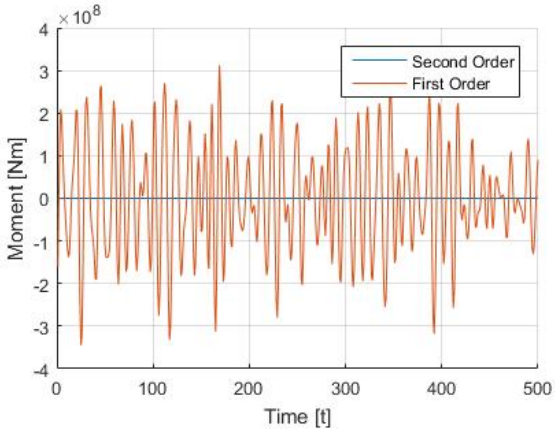

(b) First and second order

Figure 4.6: Wave excitation forces in pitch.

4.2.4 Structural Damping

The structural damping has an effect on the stress when natural frequency of the tower is excited, and hence it may be of importance for fatigue calculations. In RIFLEX the damping is set according to Rayleigh damping, and it is assumed stiffness proportional (ref. section 3.4.2).

The sensitivity on structural damping is tested the same way as for viscous damping, but now multiplying the stiffness proportional coefficient by a factor ($C_{scaling}$):

$$a_2' = a_2 \cdot C_{scaling} \tag{4.4}$$

Where a_2 is the original stiffness proportional coefficient and equals 0.007 (corresponds to approximately 1 % of critical damping at first tower bending mode frequency). The difference in damage compared to damage when using the original damping, a_2, is presented in Figure 4.7 and Figure 4.8. Environment is taken as combined wind/wave. It is seen that the magnitude of structural damping has an effect on fatigue. For point 3, which gives the largest yearly damage, an increase in structural damping by 50 % gives a reduced yearly damage of approximately 10 %. Point 1 has large percentage variation, but from Figure 4.8 it is seen that the total damage for point 1 is small compared to the most critical point.

There are some uncertainties for structural damping, and it is not unlikely that the deviation between damping used in calculations and real damping is 50 %, giving a fatigue damage deviation of 10 %. 3p effects will dominate the fatigue damage for current design, and this will be further outlined in section 5.3. For other cases, where the 3p effects don't dominate fatigue, it is expected that sensitivity of structural damping on fatigue damage is decreased.

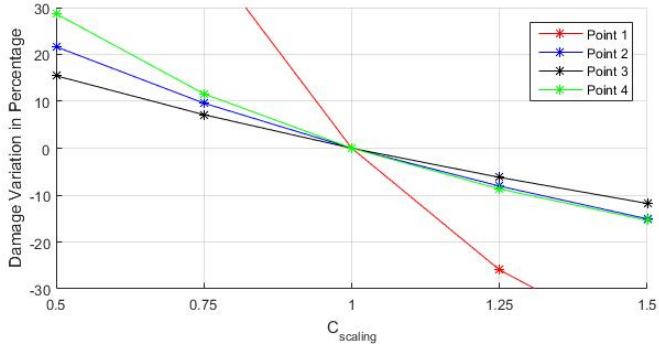

Figure 4.7: Damage variation as a function of $C_{scaling}$ as used in equation (4.4).

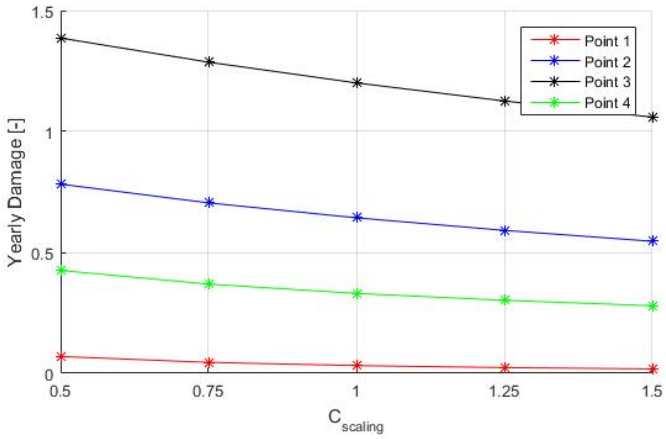

Figure 4.8: Damage variation as a function of $C_{scaling}$ as used in equation (4.4).

4.2.5 Effect on Tower Eigenfrequency When Mounted on a Semi-submersible Floater

The natural frequency of the steel tower is of interest for fatigue on floating wind turbines. Normally one wants to design the tower such that the eigenfrequency is outside the 1p and 3p range, in order to avoid large stress due to dynamic effects from the turbine. The effect of having a load frequency close to the natural frequency was shown in section 2.1.4, seeing that the response in the resonance area may be large.

When investigating the steel tower eigenfrequency for Case 0, one found that the impact of being mounted on a semi-submersible floater is of importance. The effect of the water plane stiffness tends to increase the the eigenfrequency compared to the case where the tower is fixed.

For the case where the tower is fixed, SIMA is able to perform eigenvalue analysis. The eigenvalue analysis showed an eigenfrequency equal to 0.36 Hz for the first bending mode. The eigenmode is shown in Figure 4.9.

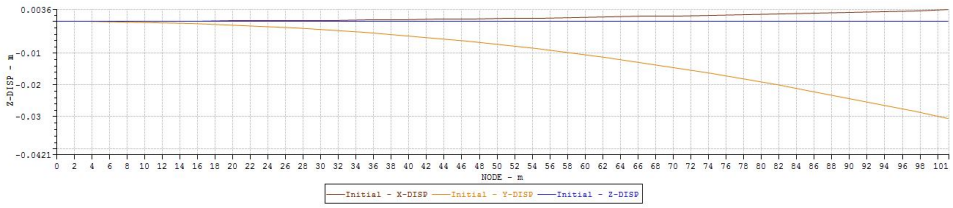

Figure 4.9: Eigenmode steel tower for Case 0 when the tower is fixed, and not mounted on a floater.

SIMA is not able to perform an eigenvalue analysis for a coupled SIMO-RIFLEX model.

The eigenfrequency of the steel tower when mounted on the OO Star 10 MW floater must hence be found by another method. Two methods are used to find this:

1. Performing a FFT of moment force in bottom part of steel tower during first part of a pitch decay test. The natural frequency of the tower is triggered in this time range, as seen in Figure 4.10a. The peak of the response spectrum will then indicate the eigenfrequency.
2. Calculating the energy spectrum for wave elevation (wave spectrum) and moment at a given point on the tower (moment spectra) when the system is exposed to wave forces. Knowing these spectra, the transfer function can be found from equation (2.15), and plotted as in Figure 4.10b. The peak of the transfer function gives the eigenfrequency.

Both methods give approximately the same answer. The eigenfrequency was found to be approximately 0.42 Hz for Case 0, which is 0.06 Hz larger than when the same tower is fixed. This increase in eigenfrequency makes the structure more vulnerable for 3p effects, and decreases therefore the fatigue life time. The transfer function, as seen in Figure 4.10b, illustrates this in a good way. The transfer functions gives a relation between excitation force and corresponding response, and it is seen that the transfer function is much higher around its peak, which indicates the natural frequency.

The findings are supported by Bachynski et al. (2014), which found that different designs for floating offshore wind with the same tower (OC3 Hywind) and turbine structure, gave different eigenfrequencies for tower bending. When mounted on a spar, the tower had an eigenfrequency equal 0.48 Hz, while mounted on a semi-sub it gave an eigenfrequency of 0.42 Hz and 0.43 Hz, depending on the design. The eigenfrequency of OC3 Hywind tower equals 0.36 Hz when it is fixed instead of mounted on a floater (Kvittem and Moan, 2015).

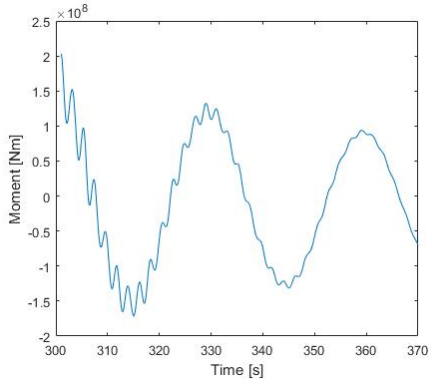

(a) Moment at a given point at steel tower during pitch-decay test.

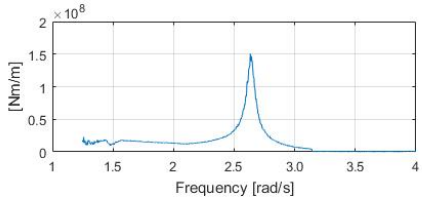

(b) Transfer function steel tower.

Figure 4.10: Illustration of methods to find eigenfrequency of first tower bending mode when mounted on a semi-submersible.

Chapter 5

Results and Discussion for Fatigue

The main objective of this thesis was to investigate the effect of an increased elevation level between concrete and steel on fatigue life time for OO Star 10 MW. The two previous chapters, containing methodology and sensitivity studies, have described important steps in order to establish results for steel tower fatigue.

Current chapter will present results related to design differences between Case 0, Case 20 and Case 40. Mainly fatigue results are given, but also results from decay analyses, eigenfrequency for first tower bending mode and possible cost reductions are presented.

5.1 Decay Analyses

A decay analysis can provide important information such as natural period, added mass and damping for the system. This information helps to understand the behaviour of the system, such as what forces are critical for the system and how fast an oscillation will die out. A decay analysis is also useful to verify that correct mass and stiffness is modelled in SIMA.

Decay analyses for the three different cases were performed by use of the theory described in section 2.7, and methodology described in section 3.6.2. As expected, the three designs have similar behaviour. The results are presented as numbers in Table 5.1. They are also presented visually for Case 0 in Figure 5.1, while Case 20 and Case 40 are presented visually in Appendix D.

Table 5.1: Results for decay analyses for Case 0, Case 20 and Case 40. Note that it is the damped natural period that is given, which for low damping ratios is approximately equal to undamped natural period.

	Natural period [s]			Linear damping ratio [-]			Quadratic damping ratio [-]		
DOF \ Case	0	20	40	0	20	40	0	20	40
Surge	158.1	161.1	161.6	0.0357	0.0434	0.0363	0.0077	0.0039	0.0071
Sway	158.1	161.1	161.6	0.0398	0.0437	0.0445	0.0075	0.0048	0.0042
Heave	22.9	22.8	22.6	0.0039	0.0035	0.004	0.0150	0.0154	0.0151
Roll	29.9	29.5	28.1	0.0022	0.0017	0.0014	0.0066	0.0065	0.0066
Pitch	29.9	29.5	28.1	0.0018	0.0018	0.0015	0.0071	0.0067	0.0067
Yaw	128.4	130.0	132.1	0.0034	0.0034	0.0031	0.0066	0.0065	0.0065

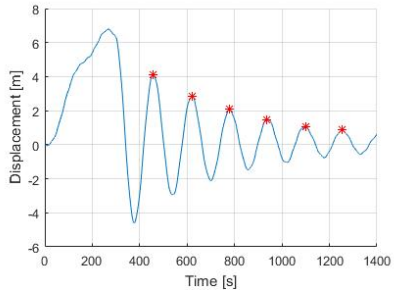

(a) Surge

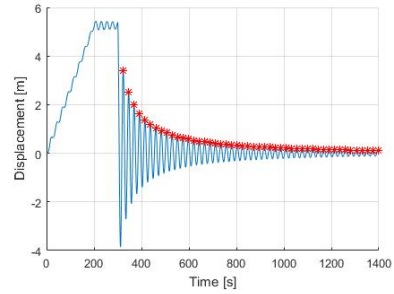

(b) Heave

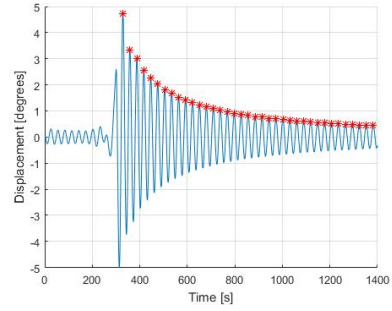

(c) Pitch

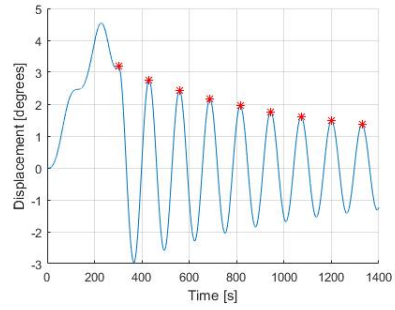

(d) Yaw

Figure 5.1: Decay tests for Case 0 in SIMA.

The equation for natural period was given for an uncoupled system in the theory chapter (see equation 2.3). The system in SIMA is not uncoupled, but this equation can still be used to verify that correct mass and stiffness is given in the numerical model. When estimating natural period, added mass is taken from Wadam calculations (as given in Appendix E).

It is the mooring system that provides a stiffness in surge, sway and yaw direction. The mooring stiffness is relative small compared to the mass, and therefore these directions have high natural periods. The results from decay analyses show that the natural period in these directions are higher for Case 40 than Case 0. Knowing that the mass is increased for Case 40 compared to Case 20, but the same mooring system (and hence stiffness) is used, it is found logical that the natural period in these directions increases slightly.

Natural periods in heave are found to be close to values calculated from known mass, added mass and water plane stiffness.

The natural period in pitch for all three cases are close to 36 seconds when using the equation for an uncoupled system with no mooring system (equation 2.3). Natural periods found from decay analyses are lower than estimated in pitch. The reasons for this is that the mooring system contributes with an increased stiffness in pitch/roll and that there is significant coupling effects between surge/pitch and sway/roll. A decrease in natural period due to coupling effects may be of importance for the ultimate limit state condition for the system.

In section 2.1.4 the dynamic effects when excitation load has a period close to natural period of the system was shown. First order excitation loads from waves have typically a period between 6-15 seconds, and the natural periods of the system are above this, avoiding large dynamic effects from wave loads in a fatigue analyses.

5.2 Eigenfrequency for First Tower Bending Mode

When the tower structure is exposed to excitation loads with a frequency close to its eigenfrequency, the response is large due to a large dynamic effect. First order wave forces and wind forces will not excite the first bending eigenfrequency of the tower, but forces due to an operating wind turbine may. When the blades rotate, excitation forces with a frequency equal to rotational frequency of turbine rotor (1p) and blade passing frequency (3p) are created. These forces are created due to tower shadow effect, wind shear and oblique inflow (ref. section 2.3.3). It is therefore important to be aware of the eigenfrequency for first tower bending mode.

The eigenfrequency for first tower bending mode was estimated as described in section 4.2.5. The transfer functions are presented in Figure 5.2, and the eigenfrequencies are given in Table 5.2.

Table 5.2: Eigenfrequency first tower bending mode.

Case	f_t [Hz]
0	0.42
20	0.46
40	0.47

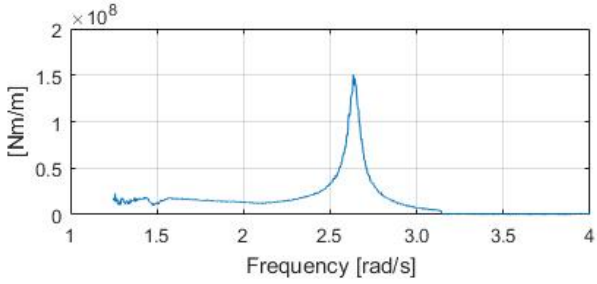

(a) Case 0

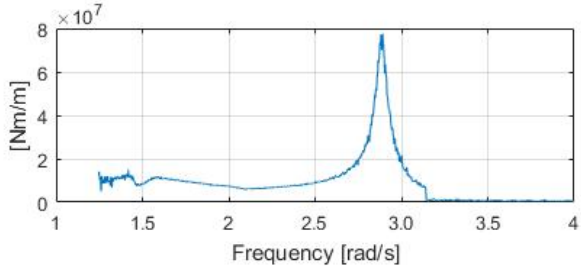

(b) Case 20

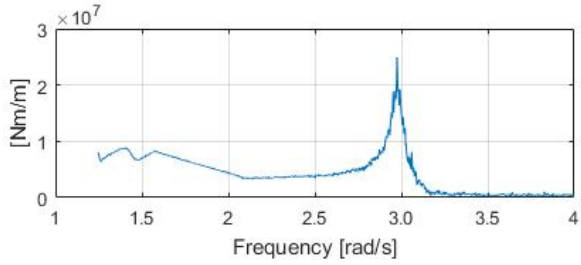

(c) Case 40

Figure 5.2: Transfer functions for tower structure. They are taken in the bottom part of the steel tower, i.e. variable vertical position for the three cases.

The three towers have all eigenfrequencies in the 3p-range. By 3p-range it is meant the range of possible blade-passing frequencies for an operating turbine. The mean 3p frequency in rated operation equals 0.48 Hz, which is close to the eigenfrequencies for the tower structures, as illustrated in Figure 5.4. The wind field is turbulent, and rotor speed is not constant. This implies that the 3p frequency fluctuates around a mean value, and all of the three towers will be exposed to excitation forces with frequencies equal to their natural frequency. This fluctuation is shown in Figure 5.3. Large dynamic effects in combination with a high-frequent load gives a large contribution to fatigue damage, as will be shown in section 5.3.

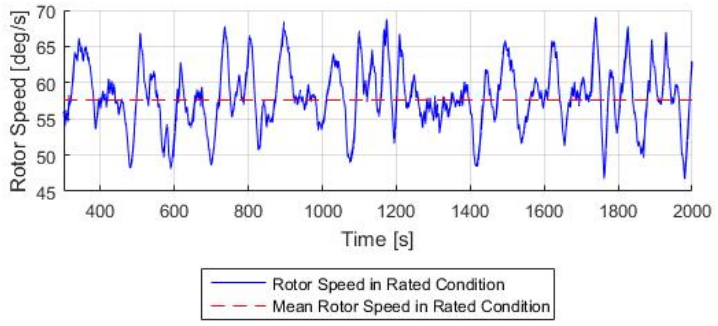

Figure 5.3: Example of rotor speed in rated condition.

One wants to design the tower structure in order to avoid eigenfrequency in the 3p range. The eigenfrequency is then located between 1p and 3p, or above the 3p range. Dr. techn. Olav Olsen AS is still in an early phase of modifying the OO-star from 5 MW to 10 MW, and the tower structure needs further improvement. Some effort was invested trying to solve the problem, but a design was not found that satisfied eigenfrequency, needed stiffness and sufficiently low weight. The task was therefore continued for the given design.

If one wants to design the tower such that it has an eigenfrequency above 3p range for OO Star 10 MW, Case 40 will be the best initial design. Case 40 has the highest tower eigenfrequency, which is currently closest to mean rated 3p frequecy, but this design will probably require the least additional steel weight to get an eigenfrequency above the 3p range.

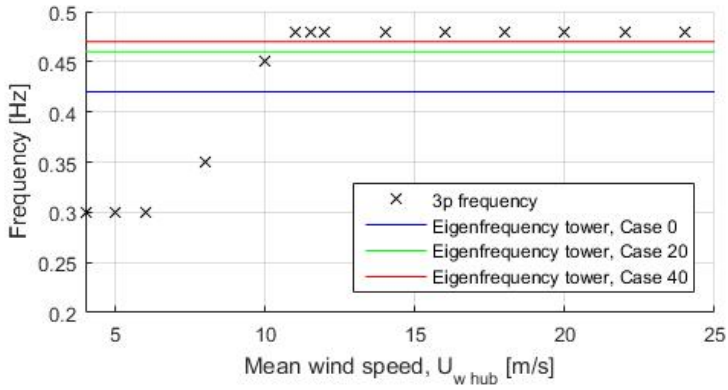

Figure 5.4: Illustration of 3p frequency compared to the natural frequency for the tower structure.

5.3 Fatigue

In this section, results directly related to fatigue of the three cases will be given. Yearly fatigue damage for variable vertical positions in the steel tower will be given for all three cases. Also some discussions on which loads that contribute to fatigue and critical angular positions will be presented.

5.3.1 Contributions to Fatigue

In order to map what gives a contribution to fatigue, FFT of several tower bending moment time realizations was performed. The spectra showed that there were three main contributions; wind loads, wave loads and loads due to 3p effects. The size of each contribution, and at what frequency the peak is located, depends on environmental conditions.

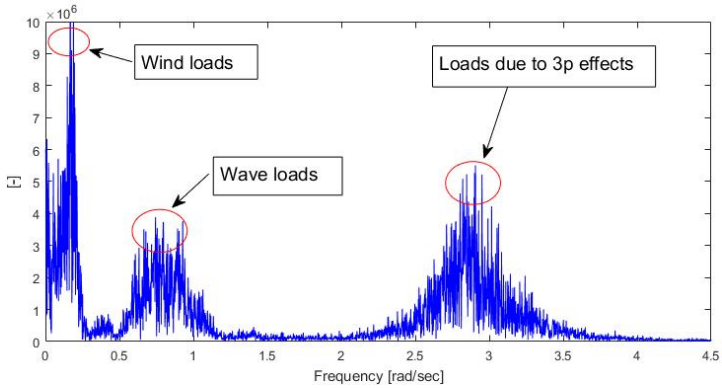

Figure 5.5: Illustration of peaks in a typical spectrum of a FFT of bending moment in steel tower. Note that there is a clear peak in natural frequency for pitch that is probably caused by wind loads. Fatigue damage for lower frequencies than this is also caused by wind loads.

5.3.2 Case 0

The fatigue damage is calculated as described in the theory and methodology chapter. It has included SCF and a safety factor, as recommended by regulations (see section 3.6.3). The damage is calculated for variable vertical positions and for eight points evenly distributed around the tower at each vertical level. The damage is taken for the most critical point, i.e. the point where fatigue damage will occur first.

In order to quantify the contributions from 3p effects and wind/waves, filtering of the time series is performed. The filtering has been done before using rainflow counting. The 3p effects are estimated by performing a band-pass filter from 0.3 Hz $-$ 0.8 Hz, while the contributions from wind/waves are found by a low-pass filter with cut-off frequency equal

to 0.3 Hz. Background theory for filtering of a time series was given in section 2.6.1. Note that when filtering the time series, it will not give exact results on how large the different contributions are, but it gives an indication. This is also seen if one compares the total damage from a time series with the sum of 3p effects and wind/waves calculated by use of filtering. The sum of 3p and wind/wave is not equal the total damage.

The results for Case 0 is presented in Figure 5.6. It is found that the yearly damage for bottom part of the steel tower with given design equals 0.83. The total lifetime is approximately 1.2 years. This fatigue life time is obviously too low, and must be improved.

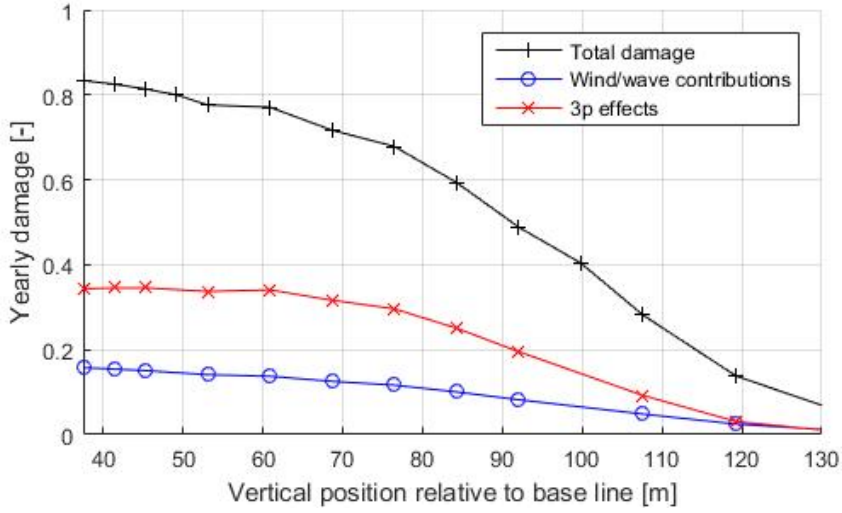

Figure 5.6: Fatigue damage for Case 0. Damage is taken equal damage for the most critical point (out of eight). Wind/wave contributions and 3p effects are estimated by use of low-pass and band-pass filtering, respectively.

It is seen that 3p effects gives the largest contribution to fatigue damage. If assuming that the filtered data for 3p and wind/wave give a correct indication of contribution ratio, the wind/wave contribution damage can be estimated the following way:

$$D_{wind/waves} = D_{total} \cdot \frac{D'_{wind/waves}}{D'_{3p}} \tag{5.1}$$

Where $D'_{wind/waves}$ is damage from wind/waves after a low-pass filtering of the data, while D'_{3p} is the damage due to 3p effects after band-pass filtering. The estimates for fatigue lifetime, if being able to avoid the large 3p effects, is equal to 2.63 years for Case 0. This is an increase of 119 %, but the life time is still low.

5.3.3 Case 20

Case 20 has an increased elevation level for transition point between concrete and steel of 20 metre compared to Case 0. The steel tower has an increased bending stiffness for comparable vertical positions compared to Case 0, as was described in section 3.4.2. The fatigue lifetime for Case 20 is estimated similar as for Case 0 (as described in section 5.3.2). The results are presented in Figure 5.7.

The yearly damage for Case 20 is equal to 0.74, which gives a fatigue lifetime of 1.32 years. If using equation (5.1) to estimate damage without 3p effects, the damage from wind/waves are found to be 0.12. This gives a fatigue lifetime equal to 8.5 years.

The fatigue life time for Case 20 is too low. It seems like the 3p effect gives the largest contribution, which is expected due to first tower bending mode eigenfrequency. If being able to design the tower outside the 3p range, the fatigue life time is estimated to increase significantly.

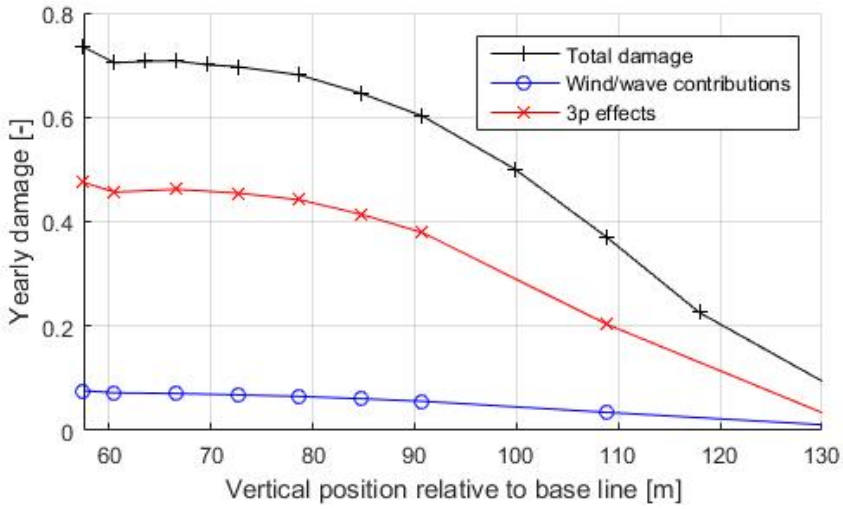

Figure 5.7: Fatigue damage for Case 20. Damage is taken equal damage for the most critical point (out of eight). Wind/wave contributions and 3p effects are estimated by use of low-pass and band-pass filtering, respectively.

5.3.4 Case 40

Case 40 has an increased elevation level for transition point between concrete and steel of 40 metre compared to Case 0. Also the steel tower has an increased bending stiffness for comparable vertical positions compared to Case 0, as was described in sub-section 3.4.2. The fatigue lifetime for Case 20 is estimated similar as for Case 0 (as described in section 5.3.2). The results are presented in Figure 5.8.

The yearly damage for Case 40 is equal to 0.72, which gives a fatigue lifetime of 1.39 years. If using eq. (5.1) to estimate damage without 3p effects, the damage from wind/waves are found to be 0.08. This gives a fatigue lifetime equal to 12.5 years.

The fatigue life time for Case 40 is too low, and needs to bo improved. It seems like the 3p effect gives the largest contribution, which is expected due to first tower bending mode frequency. If it is possible to increase the stiffness of the tower such that the tower eigenfrequency is above 3p range, fatigue life time will increase significant, and fatigue life time is expected to be close to an acceptable value.

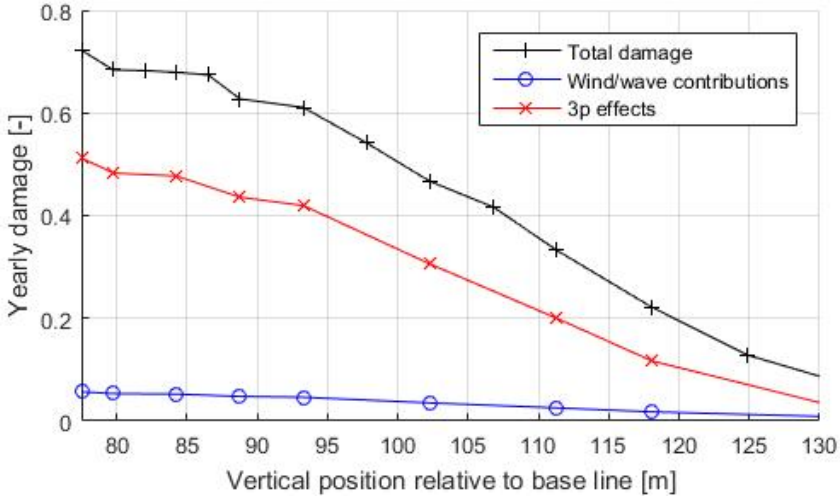

Figure 5.8: Fatigue damage for Case 40. Damage is taken equal damage for the most critical point (out of eight). Wind/wave contributions and 3p effects are estimated by use of low-pass and band-pass filtering, respectively.

5.3.5 Comparison of the Cases

DNV (2013) states that wind turbine components should be designed for a lifetime equal to 20 years. None of the three systems have a steel tower close to fulfil this requirement. A further improvement of the steel tower is needed. In this section, a discussion on which design will be best suited to achieve wanted lifetime is given.

Total damage for the three cases as a function of vertical position relative to transition point between concrete and steel is given in Figure 5.9. It is found that the bottom part of the steel tower will have a longer lifetime for an increased elevation height between concrete and steel. The main contribution for this is the reduced moment force in bottom part of the tower due to a decreased distance from the wind turbine. This leads to lower moment force for wind loads, and the effects from nacelle and blade mass when system is pitching.

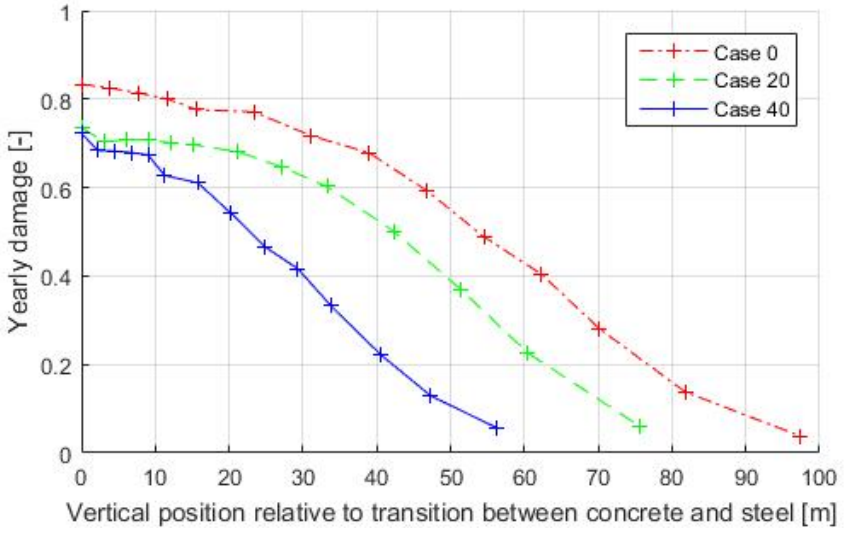

Figure 5.9: Total damage as function of vertical position relative to transition point between concrete and steel.

If comparing the three cases such that they have the same vertical position relative to base line, the result will be as given in Figure 5.10. It is interesting to see that Case 20 and Case 40 in most vertical positions have a larger damage than Case 0 for similar vertical positions. Knowing that Case 20 and Case 40 have a larger stiffness than Case 0 at comparable vertical positions relative to base line (see Figure 3.5), this means that Case 20 and Case 40 have a larger response on excitations loads. Case 20 and Case 40 have steel towers with a natural frequency closer to 3p frequency in rated condition, and it seems like this 3p effects makes a larger contribution to the fatigue damage for Case 20 and Case 40.

A comparison of the 3p effects are given in Figure 5.11. The 3p effects are estimated by use of a band-pass filtering before using rainflow counting. The results show that Case 20 and Case 40 are excited to the largest 3p effects, which is logical taking in mind the eigenfrequencies of the towers. As was mentioned in section 5.2, is Case 40 the most suitable option if one wants to design the tower such that eigenfrequency is above the 3p range.

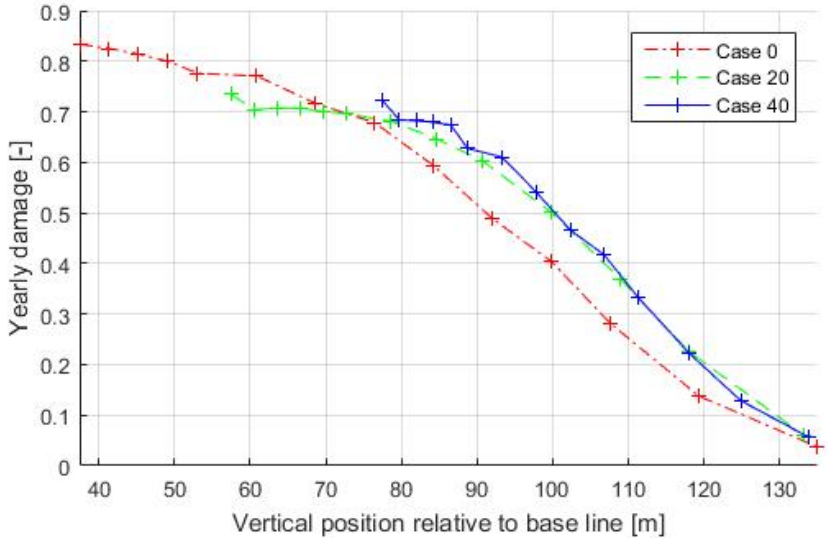

Figure 5.10: Total damage as function of vertical position relative to baseline.

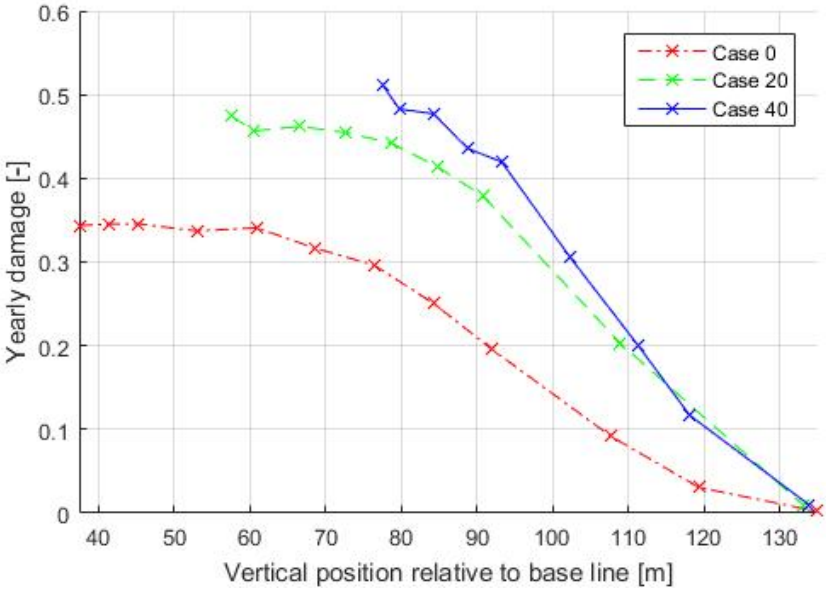

Figure 5.11: Damage due to 3p effects estimated by use of a band-pass filter. Presented as function of vertical position relative to baseline.

A comparison of the estimated damage due to wind and wave forces is given in Figure 5.12. The damage is estimated by use of a low-pass filtering before using rainflow counting. The results show that Case 0 has the largest fatigue damage due to wind and waves.

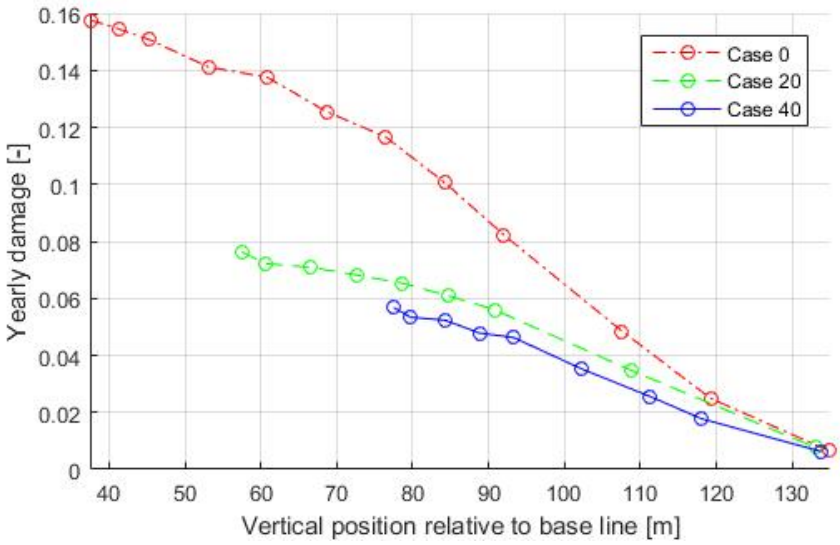

Figure 5.12: Damage due to wind and wave forces. Damage is estimated by use of a low-pass filter. Presented as function of vertical position relative to baseline.

Equation (5.1) is used in order to provide some estimates on the fatigue damage and lifetime if the 3p effects can be minimized. It is found that increasing the elevation height will reduce the yearly damage. If comparing Case 0 and Case 40, the lifetime is estimated to increase from 2.6 years to 12.5 years by increasing the elevation level between concrete and steel with 40 meter. This increase is caused by a reduced moment force from wind and a slightly stiffer tower structure. When comparing Case 20 and Case 40, which has the same steel tower geometry at respective equal vertical heights, the lifetime increases from 8.5 to 12.5 years. Note that equation (5.1) do not give an exact answer, and that the equation is only valid to use for providing indications of how large the fatigue damage will be if the 3p effects are avoided.

5.3.6 Critical Direction

In the long-term statistic, probability for environmental direction varies. Due to this, the damage will not be evenly distributed around the tower, and it is of interest to know how much the damage varies with variable angular position.

For given environmental loads and headings, fatigue at 32 points evenly distributed around the tower is calculated. The result is presented in Figure 5.13 and Figure 5.14. The result is presented as yearly damage, and the position is given by the angle θ, which was described in Figure 3.15.

For Case 0 it seems like the damage is largest for an angle around 90 and 270 degrees, giving a yearly damage of 0.8. The plot shows that the damage is not evenly distributed, and for some points it is as low as 0.52. Also for Case 20 and Case 40 the damage is not evenly distributed around the steel tower. It seems like Case 20 and Case 40 have a difference in peak location of approximately 10-20 degrees compared to Case 0. A possible explanation to this difference is that there are some differences on which environmental conditions the three cases are sensitive to with respect to fatigue damage, as will be described in section 5.3.7.

Due to the damage variation around the steel tower, it can be an option to use a tower design with variable bending stiffness for different angular positions on the tower. Especially in bottom part of the steel tower, which is most sensitive to fatigue, this can be beneficiary. This can be achieved by using an elliptic cross sectional tower shape, or have varying steel thickness for different angular positions. Both of these options might be possible without increasing the total steel weight.

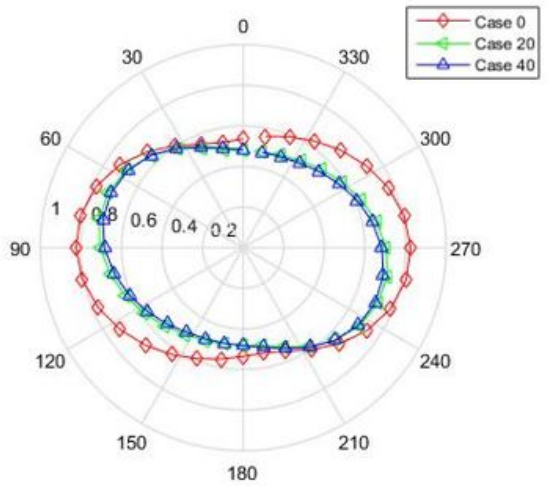

Figure 5.13: Damage for various points around the tower. Vertical position taken in bottom part of steel tower for each case. Point location is described by the angle θ, as described in Figure 3.15.

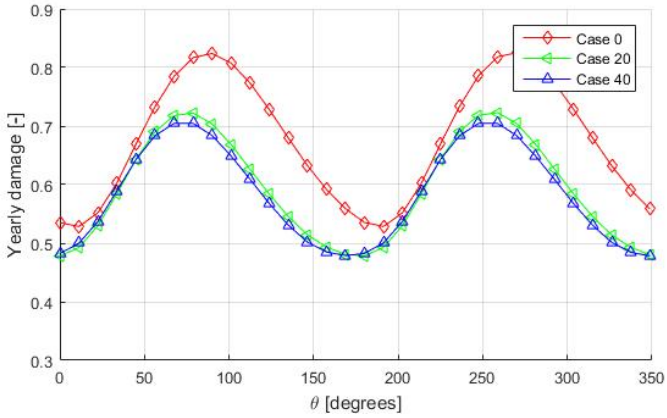

Figure 5.14: Damage for various points around the tower. Vertical position taken in bottom part of steel tower for each case. Point location is described by the angle θ, as described in Figure 3.15.

5.3.7 Critical Environment

It is of interest to quantify which environmental realizations contribute to fatigue damage. The environment is divided into 70 runs based on long-term statistics, as was described in section 3.5. A weighted yearly damage, based on probability and calculated damage, is presented for each environment in Figure 5.15. Environment that corresponds to a peak in the figure does therefore not necessarily correspond to larger damage, but can also be due to large probability.

The turbine condition for different environments is described in Table 5.3. Values for cut-in, rated and cut-out speeds was given in Table 1.1. It is seen that when the wind speed is below cut-in speed and above cut-out speed, the fatigue damage is approximately zero. This implies that fatigue damage from parked condition is low.

For wind speeds between cut-in and rated, the damage is low. For these wind speeds the damage is larger for Case 0 than Case 20 and Case 40, which is expected since the mean 3p effect is closer to tower eigenfrequency for these environments.

The largest fatigue contribution is for environments with wind speed between rated and cut-off. Many of these environments have a large probability and in combination with large 3p effects and wind/wave contributions, this gives a relative large weighted damage.

For most wind speeds, damage on Case 0 is higher than Case 20 and Case 40. Exception is for environments with wind speeds equal to 15.18 m/s at hub height (U_{w10}=12.35 m/s). For these environments, corresponding to number 33-40, some realizations gives a larger damage on Case 20 and Case 40 than Case 0. This implies that for this specific wind speed, the 3p effects are of high importance.

Table 5.3: Operation conditions for wind turbine for variable environments. Environment numbers are taken according to Table B.1 and Table B.2.

Environment Number	Operation Condition
1-8	Wind speed below cut-in speed. Turbine is parked.
9-24	Wind speed between cut-in and rated speed. Turbine is operating.
24-56	Wind speed between rated and cut-out speed. Turbine is operating.
57-70	Wind speed above cut-out wind speed. Turbine is parked.

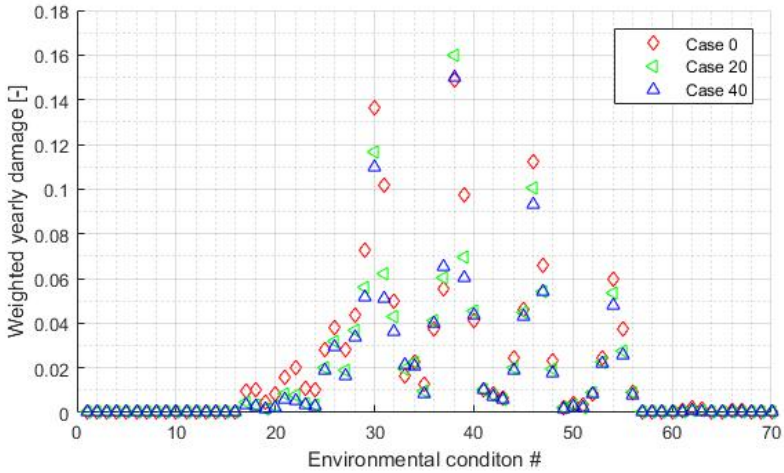

Figure 5.15: Weighted damage bottom part of steel tower in each case. Damage is taken as most critical out of 8 points for each run. Environmental condition number corresponds to environments given in Table B.1 and Table B.2.

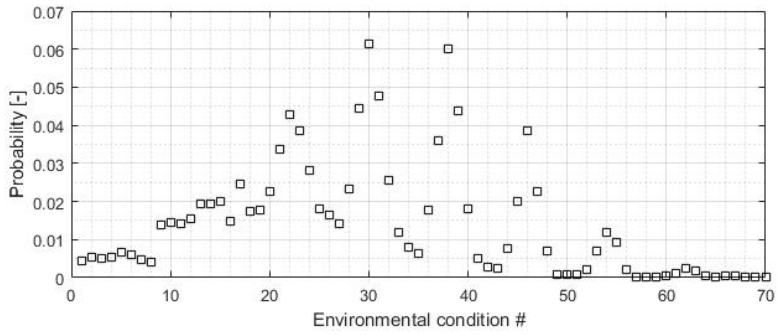

Figure 5.16: Probability for environmental conditions. Environmental condition number corresponds to environments given in Table B.1 and Table B.2.

5.4 Cost Reduction

Currently, cost is a major problem for the offshore wind energy industry. It is important to account for cost when trying to improve the fatigue lifetime for OO Star 10 MW. One important reason for studying the effect of increased elevation height between concrete and steel is that one can reduce the steel weight, and hence the total new building cost. Original design, Case 0, has a steel thickness of what is close to both practical and economical efficient to use.

The cost for steel and concrete is taken as (Landbø, 2016a):

- Steel: 30 000 $\frac{NOK}{t}$
- Concrete: 15 000 $\frac{NOK}{m^3}$

Cost estimates for concrete and steel is given in Table 5.4. It is seen that Case 40 will reduce the total cost by approximately 5 mNOK compared to Case 0, reducing the material cost for steel tower and concrete floater by 4.7 %. This means that Case 40 will both increase the fatigue life time and decrease the material cost, compared to Case 0.

Table 5.4: Estimation for total material cost (steel and concrete) for the three different design cases. The material cost is here taken for floater and tower, i.e. material cost for rotor blades is not included.

	Concrete		Steel		Steel + concrete
Case	Volume [m^3]	Cost [mNOK]	Mass [t]	Cost [mNOK]	Cost [mNOK]
0	5587.2	83.81	834.4	25.03	108.84
20	5822.4	87.34	604.7	18.14	105.48
40	6124.4	91.87	393.76	11.81	103.68

Chapter 6

Results and Discussion for Additional Design Aspects

In addition to testing fatigue sensitivity for variable elevation level between concrete and steel, some additional design aspects have been investigated. The design process of OO Star 10 MW is still in an early stage, and it it therefore of interest to screen important design aspects. Analyses have been used to see if any of the aspects seems to be a limitation for the current design. Aspects tested are outer column freeboard, mooring system, offset, air gap, accelerations at hub level and pitch motions.

The results are established by use of the same numerical model as was used for fatigue calculations. All aspects are tested for Case 0 (base case), and it is assumed that the properties for tested aspects will be similar for Case 20 and Case 40. Aspects are tested for variable wind speeds. Significant wave height and wave period are taken as the most probable for given wind speed.

Additional design aspects are tested for one time realization with one hour duration for each environmental condition. Responses are assumed to be Gaussian distributed (see section 2.6.3), and results are presented by use of mean value and standard deviation. Optimally one should perform several realizations for each environmental condition in order to establish extreme value distributions. This is not done due to high computational time and storage.

There are some limitations on the numerical model and methods used. Current is not included, potential flow theory only accounts for forces up till mean water level etc. Anyhow, the results are used in order to give an indication of whether or not different aspects will be a limitation. Further analyses are required in a later stage of design process.

6.1 Mooring Line Tension

Three mooring lines keep the system in position. In harsh environment the mooring lines will be exposed to large tensions due to environmental loads, and it is important that mooring lines have sufficient breaking strength. Failure on a line can lead to critical damages, such as collision.

The mooring system is analysed as a quasi-static system, as was described in section 3.4.1. Tension in mooring line is tested for variable environmental loads propagating in true NE direction, and the tension is measured for mooring line at windward side. The results are presented in Figure 6.1.

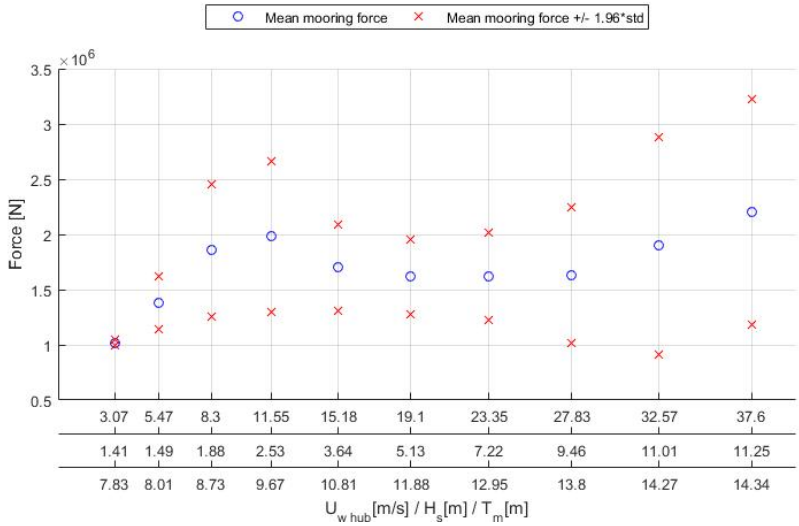

Figure 6.1: Tension in mooring line located at windward side for Case 0 in variable environmental loads propagating in NE direction.

It is seen that the environment with wind speed equal to 37.6 m/s at hub height gives the largest tension in the mooring lines. 2.5 % of the time will the line tension in this environment be above 3.2 MN. This value is much lower than minimum load bearing capacity, which is equal to 21.2 MN for the mooring lines (Vicinay, 2016).

Anyhow, mooring line failure can occur if breaking strength tension is exceeded only ones. One realization with one hour duration was tested for each environment. For environment with wind speed 37.6 m/s at hub height, the realization had a maximum mooring tension equal to 5.75 MN. This value is much lower than the minimum load bearing capacity. It is recommended to perform multiple analyses in order to make an extreme value distribution to verify the mooring system, but based on this screening process, it seems like current mooring system is not a limitation for the design.

There are some limitations when calculating mooring forces with the current numerical model. Second order difference frequency forces in surge/sway is not included, and these may trigger the natural period in surge/sway, giving a larger standard deviation. Also current will contribute, giving a larger mooring line tension. Note that mean drift forces are included in the numerical model.

It is also important to remember that calculations are performed quasi-static (see section 3.4.1). Dynamic effects are included by use of DAF. How large this DAF is, relative to real value, determines how conservative the method is. If DAF is higher than actual dynamic effects on the mooring lines, the method is conservative.

6.2 Horizontal Offset

A power cable is mounted on the floater. The power cable transports power generated by the turbine to a power net. In order to supply the floater with a sufficient cable length, calculations for the horizontal offset is needed.

The horizontal offset also gives an indication how closely wind turbines can be placed to other structures, and still avoid collisions. How closely two wind turbines can be located to each other might be important if the wind park area is restricted, and one wants to have a certain number of turbines located here.

6.2.1 Critical Direction

To estimate maximum horizontal offset for the system, one needs to know at what direction the offset will be largest. The critical environmental direction is tested by analysing offset with the same environment, but with variable propagation direction. The following environmental condition is used:

- $U_{w_{hub}}$ = 11.55 m/s, H_s=2.53 m, T_m=9.67 s

This condition is close to rated condition for the 10 MW DTU RWT. The result are presented in Figure 6.2 as mean offset and with a confidence interval equal to 95 %. Wind/wave propagation in true SW and E direction is found to be the most critical (see Figure 3.3 for system orientation).

6.2.2 Offset

Horizontal offset is tested for different environmental conditions propagating in SW direction. This environmental direction was found to be the most critical in previous subsection. The results are presented in Figure 6.3.

From the results it is seen that the offset has a similar pattern as for the mooring line tension presented in Figure 6.1, which is logical. The largest offset will happen for environment

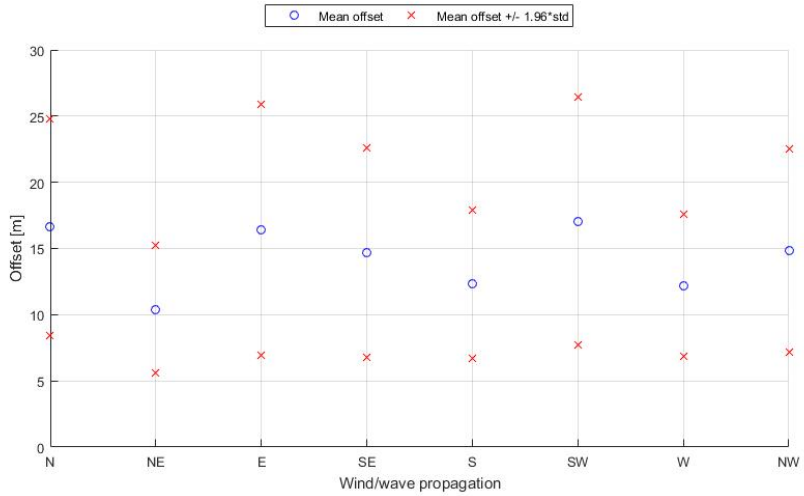

Figure 6.2: Offset for equal wind/wave environment, but with different propagation directions.

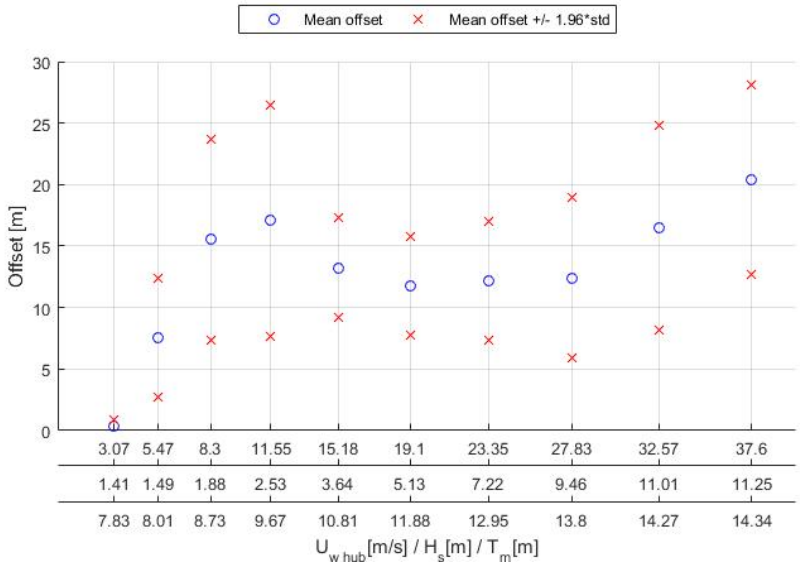

Figure 6.3: Offset for variable environmental conditions for Case 0 when environment is propagating in SW direction.

with wind speed equal to 37.6 m/s at hub height. The system will oscillate around a mean offset of 20 metre. When having in mind that the total length of the system is approximately 70 metre, it seems acceptable with a mean offset of 20 metre for critical

environmental loads. From the results it can be concluded that the power cable must be able to handle a minimum offset of 30 metre.

There are some important limitations for these offset calculations. These limitations are closely related to those described for mooring tension in section 6.1. Anyhow, the results are only used as an early stage screening of the system. The results indicates that the system offset will not be a limitation for current design.

6.3 Pitch Motion

One wants to avoid large pitch motions for a floating offshore wind turbine. A large pitch motion gives a relative angle compared to incoming wind, which reduces the efficiency of the wind turbine. Also the hydraulic system can have problems operating optimal in large pitch motions.

Pitch motion is tested for different environmental conditions propagating in true SW direction, i.e. along the x-axis in SIMA. For this environmental direction, the pitch motion is much larger than roll. The results for pitch are given in Figure 6.4 for variable environmental conditions.

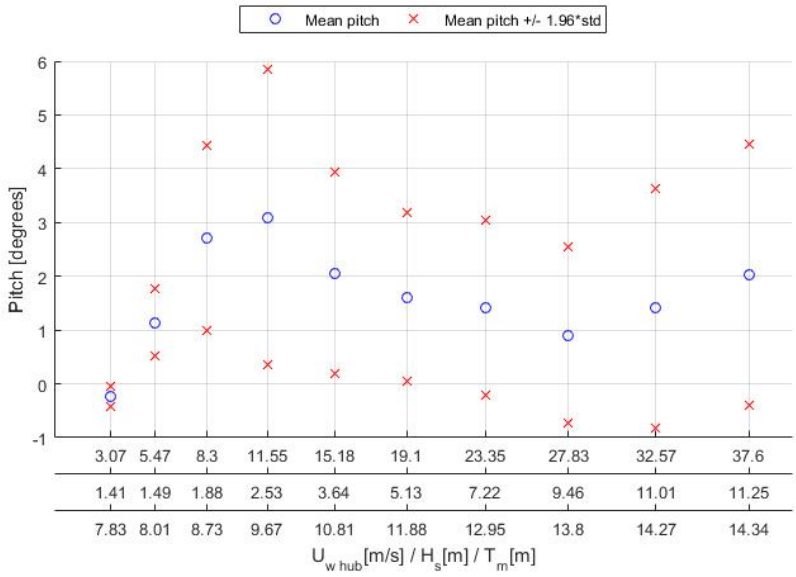

Figure 6.4: Pitch motion for variable environmental conditions for Case 0. Environment is propagting in true SW direction.

It is seen that environment with wind speed equal to 11.55 m/s at hub height gives the largest pitch motion. This is expected since this wind speed is close to rated for the 10

MW DTU RWT, and rated condition gives the largest aerodynamic thrust (see Figure 4.2). The pitch angle will be lower than 6 degrees 97.5 % of the time at this environment.

A rule of thumb is that the pitch angle should be below 10 degrees. It seems like the current design is within this requirement. It can be discussed how critical it is to exceed 10 degrees for short periods. A reduced wind efficiency in short periods due to a pitch angle is not critical, but it might be critical if the hydraulic system has problems working optimal.

6.4 Acceleration Hub Level

It is normal that producers of wind turbine systems give a limit on the acceleration at hub level. This is given in order to avoid high loads on components, which can lead to critical damages. Examples of such components are gear box and shaft.

The acceleration is found for variable environmental conditions propagating in true SW direction. The process is assumed to be Gaussian distributed, and the results are presented in Figure 6.5. It is the acceleration in x-direction that is given, and it is assumed that this direction will dominate for the given environment.

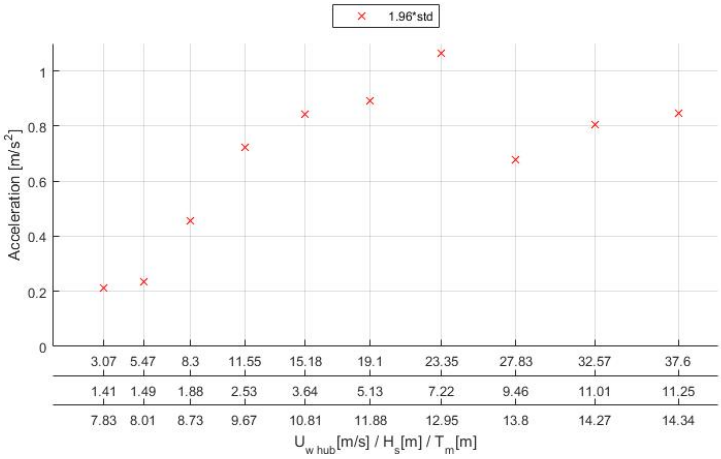

Figure 6.5: Acceleration in x-direction at hub level for variable environment propagating in true SW direction. Mean value is equal to zero, and the results are presented as $1.96 \cdot$ std.

The mean value is found to be approximately zero for all cases. The environment giving the largest accelerations is wind equal to 23.35 m/s with corresponding waves. This environment has a standard deviation equal to 0.54 m/s^2. Of the environments that are tested, this is the environment with wind speed closest to cut out wind speed. It is therefore logical that this environment will provide the largest acceleration at hub height (of those tested).

Dr.techn. Olav Olsen AS wants to avoid accelerations higher than 0.5g ($\approx 5m/s^2$) at hub level for current design. Seeing from the results, 97.5 % of the process will have an acceleration below 1.1 m/s^2. It is therefore reasonable to assume that accelerations at hub level will not be a limitation for current design.

6.5 Outer Column Freeboard

Freeboard on the three outer columns of the floater is of importance. The columns provides a stiffness both in heave and pitch for the system. When the columns are submerged (relative to its initial condition), this provides a positive buoyancy force. This force is in particular important for making the system stable in pitch and roll. The force is determined by submerged volume. The largest stiffness force is established when the column is fully submerged. A further submerging of the column will then not provide any larger stiffness force, and the consequence can in worst case be that the system capsize. It is therefore important to have sufficient freeboard on outer columns.

The freeboard was tested at centre of lee ward side column with environment propagating in true SW direction. The effect of pitch (η_5), heave (η_3) and wave elevation (ζ) for freeboard (z_f) at the centre of the column was accounted for in the following way:

$$z_f = z_{f0} + \eta_3 - sin(\eta_5)x_c - \zeta \tag{6.1}$$

z_{f0} is initial freeboard (=13 metre) and x_c is the distance between column and shaft centre. Also note that ζ here represent the wave elevation at centre of the column position. The results are presented in Figure 6.6 for variable environmental conditions.

It is found that environment corresponding to wind speed 19.1 m/s is most critical for freeboard. This environment has a mean value equal to 11.47 metre and a standard deviation of 4.78 metre. 2.5 % of the time will the process have a freeboard of less than 2.1 metre. This implies that the freeboard in current design may be too small. There are several possible factors causing this environment to be the most critical for the freeboard. The phase between heave, pitch and wave elevation is one possible explanation. Another is the mean wave period.

It will be of interest to estimate a minimum value for the freeboard at the column. If looking at the time series of the freeboard (for critical environment), as given in Figure 6.7, it seems like there are two frequencies creating the peaks; wind and wave frequencies. This is more clearly illustrated in Figure 6.8. The wave frequency is much higher than the wind frequency, and it is therefore assumed that the process are broadbanded. Since the process is assumed Gaussian, the distribution for peaks will then also be Gaussian distributed since the process is broadbanded.

The time series showed that the process had 458 peaks in a simulation with 1 hour duration. For a 3 hour duration, it is therefore assumed that the process will have approximately 1350 peaks. An estimate for a minimum value is found as the value that is below a confidence

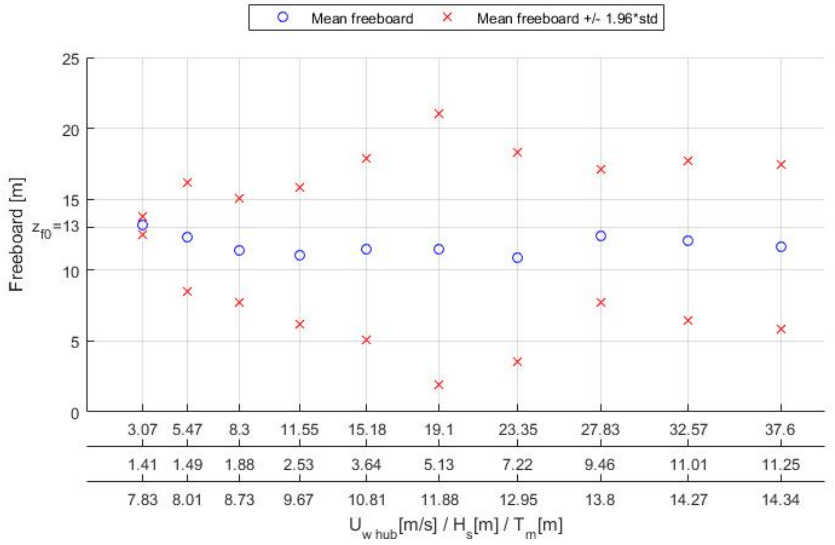

Figure 6.6: Freeboard for outer column with variable environment propgating in true SW direction.

interval with probability $1 - \frac{2}{1350}$. The estimated minimum freeboard was found to be -3.69 metre for environment corresponding to wind speed equal to 19.1 m/s at hub level with a 3 hour duration, which is a critical low value.

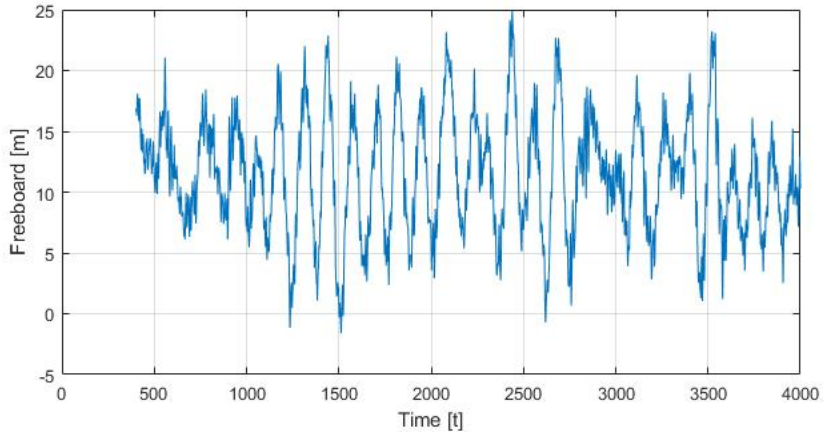

Figure 6.7: Time series of freeboard for environment wind speed at hub height equal to 19.1 m/s, significant wave height equal to 5.13 metre and a mean wave period of 10.81 second.

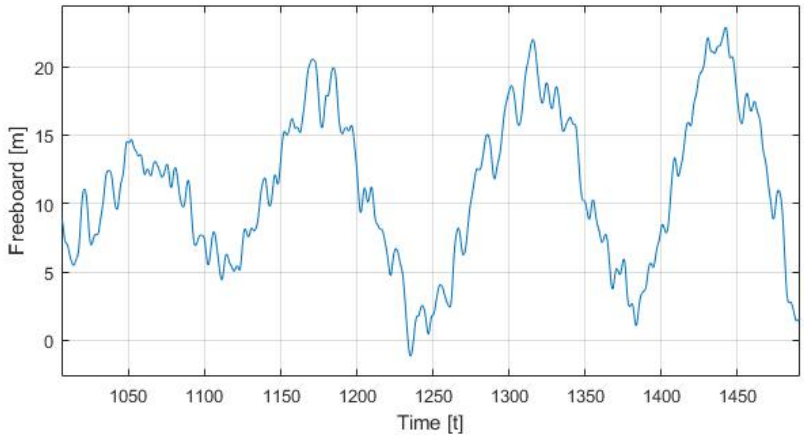

Figure 6.8: Time series of freeboard for environment corresponding to a wind speed at hub height equal to 19.1 m/s, significant wave height equal to 5.13 metre and a mean wave period of 10.81 second.

There are two main limitations for the performed calculations. The first is that drag forces may be a bit smaller than in reality (since they are estimated by use of more simple geometries). The drag forces will contribute with quadratic damping, and this may reduce the motions of the system in both pitch and heave, making it less sensitive to a small freeboard.

Another limitation is that the stiffness is found from potential flow theory, and the stiffness coefficient is therefore taken equal to the water plane stiffness in calm condition. This means that the stiffness is over estimated when the column is fully submerged in the time-domain simulations. Despite the limitations, it seems like the column freeboard must be increased, and a further investigation on the column height is therefore recommended.

6.6 Rotor Air Gap

It is important to have sufficient air gap between blade tip and water. The blade will be exposed to a slamming load if the blade hits the water when it rotates, and this can cause a critical damage to the blade structure.

The rotor air gap is tested similar as column freeboard (see section 6.5), but with modified x_c and ζ since air gap and freeboard are testen in different positions. The results are given in Figure 6.9 for variable environmental conditions. The environment propagated in true SW direction, and the process was assumed to be Gaussian distributed.

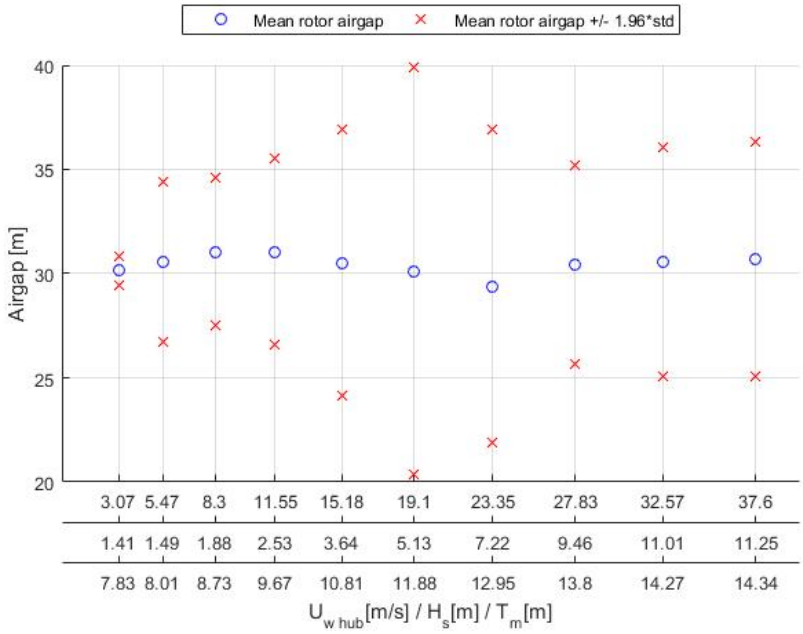

Figure 6.9: Rotor air gap for variable environmental conditions propagating in true SW direction.

Similar as for column freeboard; environment corresponding to wind speed 19.2 m/s at hub height is most critical for rotor air gap. For this environment the air gap will be above 20 metre at 97.5 % of the time. The mean air gap is approximately 30 metre.

Only looking at air gap, it seems like a possibility to decrease the hub level. This would lead to lower moment forces from aerodynamic forces on the bottom part of the steel tower, and hence improve the fatigue lifetime. Anyhow, there are several factors that are important when determining the hub level. A low hub level will be beneficiary for material cost and fatigue. In the same time one wants to have a certain hub height to minimize wind shear and have a more stable power generation.

Chapter 7

Conclusion

In this report, three different design cases for the OO Star 10 MW design have been tested. The main objective was to investigate the effect of an increased elevation level between concrete and steel on the fatigue damage in the steel tower.

The sensitivity studies showed that water plane stiffness affects the first tower bending mode frequency, and this effects increases the eigenfrequency compared to a fixed tower. All three cases have a steel tower eigenfrequency close to the blade passing frequency. This gives a large dynamic effect, and in addition to being a high frequent load, this give large fatigue damage from 3p effects. The 3p effects was found to dominate the fatigue damage, and this is found to be a major problem for the fatigue life time.

The fatigue damage is largest in bottom part of the steel tower. The fatigue life time was found to be approximately 1.2 years for Case 0. Case 20 has a fatigue life time equal to 1.32 years, while Case 40 has a fatigue life time equal to 1.39. Case 40 will increase the fatigue life time with 15.8 % compared to Case 0, which is the base case. Preliminary results show that an increase of the elevating level between concrete and steel will increase the fatigue life time, even though none of the current designs have a sufficient fatigue life time.

To improve the fatigue life time, damage from 3p effects must be reduced. It is recommended to design the steel tower such that first tower bending mode eigenfrequency is outside the 3p range. If one wants to design the tower such that the eigenfrequency is above the 3p range, Case 40 will require the least additional steel weight. For current designs, Case 40 has the lowest material cost for concrete and steel tower. Case 40 will reduce the material cost by more than 5 mNOK compared to Case 0.

To estimate the fatigue life time if being able to minimize 3p effects, filtering of results before a rainflow counting is used. Filtered results are used to find fatigue contribution ratio between wind/wave and 3p effects. This ratio, in combination with total damage calculated in SIMA, is used to estimate fatigue life time if 3p effects are minimized. The

fatigue life time for Case 0 is estimated to be 2.6 years, Case 20 to be 8.5 years and Case 40 to be 12.5 years with minimized 3p effects.

The damage is not evenly distributed around the steel tower for neither of the three designs. This happens due to variation of probability for different environmental headings. An option for increasing the fatigue life time is therefore to have a varying bending stiffness around the steel tower, either by using an elliptic cross sectional shape on the tower, or varying the steel thickness around the tower.

Additional design aspects were tested for Case 0 to be used in a screening process of the design. The results shows that mooring line tension, horizontal offset, pitch motion, acceleration at hub height and rotor air gap is within requirements. These design aspects are not a limitation for the current design. The calculations have some limitations, but they are assumed to be valid to be used in an early-stage process.

Freeboard on outer columns seems to be critical low. For the most critical environment (of those tested), the minimum freeboard was estimated to be -3.9 metre during a three hour realization, i.e. column will be fully submerged.

Chapter 8

Recommendations for Further Work

This thesis has been carried out during one semester, and the time duration has been limited. There are still aspects that can be further studied and developed. The most important task will be to improve the steel tower geometry. The steel towers should be designed with an eigenfrequency outside the 3p range. It is recommended to investigate the possibility of having a varying bending stiffness at different angular positions of the steel tower, especially in bottom part of the steel tower, which is most sensitive to fatigue.

Preliminary results show that increasing the transition point between concrete and steel will increase the fatigue life time. Anyhow, these results are strongly affected by the 3p effects. If steel tower designs are modified in order to minimize 3p effects, new fatigue calculations should should be performed for variable vertical transition points between concrete and steel. In this way, the effect of an increased concrete shaft when wind and wave forces dominates the fatigue can be determined.

In this thesis the fatigue damage has been large, and therefore it has not been any focus on detail engineering of possible coupling mechanisms between concrete floater and steel tower. It can be useful to study if such coupling mechanism will increase the stiffness in bottom part of the steel tower. If so, the critical fatigue damage may occur at a slightly higher vertical position, and the total fatigue life time can be increased.

Additional design aspects are only studied for Case 0 in this thesis, and it is assumed that Case 20 and Case 40 will have similar results. It would be of interest also to perform analyses for additional design aspects for Case 20 and Case 40 to see the effect of an increased concrete shaft on these aspects. These analyses can be used to verify that Case 20 and Case 40 do not have any large drawbacks on additional design aspects.

References

Bachynski, E., 2015. Basic Aerodynamics for Wind Turbines, Lecture Notes.

Bachynski, E. E., Kvittem, M. I., Luan, C., Moan, T., 2014. Wind-Wave Misalignment Effects on Floating Wind Turbines : Motions and Tower Load Effects 136 (7491), 1–12.

Bak, C., Zahle, F., Bitsche, R., Yde, A., Henriksen, L. C., Nata, A., Hansen, M. H., 2013. Description of the DTU 10 MW Reference Wind Turbine Department of Wind Energy I-Report (July), 1–138.
URL https://dtu-10mw-rwt.vindenergi.dtu.dk

Bearman, W., Downie, J., Obasaju, D., 1985. Forces on cylinders in viscous oscillatory flow at low Keulegan-Carpenter numbers 154, 337–356.

Berge, S., 2006. Fatigue and Fracture Design of Marine Structures 2; Fatigue Design of Welded Structures.

Blevins, R. D., 1992. Applied Fluid Dynamics Handbook.

DNV, 2010. DNV-RP-C203 FATIGUE DESIGN OF OFFSHORE STEEL STRUCTURES.

DNV, 2011. SESAM User Manual HydroD.

DNV, 2013. OS-J103 - Design of Floating Wind Turbine Structures (June), 124.

DNV, 2014. DNV-RP-H103 Modelling and Analysis of Marine Operations (February).

EWEA, 2013. The European Wind Initiative - Wind Power Research and Development to 2020.

Faltinsen, O. M., 1990. Sea Loads on Ships and Offshore Structures.

Gómez, P., Sánchez, G., Llana, A., Gonzalez, G., 2015. Qualification of innovative floating substructures for 10MW wind turbines and water depths greater than 50m.

Greco, M., 2012. Lecture Notes; TMR 4215 Sea Loads.

Hansen, M. H., Hansen, A., Larsen, T. J., Øye, S., Sørensen, P., Fuglsang, P., 2005. Control design for a pitch-regulated , variable speed wind turbine. Vol. 1500.

Hansen, M. O. L., 2015. Aerodynamics of Wind Turbines, 3rd Edition.

IEC, 2005. IEC61400-1: "Wind turbines - Part 1: Design requirements", 3rd Edition.

ISO, 2005. Specific requirements for offshore structures. Part 1: Metocean design and operating consderations.

Jonkman, J., Butterfield, S., Musial, W., Scott, G., 2009. Definition of a 5-MW Reference Wind Turbine for Offshore System Development (February).

Jonkmann, B., Kilcher, L., 2012. TurbSim User ' s Guide : Version 1 . 06 . 00 (September).

Kvittem, M. I., Moan, T., 2015. Frequency versus time domain analysis for fatigue of a semi-submersible wind turbine tower. Journal of Offshore Mechanics and Arctic Engineering 137(1).

Landbø, T., 2016a. Personal conversation, 12.04.2016.

Landbø, T., 2016b. Personal conversation, 30.03.2016.

Larsen, C. M., 2014. TMR4182 Marin dynamikk.

Lee, Y.-L., Barkley, M. E., Kang, H.-T., 2012. Metal Fatigue Analysis Handbook; Practical Problem-Solving Techniques for Computer-Aided Engineering. Ch. 3.

Marintek, 2015a. RIFLEX Theory Manual, V4.6v0.

Marintek, 2015b. SIMO - Theory Manual Version 4.6 rev 0. Tech. rep.

Newland, D. E., 1993. An introduction to random vibrations, spectral and wavelet analysis.

Steen, S., 2014. Lecture Notes; Experimental Methods in Marine Hydrodynamics.

Vicinay, 2016. Offshore Mooring Chain: Date visited (2016.04.28).
URL http://www.vicinaycadenas.net/mooring-chain/offshore-mooring-chain.asp

Xu, K., 2015. Design and Analysis of Mooring System for a Semi-submersible Floating Wind Turbines in Shallow Water. M.Sc. thesis.

Appendix A

Steel Tower Geometry

TOWER DATA		
Nacelle level	141.50	m
Tower bottom level	37.50	m
Distance tower top to Nacelle CL	2.75	m
Tower Height	101.25	m
Lower diameter	8.3	m
Lower thickness	60	mm
Upper diameter	5.5	m
Upper thickness	30	mm

Added weight for flanges	5 %	
Calculated plate weight tower	794.6929	t
Weight included flanges	834	t

TOWER SPECIFICATION

sect. nr.	Level ab. WL	Step 1.2	Weight (t)	CoG	Moment
Diam (m)	Height (m)	t(mm)			
5.5	138.75				
26	3.89	30.0	15.91	136.80	2177.20
5.607692	134.86				
25	3.89	32.0	17.30	132.91	2299.41
5.715385	130.96				
24	3.89	33.0	18.18	129.01	2345.42
5.823077	127.07				
23	3.89	34.0	19.08	125.12	2387.14
5.930769	123.17				
22	3.89	35.0	20.00	121.23	2424.34
6.038462	119.28				
21	3.89	36.0	20.94	117.33	2456.78
6.146154	115.38				
20	3.89	38.0	22.49	113.44	2550.96
6.253846	111.49				
19	3.89	39.0	23.48	109.54	2571.99
6.361538	107.60				
18	3.89	40.0	24.49	105.65	2587.46
6.469231	103.70				
17	3.89	41.0	25.52	101.75	2597.13
6.576923	99.81				
16	3.89	42.0	26.58	97.86	2600.77
6.684615	95.91				
15	3.89	44.0	28.29	93.97	2658.16
6.792308	92.02				
14	3.89	45.0	29.39	90.07	2647.44
6.9	88.13				
13	3.89	46.0	30.52	86.18	2629.89
7.007692	84.23				
12	3.89	47.0	31.66	82.28	2605.26
7.115385	80.34				
11	3.89	48.0	32.83	78.39	2573.33
7.223077	76.44				
10	3.89	50.0	34.70	74.50	2585.19
7.330769	72.55				
9	3.89	51.0	35.92	70.60	2535.95
7.438462	68.65				
8	3.89	52.0	37.16	66.71	2478.59
7.546154	64.76				
7	3.89	53.0	38.41	62.81	2412.89
7.653846	60.87				
6	3.89	54.0	39.69	58.92	2338.60
7.761538	56.97				
5	3.89	56.0	41.73	55.02	2296.20
7.869231	53.08				
4	3.89	57.0	43.06	51.13	2201.65
7.976923	49.18				
3	3.89	58.0	44.41	47.24	2097.72
8.084615	45.29				
2	3.89	59.0	45.78	43.34	1984.17
8.192308	41.39				
1	3.89	60	47.17	39.45	1860.75
8.3	37.50				

Height	101.25	Weight	794.69	79.16	62904.40

Figure A.1: Tower geometry for Case 0. Provided by Dr.techn. Olav Olsen AS.

TOWER DATA		
Nacelle level	141,50	m
Tower bottom level	57,50	m
Distance tower top to Nacelle CL	5,40	m
Tower Height	78,60	m
Lower diameter	8,3	m
Lower thickness	54	mm
Upper diameter	5,5	m
Upper thickness	30	mm
Added weight for flanges	5%	
Calculated plate weight tower	575,9593	t
Weight included flanges	605	t

TOWER SPECIFICATION

sect. nr.	Level ab. WL	Step 1,0	Weight (t)	CoG	Moment
Diam (m)	Height (m	t(mm)			
5,5	136,10				
26	3,02	30,0	12,35	134,59	1662,80
5,607692	133,08				
25	3,02	31,0	13,01	131,57	1712,07
5,715385	130,05				
24	3,02	32,0	13,69	128,54	1759,41
5,823077	127,03				
23	3,02	33,0	14,38	125,52	1804,67
5,930769	124,01				
22	3,02	34,0	15,08	122,50	1847,70
6,038462	120,98				
21	3,02	35,0	15,81	119,47	1888,37
6,146154	117,96				
20	3,02	36,0	16,54	116,45	1926,52
6,253846	114,94				
19	3,02	37,0	17,30	113,43	1962,01
6,361538	111,92				
18	3,02	38,0	18,07	110,40	1994,71
6,469231	108,89				
17	3,02	39,0	18,85	107,38	2024,45
6,576923	105,87				
16	3,02	40,0	19,65	104,36	2051,11
6,684615	102,85				
15	3,02	41,0	20,47	101,33	2074,53
6,792308	99,82				
14	3,02	42,0	21,31	98,31	2094,58
6,9	96,80				
13	3,02	43,0	22,15	95,29	2111,10
7,007692	93,78				
12	3,02	44,0	23,02	92,27	2123,96
7,115385	90,75				
11	3,02	45,0	23,90	89,24	2133,00
7,223077	87,73				
10	3,02	46,0	24,80	86,22	2138,08
7,330769	84,71				
9	3,02	47,0	25,71	83,20	2139,07
7,438462	81,68				
8	3,02	48,0	26,64	80,17	2135,81
7,546154	78,66				
7	3,02	49,0	27,58	77,15	2128,16
7,653846	75,64				
6	3,02	50,0	28,55	74,13	2115,99
7,761538	72,62				
5	3,02	51,0	29,52	71,10	2099,13
7,869231	69,59				
4	3,02	52,0	30,51	68,08	2077,45
7,976923	66,57				
3	3,02	53,0	31,52	65,06	2050,81
8,084615	63,55				
2	3,02	54,0	32,55	62,03	2019,05
8,192308	60,52				
1	3,02	54	32,98	59,01	1946,25
8,30	57,50				
Height	78,60	Weight	575,96	90,32	52020,78

Figure A.2: Tower geometry for Case 20. Provided by Dr.techn. Olav Olsen AS.

TOWER DATA		
Nacelle level	141,50	m
Tower bottom level	77,50	m
Distance tower top to Nacelle CL	5,40	m
Tower Height	58,60	m
Lower diameter	7,6	m
Lower thickness	48	mm
Upper diameter	5,5	m
Upper thickness	30	mm

Added weight for flanges	5%	
Calculated plate weight tower	375,9707	t
Weight included flanges	395	t

TOWER SPECIFICATION

sect. nr.	Level ab. WL	Step 0,7	Weight (t)	CoG	Moment
Diam (m)	Height (m	t(mm)			
5,5	136,10				
26	2,25	30,0	9,19	134,97	1240,21
5,580769	133,85				
25	2,25	31,0	9,63	132,72	1278,39
5,661538	131,59				
24	2,25	32,0	10,08	130,47	1315,73
5,742308	129,34				
23	2,25	33,0	10,55	128,21	1352,16
5,823077	127,08				
22	2,25	33,0	10,69	125,96	1347,06
5,903846	124,83				
21	2,25	34,0	11,17	123,70	1381,69
5,984615	122,58				
20	2,25	35,0	11,65	121,45	1415,26
6,065385	120,32				
19	2,25	36,0	12,15	119,20	1447,71
6,146154	118,07				
18	2,25	36,0	12,31	116,94	1439,23
6,226923	115,82				
17	2,25	37,0	12,81	114,69	1469,52
6,307692	113,56				
16	2,25	38,0	13,33	112,43	1498,52
6,388462	111,31				
15	2,25	38,0	13,50	110,18	1487,28
6,469231	109,05				
14	2,25	39,0	14,03	107,93	1513,85
6,55	106,80				
13	2,25	40,0	14,56	105,67	1538,99
6,630769	104,55				
12	2,25	41,0	15,11	103,42	1562,62
6,711538	102,29				
11	2,25	41,0	15,29	101,17	1547,18
6,792308	100,04				
10	2,25	42,0	15,85	98,91	1568,03
6,873077	97,78				
9	2,25	43,0	16,42	96,66	1587,21
6,953846	95,53				
8	2,25	43,0	16,61	94,40	1568,42
7,034615	93,28				
7	2,25	44,0	17,20	92,15	1584,56
7,115385	91,02				
6	2,25	45,0	17,79	89,90	1598,87
7,196154	88,77				
5	2,25	46,0	18,38	87,64	1611,30
7,276923	86,52				
4	2,25	46,0	18,59	85,39	1587,50
7,357692	84,26				
3	2,25	47,0	19,20	83,13	1596,52
7,438462	82,01				
2	2,25	48,0	19,83	80,88	1603,50
7,519231	79,75				
1	2,25	48	20,04	78,63	1575,76
7,60	77,50				
Height	58,60	Weight	375,97	102,98	38717,06

Figure A.3: Tower geometry for Case 40. Provided by Dr.techn. Olav Olsen AS.

Appendix B

Environmental Data

Hs [m]	Tp [s]																				
	0-1	1-2	2-3r	3-4r	4-5	5-6	6-7	7-8	8-9	9-10	10-11	11-12	12-13	13-14	14-15	15-16	16-17	17-18	18-19	19-20	20-21	21-22
0.0-0.5			1																			
0.5-1.0				129	337	681	581	1242	774	341	88	24	11	40	28	11						
1.0-1.5				18	589	1721	1189	2403	3333	1824	754	284	120	23	20	6						
1.5-2.0					21	1260	1855	1644	2765	2720	1444	744	235	131	50	27	3	2				
2.0-2.5				1	4	164	1804	1614	1843	2055	1773	1273	562	222	40	31		4	1			
2.5-3.0					1	8	607	1536	1290	1462	1659	1184	686	338	101	40	1	8	3			
3.0-3.5							85	989	970	1014	1170	1140	749	265	167	61	11	9	1			
3.5-4.0							10	397	846	859	971	873	754	319	221	76	20	5				
4.0-4.5							1	53	646	706	744	893	791	353	206	127	30	4				
4.5-5.0								8	221	529	586	790	659	414	167	76	44	27	4			
5.0-5.5									44	340	558	517	441	250	252	56	9	10	4			
5.5-6.0									7	169	293	433	424	214	182	75	9	16				
6.0-6.5									1	67	101	315	263	186	100	54	21	13	6			
6.5-7.0										3	42	220	301	218	101	35	17	13	2			
7.0-7.5											15	106	160	156	69	54	17	1				
7.5-8.0											8	32	145	117	59	50	1	4				
8.0-8.5												10	121	112	67	37		3				
8.5-9.0												3	115	148	62	25	4	2				
9.0-13.5													78	277	321	197	15	21				

Figure B.1: Scatter Hs/Tp for location West of Barra (Gómez et al., 2015).

Significant Wave Height [m]	Dominant Wave Direction [°] 21							
	0	45	90	135	180	225	270	315
0,00-0,50				1				
0,50-1,00	410	568	151	44	59	1100	1435	520
1,00-1,50	1159	950	330	326	311	2933	5156	1119
1,50-2,00	1344	597	324	376	490	3279	5111	1380
2,00-2,50	1029	356	190	541	684	2951	4507	1133
2,50-3,00	624	217	89	403	499	2375	3755	962
3,00-3,50	343	175	63	227	371	1972	2870	610
3,50-4,00	234	107	65	170	294	1587	2544	350
4,00-4,50	151	44	58	117	301	1343	2292	248
4,50-5,00	104	14	14	81	160	1221	1705	226
5,00-5,50	73	12	13	28	136	870	1191	158
5,50-6,00	56	2	8	26	84	542	1030	74
6,00-6,50	9		11	24	35	339	658	51
6,50-7,00				1	15	316	582	38
7,00-7,50					9	192	348	29
7,50-8,00					9	114	268	25
8,00-8,50						100	233	17
8,50-9,00						105	237	17
9,00-13,50						190	664	55
13,50-20,00								

Figure B.2: Scatter Hs/α_{Wa} for location West of Barra (Gómez et al., 2015).

Mean Wind Speed at 10 m [m/s]	Mean Wind Direction [°] 19							
	0	45	90	135	180	225	270	315
0,00-0,30								
0,30-1,60	2	4	6	2	3	4	2	
1,60-3,40	333	413	403	430	535	469	366	326
3,40-5,50	1091	1138	1116	1229	1515	1527	1576	1170
5,50-8,00	1932	1385	1395	1782	2668	3385	3049	2217
8,00-10,80	1421	1294	1105	1841	3496	4850	3750	2016
10,80-13,90	928	641	510	1408	2847	4729	3451	1420
13,90-17,20	397	215	192	605	1576	3035	1782	549
17,20-20,80	52	55	68	162	561	948	731	160
20,80-24,50	5	5	1	30	86	182	132	46
24,50-28,50					3	27	46	10
28,50-32,70							1	1
32,70-51,50								

Figure B.3: Scatter Uw/α_{Wi} for location West of Barra (Gómez et al., 2015).

Significant Wave Height [m]	Mean Wind Speed at 10 m [m/s]												
	0,00-0,30	0,30-1,60	1,60-3,40	3,40-5,50	5,50-8,00	8,00-10,80	10,80-13,90	13,90-17,20	17,20-20,80	20,80-24,50	24,50-28,50	28,50-32,70	32,70-51,50
0,00-0,50						1							
0,50-1,00		5	1054	2316	897	14	1						
1,00-1,50		14	1061	4055	5701	1444	9						
1,50-2,00		1	632	2070	5126	4736	335	1					
2,00-2,50		3	284	1083	3024	5167	1809	21					
2,50-3,00			139	468	1570	3645	2933	169					
3,00-3,50			58	197	762	2080	2981	550	3				
3,50-4,00			40	119	398	1190	2586	997	21				
4,00-4,50			4	33	193	747	2157	1324	96				
4,50-5,00			2	10	81	409	1441	1418	164				
5,00-5,50			1	10	32	184	767	1180	301	6			
5,50-600				1	22	87	452	869	370	21			
6,00-6,50					4	39	207	532	320	25			
6,50-7,00					3	12	116	463	334	24			
7,00-7,50						12	64	276	194	31	1		
7,50-8,00						2	38	195	137	44			
8,00-8,50						2	22	152	138	33	3		
8,50-9,00						2	10	98	201	45	3		
9,00-13,50							6	106	458	258	79	2	
13,50-20,00													

Figure B.4: Scatter wind/wave for location West of Barra (Gómez et al., 2015).

Table B.1: Environmental conditions table 1.

Environment number	U_{w10}	Hs	T	Heading	Probability	Wave seed
1	2.5	1.41	7.833341	315	0.004249	833
2	2.5	1.41	7.833341	0	0.005289	2028
3	2.5	1.41	7.833341	45	0.005188	4096
4	2.5	1.41	7.833341	90	0.005479	3997
5	2.5	1.41	7.833341	135	0.006824	974
6	2.5	1.41	7.833341	180	0.005999	552
7	2.5	1.41	7.833341	225	0.004668	1234
8	2.5	1.41	7.833341	270	0.004135	2650
9	4.45	1.49	8.006285	315	0.013838	2749
10	4.45	1.49	8.006285	0	0.014434	1971
11	4.45	1.49	8.006285	45	0.014155	1400
12	4.45	1.49	8.006285	90	0.015588	3738
13	4.45	1.49	8.006285	135	0.019215	1669
14	4.45	1.49	8.006285	180	0.019368	3509
15	4.45	1.49	8.006285	225	0.019989	1033
16	4.45	1.49	8.006285	270	0.01484	1442
17	6.75	1.88	8.734879	315	0.024504	3481
18	6.75	1.88	8.734879	0	0.017567	217
19	6.75	1.88	8.734879	45	0.017693	836
20	6.75	1.88	8.734879	90	0.022602	2972
21	6.75	1.88	8.734879	135	0.033839	2709
22	6.75	1.88	8.734879	180	0.042933	2964
23	6.75	1.88	8.734879	225	0.038672	2750
24	6.75	1.88	8.734879	270	0.028119	460
25	9.4	2.53	9.665454	315	0.018023	1044
26	9.4	2.53	9.665454	0	0.016412	2076
27	9.4	2.53	9.665454	45	0.014015	3406
28	9.4	2.53	9.665454	90	0.02335	819
29	9.4	2.53	9.665454	135	0.044341	4683
30	9.4	2.53	9.665454	180	0.061515	3755
31	9.4	2.53	9.665454	225	0.047563	4124
32	9.4	2.53	9.665454	270	0.02557	4692
33	12.35	3.64	10.80542	315	0.01177	1136
34	12.35	3.64	10.80542	0	0.00813	3362
35	12.35	3.64	10.80542	45	0.006469	3542

Table B.2: Environmental conditions table 2. The table is a continuation of table 1 above.

Environment number	U_{w10}	Hs	T	Heading	Probability	Wave seed
36	12.35	3.64	10.80542	90	0.017858	1233
37	12.35	3.64	10.80542	135	0.03611	4791
38	12.35	3.64	10.80542	180	0.05998	2120
39	12.35	3.64	10.80542	225	0.043771	3113
40	12.35	3.64	10.80542	270	0.01801	2971
41	15.55	5.13	11.88069	315	0.005035	1006
42	15.55	5.13	11.88069	0	0.002727	661
43	15.55	5.13	11.88069	45	0.002435	3867
44	15.55	5.13	11.88069	90	0.007673	4299
45	15.55	5.13	11.88069	135	0.019989	1945
46	15.55	5.13	11.88069	180	0.038494	4457
47	15.55	5.13	11.88069	225	0.022602	2955
48	15.55	5.13	11.88069	270	0.006963	1124
49	19	7.22	12.95167	315	0.00066	301
50	19	7.22	12.95167	0	0.000698	2500
51	19	7.22	12.95167	45	0.000862	2393
52	19	7.22	12.95167	90	0.002055	4458
53	19	7.22	12.95167	135	0.007115	3912
54	19	7.22	12.95167	180	0.012024	3630
55	19	7.22	12.95167	225	0.009272	1597
56	19	7.22	12.95167	270	0.002029	4728
57	22.65	9.46	13.79848	315	6.34E-05	4262
58	22.65	9.46	13.79848	0	6.34E-05	3596
59	22.65	9.46	13.79848	45	1.27E-05	883
60	22.65	9.46	13.79848	90	0.000381	133
61	22.65	9.46	13.79848	135	0.001091	1423
62	22.65	9.46	13.79848	180	0.002308	3846
63	22.65	9.46	13.79848	225	0.001674	4566
64	22.65	9.46	13.79848	270	0.000583	4462
65	26.5	11.01	14.27397	135	3.81E-05	2561
66	26.5	11.01	14.27397	180	0.000342	1956
67	26.5	11.01	14.27397	225	0.000583	42
68	26.5	11.01	14.27397	270	0.000127	4224
69	30.6	11.25	14.34155	225	1.27E-05	482
70	30.6	11.25	14.34155	270	1.27E-05	3479

Appendix C

Input TurbSim

```
TurbSim Input File. Valid for TurbSim v1.06.00, 21-Sep-2012

---------Runtime Options-----------------------------------
910119             RandSeed1       - First random seed  (-2147483648 to
2147483647)
RANLUX              RandSeed2       - Second random seed (-2147483648 to
2147483647) for intrinsic pRNG, or an alternative pRNG: "RanLux" or "RNSNLW"
False               WrBHHTP         - Output hub-height turbulence parameters in
binary form?  (Generates RootName.bin)
False               WrFHHTP         - Output hub-height turbulence parameters in
formatted form?  (Generates RootName.dat)
False               WrADHH          - Output hub-height time-series data in
AeroDyn form?  (Generates RootName.hh)
False               WrADFF          - Output full-field time-series data in
TurbSim/AeroDyn form? (Generates Rootname.bts)
True                WrBLFF          - Output full-field time-series data in
BLADED/AeroDyn form?  (Generates RootName.wnd)
False               WrADTWR         - Output tower time-series data? (Generates
RootName.twr)
False               WrFMTFF         - Output full-field time-series data in
formatted (readable) form?  (Generates RootName.u, RootName.v, RootName.w)
True                WrACT           - Output coherent turbulence time steps in
AeroDyn form? (Generates RootName.cts)
True                Clockwise       - Clockwise rotation looking downwind? (used
only for full-field binary files - not necessary for AeroDyn)
 0                  ScaleIEC        - Scale IEC turbulence models to exact
target standard deviation? [0=no additional scaling; 1=use hub scale uniformly;
2=use individual scales]

--------Turbine/Model Specifications-----------------------
40                  NumGrid_Z       - Vertical grid-point matrix dimension
40                  NumGrid_Y       - Horizontal grid-point matrix dimension
0.05                TimeStep        - Time step [seconds]
4000                AnalysisTime    - Length of analysis time series [seconds]
(program will add time if necessary: AnalysisTime = MAX(AnalysisTime,
UsableTime+GridWidth/MeanHHWS) )
4000                UsableTime      - Usable length of output time series
[seconds] (program will add GridWidth/MeanHHWS seconds)
119.00              HubHt           - Hub height [m] (should be >
0.5*GridHeight)
200.0               GridHeight      - Grid height [m]
200.0               GridWidth       - Grid width [m] (should be >=
2*(RotorRadius+ShaftLength))
0                   VFlowAng        - Vertical mean flow (uptilt) angle
[degrees]
0                   HFlowAng        - Horizontal mean flow (skew) angle
[degrees]

--------Meteorological Boundary Conditions-------------------
"IECKAI"            TurbModel       - Turbulence model ("IECKAI"=Kaimal,
"IECVKM"=von Karman, "GP_LLJ", "NWTCUP", "SMOOTH", "WF_UPW", "WF_07D", "WF_14D",
"TIDAL", or "NONE")
```

"3"   IECstandard   - Number of IEC 61400-x standard (x=1,2, or 3 with optional 61400-1 edition number (i.e. "1-Ed2"))
"B"   IECturbc   - IEC turbulence characteristic ("A", "B", "C" or the turbulence intensity in percent) ("KHTEST" option with NWTCUP model, not used for other models)
"NTM"   IEC_WindType   - IEC turbulence type ("NTM"=normal, "xETM"=extreme turbulence, "xEWM1"=extreme 1-year wind, "xEWM50"=extreme 50-year wind, where x=wind turbine class 1, 2, or 3)
default   ETMc   - IEC Extreme Turbulence Model "c" parameter [m/s]
LOG   WindProfileType - Wind profile type ("JET";"LOG"=logarithmic;"PL"=power law;"H2L"=Log law for TIDAL spectral model;"IEC"=PL on rotor disk, LOG elsewhere; or "default")
10   RefHt   - Height of the reference wind speed [m]
12   URef   - Mean (total) wind speed at the reference height [m/s] (or "default" for JET wind profile)
default   ZJetMax   - Jet height [m] (used only for JET wind profile, valid 70-490 m)
default   PLExp   - Power law exponent [-] (or "default")

0.0002   Z0   - Surface roughness length [m] (or "default")

--------Non-IEC Meteorological Boundary Conditions------------
default   Latitude   - Site latitude [degrees] (or "default")
0.05   RICH_NO   - Gradient Richardson number
default   UStar   - Friction or shear velocity [m/s] (or "default")
default   ZI   - Mixing layer depth [m] (or "default")
default   PC_UW   - Hub mean u'w' Reynolds stress (or "default")
default   PC_UV   - Hub mean u'v' Reynolds stress (or "default")
default   PC_VW   - Hub mean v'w' Reynolds stress (or "default")
default   IncDec1   - u-component coherence parameters (e.g. "10.0 0.3e-3" in quotes) (or "default")
default   IncDec2   - v-component coherence parameters (e.g. "10.0 0.3e-3" in quotes) (or "default")
default   IncDec3   - w-component coherence parameters (e.g. "10.0 0.3e-3" in quotes) (or "default")
default   CohExp   - Coherence exponent (or "default")

--------Coherent Turbulence Scaling Parameters-------------------
"M:\coh_events\eventdata" CTEventPath   - Name of the path where event data files are located
"Random"   CTEventFile   - Type of event files ("LES", "DNS", or "RANDOM")
true   Randomize   - Randomize the disturbance scale and locations? (true/false)
 1.0   DistScl   - Disturbance scale (ratio of wave height to rotor disk). (Ignored when Randomize = true.)

```
                                     Input9ms
 0.5                CTLy            - Fractional location of tower centerline
from right (looking downwind) to left side of the dataset. (Ignored when
Randomize = true.)
 0.5                CTLz            - Fractional location of hub height from the
bottom of the dataset. (Ignored when Randomize = true.)
50.0                CTStartTime     - Minimum start time for coherent structures
in RootName.cts [seconds]

================================================
NOTE: Do not add or remove any lines in this file!
================================================
```

Appendix D

Decay Analyses

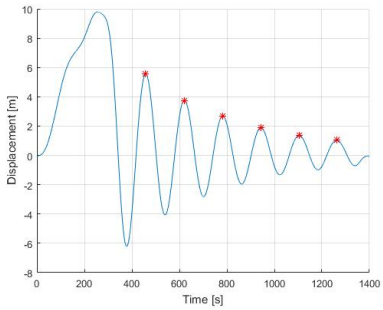

(a) Surge

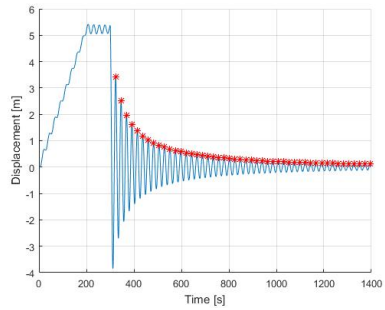

(b) Heave

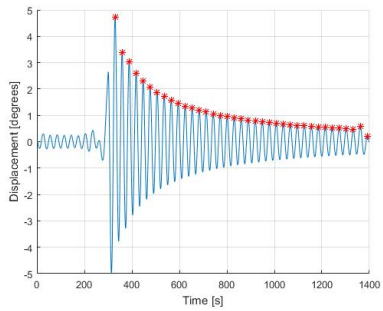

(c) Pitch

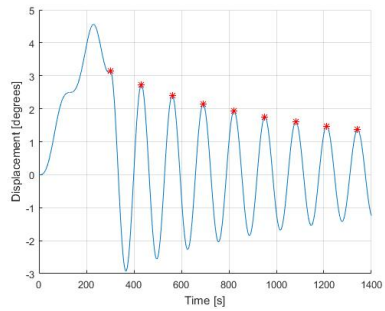

(d) Yaw

Figure D.1: Decay tests for Case 20.

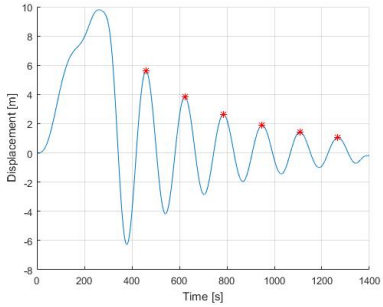

(a) Surge

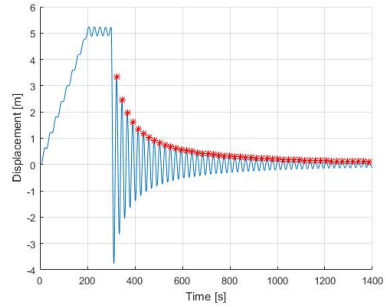

(b) Heave

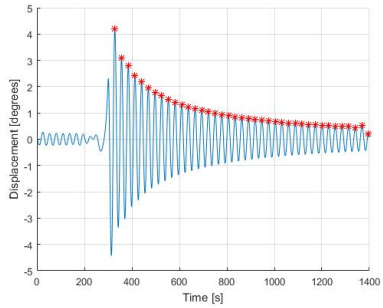

(c) Pitch

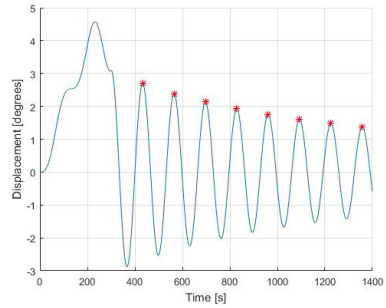

(d) Yaw

Figure D.2: Decay tests for Case 40.

Appendix E

Hydrodynamic Forces

E.1 Frequency Dependent Added Mass

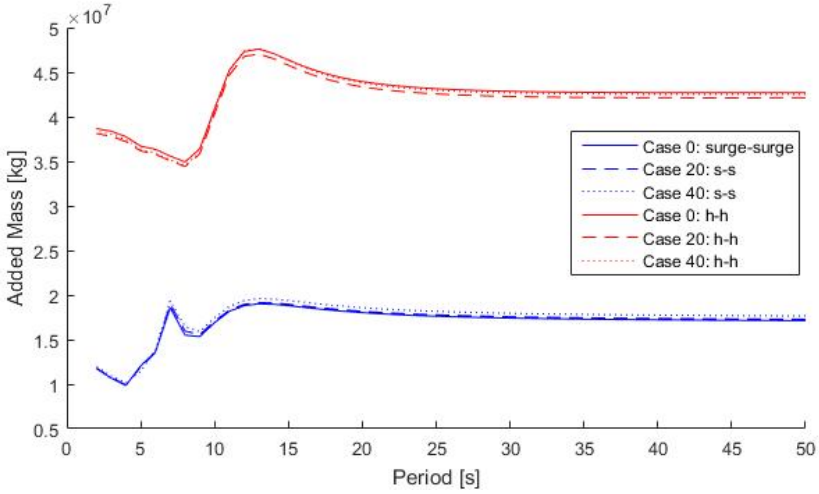

Figure E.1: Frequency dependent added mass from Wadam in surge-surge (s-s) and heave-heave (h-h) direction.

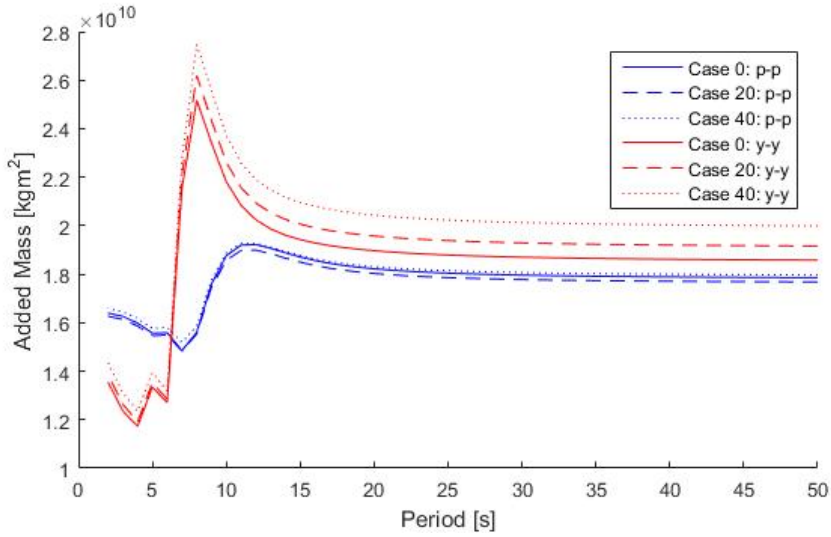

Figure E.2: Frequency dependent added mass from Wadam in pitch-pitch (p-p) and yaw-yaw (y-y) direction.

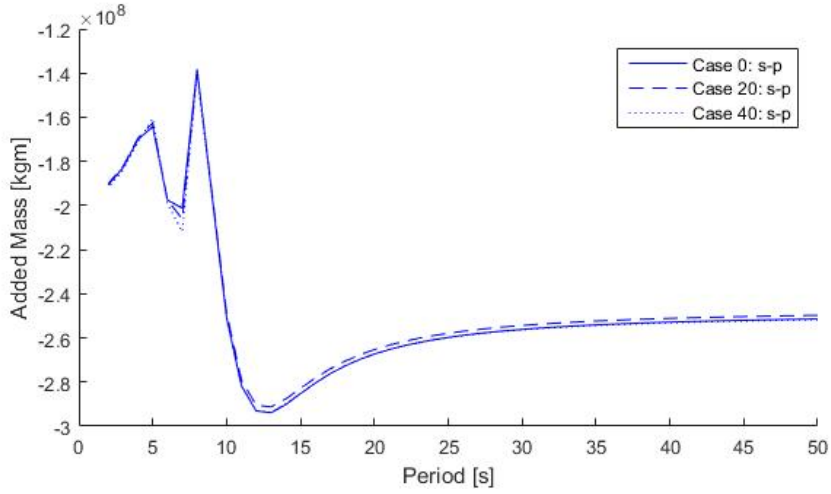

Figure E.3: Frequency dependent added mass from Wadam in surge-pitch (s-p) direction.

E.2 Frequency Dependent Linear Damping Coefficient

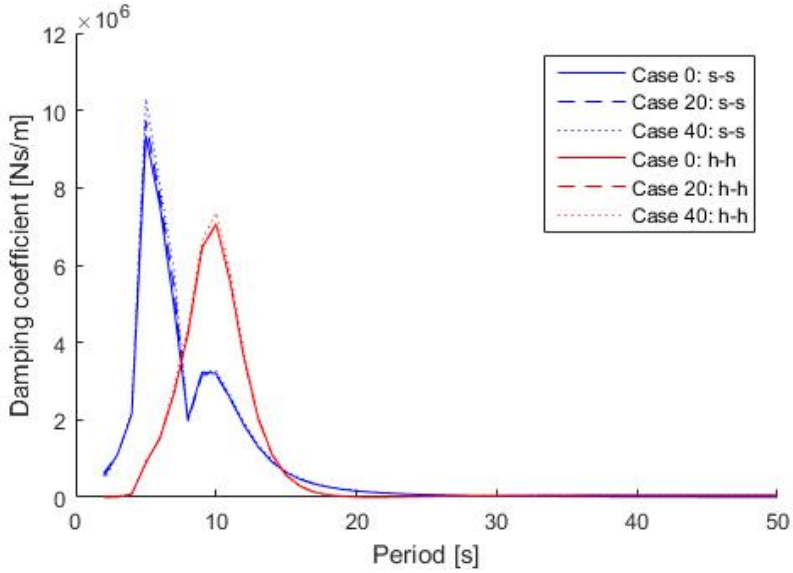

Figure E.4: Frequency dependent linear damping coefficient from Wadam in surge-surge (s-s) and heave-heave (h-h) direction.

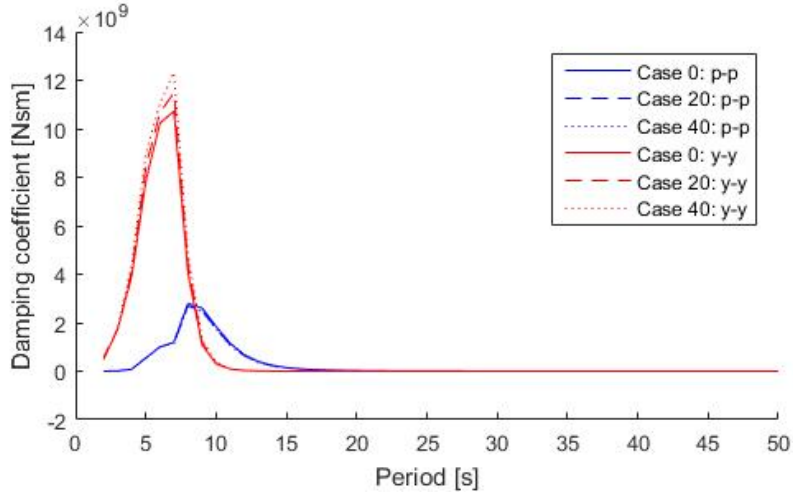

Figure E.5: Frequency dependent linear damping coefficient from Wadam in pitch-pitch (p-p) and yaw-yaw (y-y) direction.

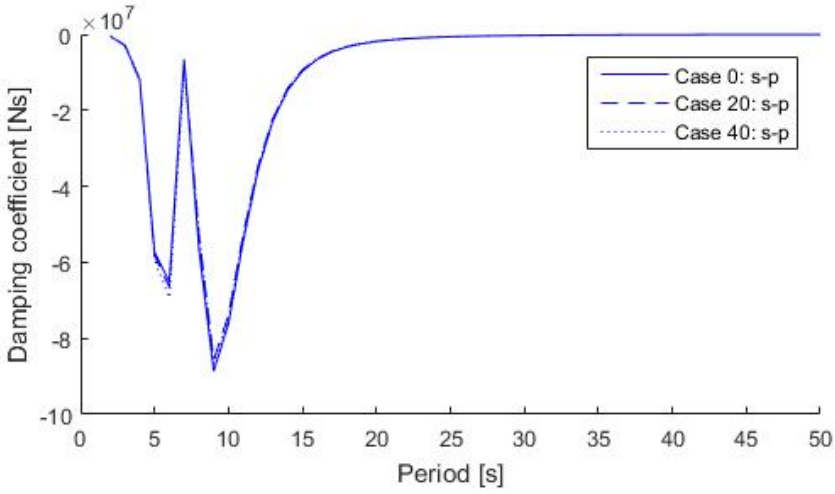

Figure E.6: Frequency dependent linear damping coefficient from Wadam in surge-pitch (s-p) direction.

E.3 First Order Wave Force Transfer Function

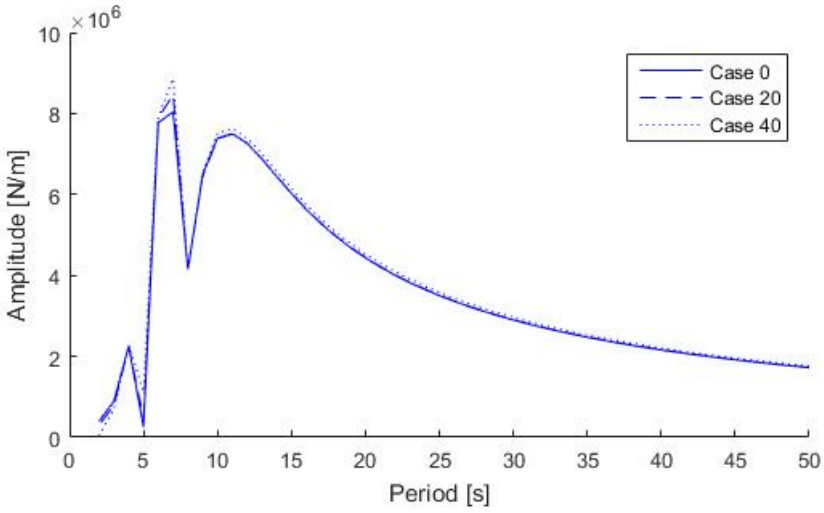

Figure E.7: First order wave force transfer function in surge direction for wave heading 0 degrees.

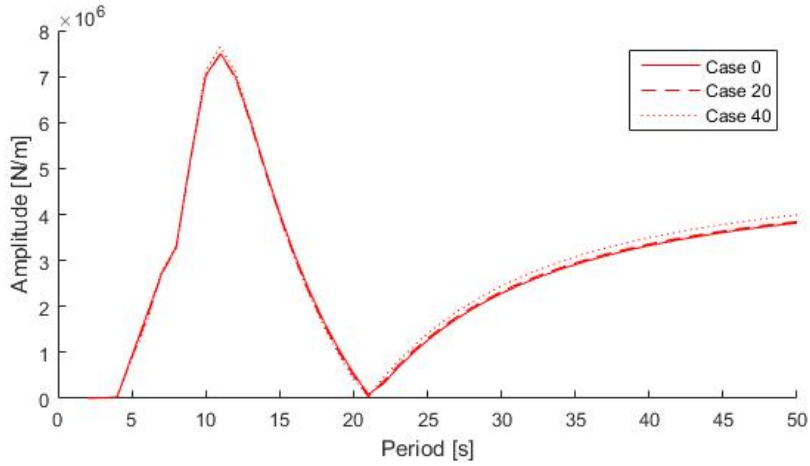

Figure E.8: First order wave force transfer function in heave direction for wave heading 0 degrees.

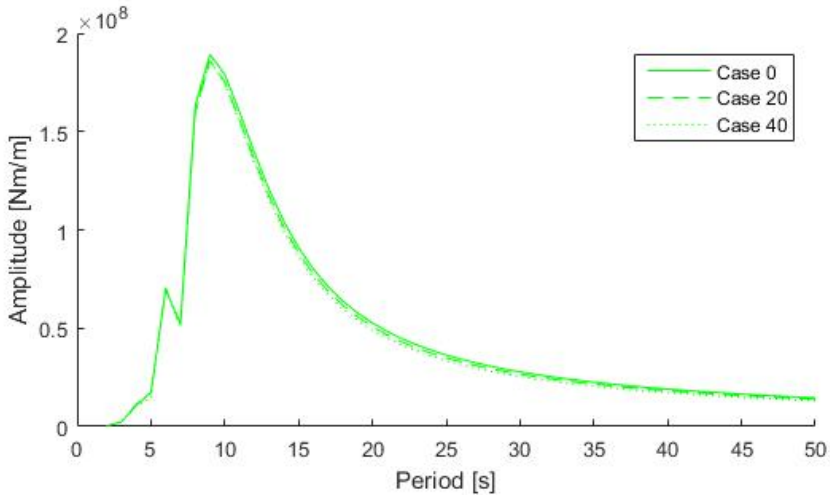

Figure E.9: First order wave force transfer function in pitch direction for wave heading 0 degrees.